Inaugural dissertation

for

obtaining the doctoral degree

of the

Combined Faculty of Mathematics, Engineering and Natural Sciences

of the

Ruprecht - Karls - University

Heidelberg, Germany.

Presented by,

M.Sc., Joshua Reginald Malapit

Born in: Mandaluyong City, Philippines

Oral examination: August 1, 2024

Insights into Autoimmune Mechanisms and the Pathogenic Role of Tumor-Infiltrating B Cells in Yo-Associated Paraneoplastic Cerebellar Degeneration

Referees:

Prof. Dr. F. Nina Papavasiliou

Prof. Dr. Hedda Wardemann

Abstract

Paraneoplastic cerebellar degeneration (PCD) is an autoimmune neurological disorder that impairs motor function through the immune-mediated death of cerebellar neurons. PCD is frequently diagnosed among ovarian or breast cancer patients, where the tumor aberrantly expresses antigens typically restricted to the cerebellum. Yo-associated PCD is the most common subtype, characterized by serum- or cerebrospinal fluid (CSF)-derived Yo antibodies. They serve as a diagnostic marker, and prompts the search for an associated tumor. Yo antibodies have been classically defined to target the canonical Yo antigen Cerebellar Degeneration-related protein 2 (CDR2), whose expression is normally restricted to Purkinje cells of the cerebellum. Much contention however exists surrounding the specificity of these autoantibodies and their contribution to the progression of the disorder. In my dissertation, I used single-cell immunoglobulin sequencing to examine the repertoire of tumor-infiltrating B cells and antibody-secreting cells from an ovarian carcinoma patient who presented with anti-Yo paraneoplastic cerebellar degeneration (Yo-PCD). Here, I show across different reactivity assays that CDR2L (Cerebellar Degeneration Related Protein 2 Like), is also a target of Yo antibodies, and may be the predominant Yo antigen. I also show that these Yo antibodies are secreted by highly-activated and somatically hypermutated antibody-secreting cells that infiltrate the tumor, and likely derive from protracted autoreactive germinal center responses. I could also show that these Yo antibodies can be taken up by Purkinje cells *in vitro*. Finally, I could show that after continuous intrathecal delivery of monoclonal Yo antibodies in mice, they are also taken up by Purkinje cells *in vivo*, and normal motor function, evaluated through rotarod assays, is affected. My results demonstrate that tumor-derived Yo antibodies mainly target CDR2L, and have a potential pathogenic contribution to the progression of Yo-PCD. Resolving the relevant Yo antigen and dissecting the epitope specificities of Yo autoantibodies may help improve the diagnosis of this disorder, and the early detection of the associated tumor. Furthermore, deeply characterizing Yo autoantibodies and elucidating antibody-mediated pathogenic mechanisms may fine-tune the prognosis for Yo-PCD, and expand current paradigms for the role of antibodies targeting intracellular antigens.

Zusammenfassung

Die paraneoplastische Kleinhirndegeneration (PCD) ist eine neurologische Autoimmunerkrankung, die die motorischen Funktionen durch das immunvermittelte Absterben von Kleinhirnneuronen beeinträchtigt. PCD wird häufig bei Patientinnen mit Eierstock- oder Brustkrebs diagnostiziert, da der Tumor in abnormaler Weise Antigene exprimiert, die normalerweise auf das Kleinhirn beschränkt sind. Die Yo-assoziierte PCD ist der häufigste Subtyp, der durch Yo-Antikörper aus dem Serum oder dem Liquor gekennzeichnet ist. Sie dienen als diagnostischer Marker und veranlassen die Suche nach einem assoziierten Tumor. Yo-Antikörper sind klassischerweise auf das kanonische Yo-Antigen Cerebellar Degeneration-related protein 2 (CDR2) ausgerichtet, dessen Expression normalerweise auf Purkinje-Zellen des Kleinhirns beschränkt ist. Die Spezifität dieser Autoantikörper und ihr Beitrag zum Fortschreiten der Erkrankung sind jedoch sehr umstritten. In meiner Dissertation untersuchte ich mit Hilfe der Einzelzell-Immunglobulin-Sequenzierung das Repertoire der tumorinfiltrierenden B-Zellen und Antikörper-sezernierenden Zellen einer Ovarialkarzinompatientin, die eine Yo-bedingte paraneoplastische Kleinhirndegeneration (Yo-PCD) aufwies. Hier zeige ich anhand verschiedener Reaktivitätstests, dass CDR2L (Cerebellar Degeneration Related Protein 2 Like) ebenfalls ein Ziel von Yo-Antikörpern ist und möglicherweise das vorherrschende Yo-Antigen darstellt. Ich konnte auch zeigen, dass diese Yo-Antikörper von hochaktivierten und somatisch hypermutierten Antikörper-sezernierenden Zellen, die den Tumor infiltrieren, abgesondert werden und wahrscheinlich von andauernden autoreaktiven Keimzentrumsreaktionen herrühren. Ich konnte auch zeigen, dass diese Yo-Antikörper von Purkinje-Zellen in vitro aufgenommen werden können. Schließlich konnte ich zeigen, dass nach kontinuierlicher intrathekaler Verabreichung von monoklonalen Yo-Antikörpern in Mäusen diese auch in vivo von Purkinje-Zellen aufgenommen werden und die normale motorische Funktion, die mit Hilfe von Rotarod-Tests ermittelt wurde, beeinträchtigt wird. Meine Ergebnisse zeigen, dass vom Tumor stammende Yo-Antikörper hauptsächlich auf CDR2L abzielen und einen möglichen pathogenen Beitrag zum Fortschreiten der Yo-PCD leisten. Die Bestimmung des relevanten Yo-Antigens und die Aufschlüsselung der Epitop-Spezifitäten von Yo-Autoantikörpern können dazu beitragen, die Diagnose dieser

Erkrankung und die Früherkennung des damit verbundenen Tumors zu verbessern. Darüber hinaus kann die eingehende Charakterisierung von Yo-Autoantikörpern und die Aufklärung von Antikörper-vermittelten pathogenen Mechanismen die Prognose für Yo-PCD verbessern und die derzeitigen Paradigmen für die Rolle von Antikörpern, die auf intrazelluläre Antigene abzielen, erweitern.

Table of Contents

1 Introduction

1.1 B cells and Tolerance

1.1.1 B cell Development and Maturation

B cells provide an extensive layer of protection against diseases through the generation of antibodies. These antibodies neutralize pathogens, mark them for destruction, activate complement proteins, recruit natural killer cells, interfere with viral replication, and enhance antigen presentation to T cells, thereby strengthening the immune response [3].

Antibodies are secreted proteins which derive from immunoglobulins on the surface of B cells. Together with the transmembrane proteins Igα and Igβ which are important docking sites for signal transduction, they form the B cell receptor (BCR)[4, 5].

Functionally, immunoglobulins play a crucial role in host defense through the recognition of different antigens on disease-causing pathogens such as bacteria, viruses and other microorganisms. Secreted antibodies can bind to and inactivate viruses and toxins thereby neutralizing them; they can coat the surface of larger foreign substances, and help target them for phagocytosis by macrophages or antibody-dependent cellular cytotoxicity [6, 7].

Structurally, immunoglobulins are composed of two identical heavy chains and two identical light chains (Figure 1)[3]. The heavy chains are encoded by the immunoglobulin heavy-chain (*IGH*) genes, and the light chains are encoded by the immunoglobulin light-chain (*IGL*) genes. Each heavy chain consists of one N-terminal variable domain (VH), which is a product of the somatic recombination of one *IGHV*, one I*GHD* and one *IGHJ* gene during B cell development. This is concatenated to three to four C-terminal constant domains (CH1, CH2, CH3, and CH4), depending on antibody class. Similarly, each light chain consists of one N-terminal variable domain (VL) from somatically recombined *IGKV* and *IGKJ* genes *or IGLV* and *IGLJ* genes, and one C-terminal constant domain (CL). The variable domains are responsible for antigen binding, and

determines much of an antibody's specificity as well as affinity, while the constant domains of the heavy chain determine downstream effector functions that allow for a tailored and effective response to a wide range of pathogens and antigens.

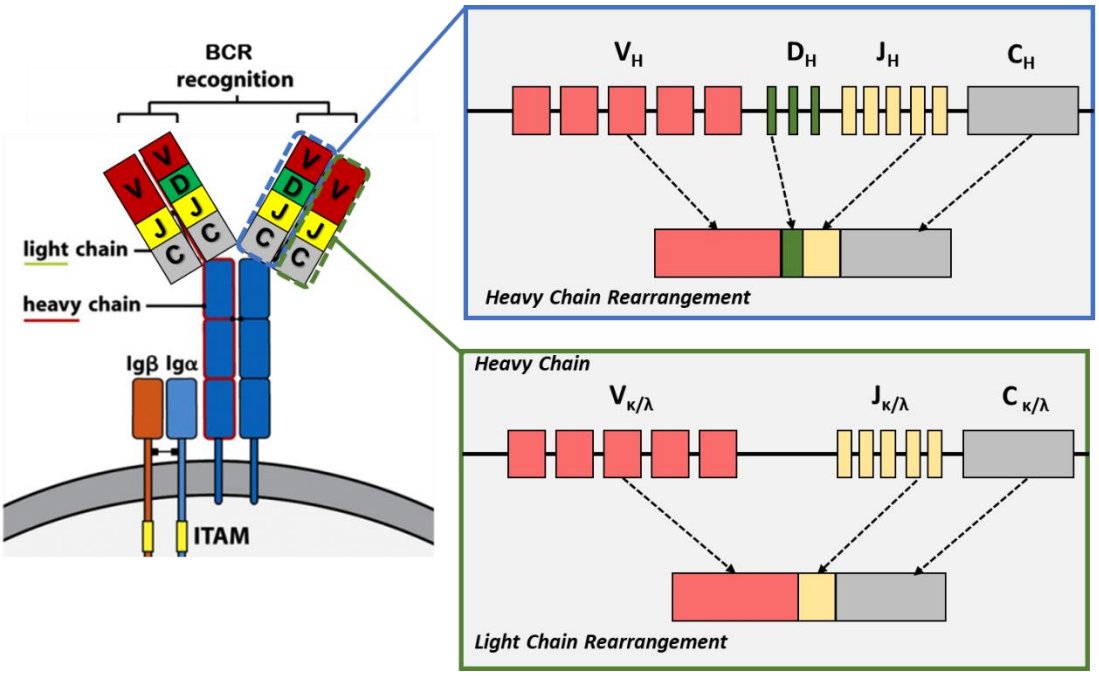

Figure 1. **Structure of the BCR, and the V(D)J recombination events that give rise to them.** B cell receptors are composed of a pair of immunogloblin heavy and light chains that result from the recombination of specific V genes, D genes (for heavy chains), J genes, and constant region genes, and dimers of the Igα:Igβ transmembrane proteins. The constant regions of the heavy chain anchor the immunoglobulin receptor via the transmembrane domain, where they interact with of Igα:Igβ, which contain (ITAMs) that initiate the signaling cascade during B cell activation.

Before B cells are able to achieve these protective functions, primarily through the secretion of antibodies, they first undergo an arduous process of developmental selection and maturation[8, 9]. B cells are generated in the bone marrow, where they go through several differentiation steps starting from being a hematopoetic stem cell (HSC)[10]. In this specialized microenvironment, external cues activate intrinsic genetic programs that transform HSCs into Common Lymphoid Progenitors (CLPs) and then direct further lineage differentiation. After having committed to the B cell lineage from the Common Lymphoid Progenitor, the pro-B cell stage begins through the rearrangement of heavy chain genes. B cells at this stage express the

RAG1 and RAG2 proteins (collectively called RAG proteins) that facilitate the assembly of a combination of one variable (V), one diversity (D), and one joining (J) gene segment within the heavy chain locus [11]. This combination creates a unique exon upstream of the immunoglobulin (C)-region exons, which is concatenated directly to the downstream μ constant (C) region exon, and drives the expression of a productive heavy chain. This heavy chain is then temporarily paired with a surrogate light chain (SLC) and is displayed on the cell surface. Several mechanisms at this stage select for cells expressing only one productive heavy chain, ensuring that each B cell carries only one unique heavy chain. Only after this do B cells enter the next stage called the pre-B cell stage [8, 12-14].

At the pre-B cell stage, a B cell strives to form a functional light chain through the rearrangement of light chain genes, starting with the kappa locus and proceeding with the lambda locus. Successful assembly of a productive light chain then replaces the SLC, and together with the heavy chain, form a functional BCR [15]. Although each B cell has the genetic potential to simultaneously express two different H-chains and four or more different L chains, a B cell usually expresses a unique H-L chain pair via allelic exclusion [14, 16]. After this functional pairing and allelic exclusion, tonic BCR signaling is triggered, which promotes positive selection for survival when the BCR does not react strongly to self-antigens in the bone marrow niche [14]. B cells then leave the bone marrow into the periphery as immature B cells.

Immature B cells travel to the spleen as new emigrant B cells. In the spleen, most B cells will not survive as they must compete with long-lived mature B cell subsets, such as memory B cells, for entry in the follicle and for the limiting amounts of the essential B cell survival factor BAFF produced there [17]. If they manage to enter the follicle and acquire BAFF, they then fully develop into mature naïve B cells, majority of which traffic into other secondary lymphoid tissues for activation [18].

1.1.2 Germinal Center Reactions

Secondary lymphoid organs such as lymph nodes, Peyer's patches, and the spleen are the primary sites for the activation, proliferation, and differentiation of B cells during T cell-dependent immune responses. When naïve B cells in the follicles of secondary lymphoid organs get activated by antigen through their BCR, they migrate to the border T:B border called the interfollicular region, where they interact with antigen-specific T cells to get T cell help [4]. Hereafter, these B cells have three main fates. A fraction of them moves into medullary chords, where they differentiate into short-lived plasmablasts and then short-lived plasma cells to secrete antibodies that typically have low affinity toward the antigen, but form the initial humoral immune response [4]. Some others differentiate into IgM (unswitched) memory B cells [4, 19] and recirculate back to the periphery. Finally, the subset of B cells that bind cognate antigen with high affinity and therefore have better access to T cell help, go on to seed germinal centers (GC) [4, 19]. Importantly, class-switch recombination or isotype switching mainly happens at these pre-GC stages, where the immunoglobulin (Ig) heavy chain μ constant region gene rearranges and switches to an Ig isotype with a more suitable effector function [20].

In germinal centers, B cells interact with T helper cells, and follicular dendritic cells (fDCs) in a highly-orchestrated process called germinal center reactions [21]. It is the mechanism responsible for affinity maturation, through which antibodies with progressively higher affinities for a specific antigen get produced. During the GC reaction, B cells within the dark zone (DZ) undergo rapid proliferation and diversification, by mutating their BCR heavy and light chain genes via the enzyme AID in a process called somatic hypermutation (SHM). The newly-generated clones then cycle to the light zone (LZ), where they interact with T follicular helper (Tfh) cells and follicular dendritic cells to test their new BCRs. In the light zone, they undergo selection based on the affinity of their BCRs and its ability to capture cognate antigens from fDCs and present them to antigen-specific Tfh cells. B cells subsequently receive T cell help based on the strength of these B:T interactions, and B cells that manage to produce higher-affinity BCRs receive more co-stimulatory T-cell help, and thus have a competitive edge to proliferate as they re-enter the dark zone for further rounds of somatic hypermutation and clonal expansion. The limiting numbers of

Tfh cells in the GC make GC reactions a highly-competitive and Darwinian selection process where B cells that have failed to acquire sufficient T cell help undergo apoptosis [21]. The end-products of GC reactions are memory B cells and antibody-secreting cells, specifically long-lived plasma cells, that have vastly improved affinities to the immunizing antigen [19]. It is a fundamental process in the adaptive humoral immune response, allowing the immune system to generate highly specific and effective antibodies tailored to prevent a broad range of diseases and pathologies.

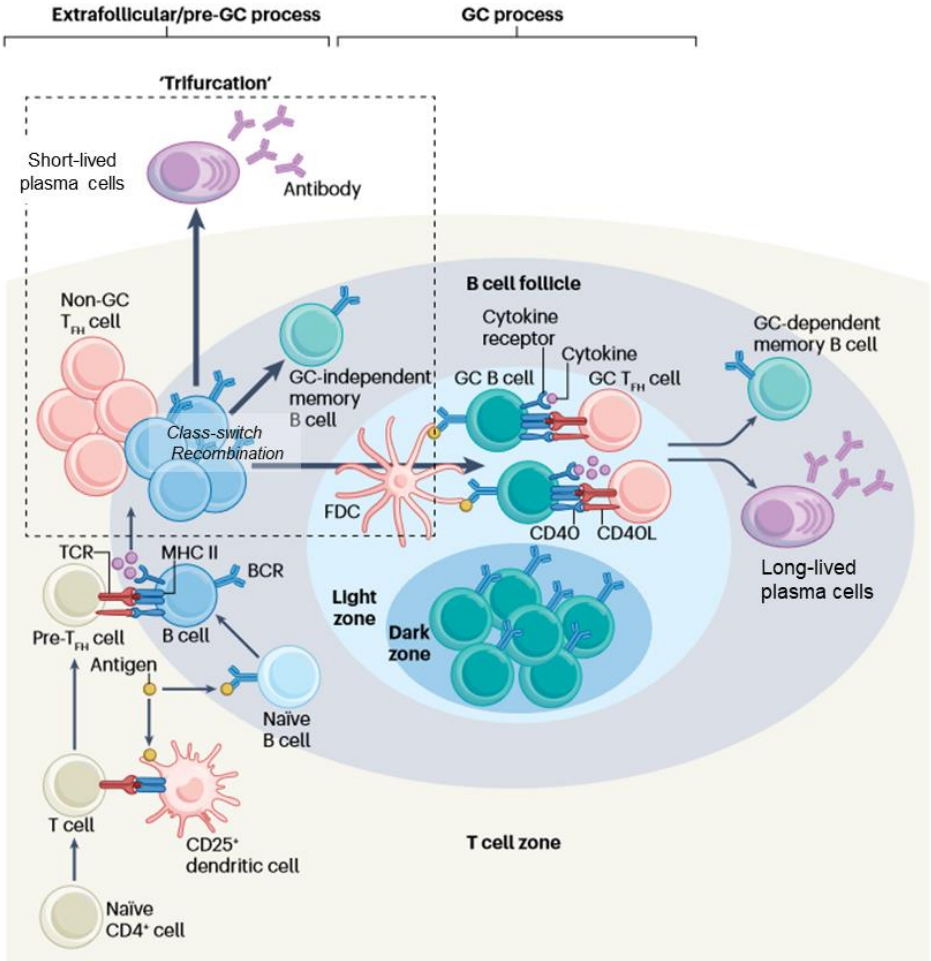

Figure 2. Germinal center reactions and the generation of memory B cells, short-lived plasma cells and long-lived plasma cells during an immune response. Activated B cells which receive T-cell help and can go through multiple fates based on the trifurcation model of B cell fate after antigen encounter. In this model, B cells can differentiate into short-lived plasma cells, GC-independent memory B cells, or can seed germinal centers which give rise to affinity matured memory B cells and long-lived plasma cells, all as a function of BCR affinity, T cell help, and signals from the microenvironment. (Adapted from Inoue, 2024 [19]).

1.1.3 B Cell Tolerance Mechanisms

Throughout B cell development and maturation, the production of autoreactive B cells – B cells bearing immunoglobulin receptors which target self-tissue – are regulated in several ways. Collectively called tolerance mechanisms, they occur at different stages of B cell development and function by reducing the number of autoreactive B cells in the B cell repertoire, attenuating BCR signals from for self-antigens, or diminishing the functionality of autoreactive clones [14]. There are three established checkpoints that purge the B cell repertoire of autoreactive B cells. In the bone marrow, during the early stages of B cell development, a considerable proportion of autoreactive B cells are removed by mechanisms of central tolerance [22].

Central tolerance is quintessential in excluding highly-autoreactive B cells from entering the naïve pre-immune B cell repertoire [14]. This first tolerance checkpoint is effectuated after pairing of the heavy and light chains, as B cells attempt to transition out of the pre-B cell stage. Here, B cells that have produced a BCR that recognizes self-antigens within the bone marrow niche with high-affinity, get overstimulated. This forces the B cell to go through a process called receptor editing [23].

During receptor editing, B cells with autoreactive receptors receive the opportunity to escape negative selection by “editing” the specificities of their receptors with additional antibody gene rearrangement. This happens in the light chain locus through the re-expression of RAG proteins, and leads to rearrangement of the remaining light chain genes starting with the kappa locus. If no productive rearrangement was achieved in the kappa loci, rearrangement of lambda light chain genes ensues, and continues until either a new BCR that is no longer autoreactive is produced, or no productive rearrangement was achieved, in which case clonal deletion happens and the B cell undergoes apoptosis [23]. Some light chain rearrangements may result in new BCRs with a low affinity toward self-antigens, and although these B cells are allowed to survive and pass the first tolerance checkpoint, they get relegated into a functionally unresponsiveness state called anergy [24, 25].

Outside of the bone marrow, peripheral tolerance mechanisms take over to further limit the potentially damaging effects of autoreactivity that might lead to autoimmunity [26]. B cells from the bone marrow and on their way to the spleen are subjected to a peripheral tolerance checkpoint that further constrains the number of immature naïve B cells, including surviving autoreactive clones [22]. Here, competition for BAFF in the follicles is a natural culling step, both for non-autoreactive and autoreactive B cells [27]. Weakly-autoreactive clones that have emigrated from the bone marrow are typically anergic, and have a significantly-reduced survival fitness due to their shorter half-life, decreased levels of surface IgM, and lower expression of the receptor for BAFF, BAFF-R [28-31]. Consequently, they have a much shorter window to reach the spleen, and a decreased competitive fitness to acquire the cytokines necessary for their survival. Some of the weakly-autoreactive B cells that survive up to this point will be retained in the periphery as normal non-autoreactive B cells, but only if their cognate autoantigen remains inaccessible to them, a state termed clonal ignorance [32]. Together, these B-cell extrinsic and B-cell intrinsic properties serve as the second tolerance checkpoint, and occurs in the periphery [33].

The stochastic nature of somatic hypermutations during germinal center reactions can inadvertently produce BCRs that can recognize self-antigen [21, 34]. When these newly-generated autoreactive B cells get exposed and bind to high amounts of GC-derived self-antigens in the LZ, without the concomitant availability of T cell help from cognate autoantigen-specific T cells, these B cells immediately undergo apoptosis [22, 35, 36]. Tingible body macrophages then clear the apoptotic cell debris, which may otherwise be a source of autoantigen-derived co-stimulatory signals via TLRs [34]. In this peripheral checkpoint in the GC, tolerance is maintained effectively by B cell-extrinsic factors that limit B-cell access to co-stimulation, primarily through the absence of cognate autoantigen specific T helper cells, but also effective clearance of apoptotic bodies [26, 34, 35]. Additionally, studies have shown the important contribution of regulatory T cells in this setting in preventing the accumulation of autoreactive clones in the periphery [37]. Autoreactive B cells that acquired only very weak affinities to GC-derived self-antigens can still persist but get relegated into an anergic state. These B cells also have the

opportunity to be rescued from anergy if they can mutate away from self-reactivity via SHM in the GC – a phenomenon termed clonal redemption [29].

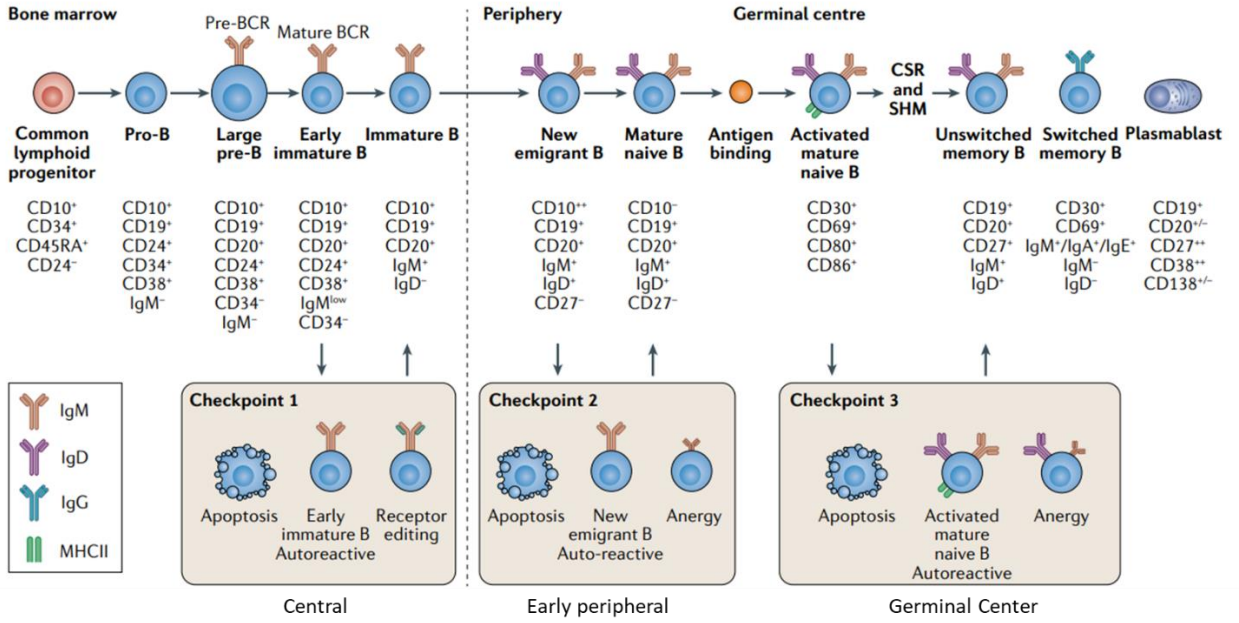

Figure 3. B cell developmental stages and tolerance checkpoints. Throughout the development of B cells from the common lymphoid progenitor to its ultimate effector fate as antibody-secreting cells, central and tolerance mechanisms impose at least three distinct checkpoints that prevent humoral immune responses from producing B cells that target self-antigens (Adapted from Sun, 2020 [22]*).*

1.2 Autoantibodies and the CNS

During B cell development and in response to diverse immunological challenges, tolerance mechanisms prevent the production of autoantibodies by B cells that recognize self-antigens [38]. Nonetheless, these mechanisms seem to be impaired in autoimmune diseases characterized by the presence of autoantibodies, as in systemic lupus erythematosus (SLE), rheumatoid arthritis (RA), multiple sclerosis (MS) and type 1 diabetes (T1D) [39].

In these autoimmune diseases, the mature naïve B cell repertoire seems to be enriched for self-reactive clones with mild affinity to cognate self-antigens, and polyreactive clones which weakly bind to structurally diverse antigens promiscuously. This implies some leakiness in the central tolerance checkpoint and the peripheral checkpoint governing new emigrant B cells in the periphery. Majority of the disease-associated antibodies however have been found to be somatically hypermutated and class-switched, also implicating dysregulated germinal center responses [34, 40, 41]. In SLE for example, the presence of class-switched highly-mutated autoantibodies specific for dsDNA comprise a significant fraction of autoantibodies in SLE patients, and is thought to be facilitated by the ineffective clearance of apoptotic bodies during the GC reaction, which provide a source of TLR-mediated co-stimulatory signals that permit autoreactive clones to affinity mature [42].

Autoantibodies that target self-antigens expressed in the central nervous system represent a unique paradigm in that autoimmunity is directed towards an organ that typically experiences reduced immune responses to protect it from excessive inflammation and immune-mediated damage – a state called immune privilege. The presence of these CNS-specific autoantibodies is a hallmark of autoimmune neurological disorders, where their detection indicates untoward immune-mediated damage to neural structures [43, 44].

In a subset of these autoimmune neurological disorders, the neurological complications are associated with malignant tumors that occur remotely from the CNS, and are called paraneoplastic neurological syndromes (PNS) [45, 46]. In these disorders, tolerance is broken and

immune privilege is breached by the malignant tumor's ectopic expression of antigens that are normally restricted to the CNS [47, 48].

Autoantibodies in this setting distinguish the presenting neurological syndrome, and are associated with distinct cancer entities, reflecting the heterogeneity of the CNS antigens that are aberrantly expressed by cancers and the specificity of the autoimmune response. The direct pathogenic contributions of autoantibodies have been extensively studied for cancers that express neuronal cell surface antigens , where antibodies are able to directly access their target epitopes, and through which several mechanisms have been described in detail [49] . They have been found to be frequently IgG-switched, with varying degrees of somatic hypermutation, indicating the role of germinal center reactions [34]. Interestingly, the presence of unmutated autoantibodies in some of these disorders, and retention of autoreactivity even after reverting somatically hypermutated clones to their unmutated germline configuration point to imperfect central tolerance mechanisms that allow for autoreactive precursors to be retained in the mature naïve B cell repertoire [22, 50-52]. On the other hand, the relevance and pathogenic involvement of autoantibodies targeting neuronal intracellular proteins has been less clear and remains unresolved.

Table 1. Autoantibodies associated with Neurological Syndromes and Co-occurring Cancers. *(Table adapted from Yshii, 2020 [1]).*

Antibody	Neurological Syndrome	Freq. of Cancer (%)	Cancer Assocation
Yo (PCA-1)	Rapidly progressive cerebellar Syndrome (RPCS)	>90	Ovary and breast cancers
SOX1	LEMS w/ and w/o RPCS	>90	SCLC
PCA2 (MAP1B)	Sensorimotor neuropathy, RPCS, and EM	80	SCLC, NSCLC, and breast cancer
Amphiphysin	Polyradiculoneuropathy, SNN, EM, SPS	80	SCLC and breast cancer
MA2 and/or MA	LE, brainstem encephalitis	>75	Testicular cancer and NSCLC
Tr (DNER)	RPCS	90	Hodgkin lymphoma
KLHL11	Brainstem/cerebellar syndrome	80	Testicular cancer
AMPAR	Limbic encephalitis	>50	SCLC and thymoma
$GABA_BR$	Limbic encephalitis	>50	SCLC
mGluR5	Encephalitis	~50	Hodgkin Lymphoma
P/Q VGCC	LEMS, rapidly progressive cerebellar syndrome	50 for LEMS; nearly 90 for RPCS)	SCLC
NMDAR	Anti-NMDAR encephalitis	38	Ovarian or extraovarian teratomas
CASPR2	Morvan Syndrome	50	Malignant thymoma

1.3 Yo-associated Paraneoplastic Cerebellar Degeneration

1.3.1 Overview of Paraneoplastic Cerebellar Degeneration

Paraneoplastic cerebellar degeneration (PCD) is a form of PNS that results from autoimmunity against cerebellar antigens. It is the one of the most common and easily recognized paraneoplastic syndromes, and comprises a suite of subtypes with diverse clinical features, prognoses, and associated tumors. Historically, the first case of PCD was described in 1919, of a patient with ovarian carcinoma co-presenting with cerebellar ataxia [53]. Only much later in the 1980s onwards did descriptions of autoantibody associations to specific cancers appear [54]. Today, PCD is classified into subtypes based on the presence of anti-neuronal antibodies that have been identified from patient-derived CSF and serum, and that primarily bind to intracellular antigens expressed by cerebellar neurons. (Table 2).

Table 2. Common Subtypes of Paraneoplastic Cerebellar Degeneration (Yshii, 2020 [1], Greenlee, 2022 [2])

Autoantibody	Target, function, localization	Associated Cancer
Anti-Yo (PCA-1)	CDR2 and its paralogue CDR2L, putative neuronal signal transduction proteins, in the cytoplasm of Purkinje cells	Ovarian tumor, breast cancer
Anti-Hu (ANNA-1)	RNA-binding protein, cytoplasmic, neuronal nuclei	SCLC, other neuroendocrine tumors
Anti-GAD65	Enzyme expressed intracellularly, allowing the conversion of glutamate to GABA in CNS neurons and pancreatic islet cell	Rarely paraneoplastic if not associated with other neuronal autoantibodies: SCLC, neuroendocrine, thymoma, breast cancer, non-Hodgkin lymphoma
Anti-CV2/CRMP5	Cytosolic protein involved in brain ontogenesis by relaying semaphorin 3A signaling. Located predominantly in dendrites of cortical pyramidal neurons, hippocampal CA1 pyramidal cells, Purkinje cells and oligodendrocytes	SCLC, thymoma, gynecological cance
Anti-Ma2 (PNMA2)	Ma2 could play a role in mRNA biogenesis, localized to structures that resemble nuclear bodies.	Testicular germ-cell tumors
Anti-Ma1 (PNMA1)	Ma1 could play a role in mRNA biogenesis, localized to structures that resemble nuclear bodies.	Variable: SCLC and non-small cell lung cancer, colon cancer, non-Hodgkin lymphoma, breast cancer
Anti-Ri (ANNA-2)	Neuron-specific RNA-binding proteins, widely express in the CNS	Breast and gynecological cancer, SCLC

1.3.2 Symptoms and Pathological Drivers

The clinical presentation of PCD begins as a mild unsteadiness in gait and problems with speech and swallowing, indicative of early neurological malfunction. This rapidly progresses to severe ataxia, where loss of muscular control in the limbs and trunk result in drastic impairment in coordination and balance [1, 55-57]. Once cerebellar dysfunction is widespread, daily activities of an afflicted patient are significantly hindered within three months before reaching a plateau.

At this point however, the immune-mediated damage to the cerebellum has become irreversible [58]. Typically, the neurological presentation precedes the diagnosis of the associated cancer. The detection of autoantibodies from patients' blood and CSF however urgently prompts for a tumor search, and is also used to confirm the diagnosis [2, 59, 60].

In majority of the subtypes of PCD, the target of the autoantibodies is an intracellular protein. This has long been used as an argument against a pathogenic role for autoantibodies, and have therefore been collectively thought to be T-cell-mediated autoimmune disorders [56]. This was corroborated by mouse studies, where the passive immunization of patient-derived autoantibodies does not lead to the same neurological outcome [61, 62]. Still, no direct evidence against the role of autoantibodies has been established, especially in models that faithfully represent the complexity of immune interactions happening within the tumor-brain axis. Yo-PCD, the most common subtype of paraneoplastic cerebellar degeneration, is at the center of this debate, where although a T-cell-mediated pathogenesis is established through the identification of cytotoxic T cells that can mediate antigen-specific killing, the pathogenic contribution of B cells specific to the Yo antigen is understudied [1, 63, 64].

1.3.3 Role of Yo Antibodies

Highly specific anti-neuronal autoantibodies found in the sera and/or cerebrospinal fluid (CSF) are crucial for the diagnosis of PCD, and the detection of these autoantibodies prompts the focused search for a tumor [60, 65]. Approximately 50% of PCD cases are associated with Yo antibodies, also called PCA-1 (Purkinje cell antibody-1), establishing anti-Yo as the most frequently identified autoantibody in PCD compared to other anti-neural antibodies.

The classical target of Yo autoantibodies is CDR2, short for Cerebellar Degeneration-Related Protein 2, a 62kDA protein localized intracellularly, and the first Yo antigen described [66-68]. Its expression is restricted to Purkinje cells and areas surrounding the brainstem, and spermatogonia despite the broad detection of CDR2 mRNA in various tissues [69, 70]. However ectopic expression in gynecological and breast cancers, even in cancer patients without

neurological symptoms, has been established [71]. No crystal structure for CDR2 exists to date, but it is inferred to have a leucine zipper motif, often associated with DNA-binding [72]. The physiological function of CDR2 however is still unclear, although some studies have found that it interacts with c-myc, and knockout of CDR2 leads to impaired cellular proliferation due to disrupted mitotic spindle formation during cell division in tumors [73], and disruption of calcium homeostasis in purkinje cells [74]. In terms of subcellular localization, it has been reported to be contained in the cytoplasm and proximal dendrites of neurons, particularly Purkinje cells, but form nuclear speckles in a model cell line of ovarian cancer [69].

Recently, another target of Yo autoantibodies, CDR2L, has been described [75, 76]. It shares about 45% sequence homology with CDR2, and is slightly smaller protein at 55kDa. CDR2L expression is also restricted to Purkinje cells and ovarian and breast cancers, but even less is known about its structure and function. Its subcellular localization has been determined to be cytoplasmic, and was found to interact with ribosomal proteins in the context of an ovarian cancer model [69].

Historically, CDR2 has been touted as the classical Yo antigen in Yo-associated Paraneoplastic Cerebellar Degeneration, principally through its inaugural detection in Yo-associated tumors in the earliest studies of Yo-associated PCD [47, 67, 77]. However growing reports on the relevance of CDR2L as another Yo antigen, perhaps even the more relevant one, have also been put forward, although this has remained a subject of much contention [78]. Resolving the main Yo antigen in PCD has profound ramifications on how this disorder is diagnosed, as current commercially-available diagnostic kits are designed based on CDR2 as the sole Yo antigen.

Furthermore, divergent from the paradigm in the field that neurological disorders associated with intracellular autoantigens are solely T-cell driven diseases, the pathogenic role of autoantibodies in the setting of Yo-PCD has remained unresolved.

In the current project, I sought to revisit long-standing questions about the origin, specificity and pathogenic role of Yo-antibodies by performing extensive characterization and exploration of their pathogenic involvement at monoclonal level. I used single-cell

immunoglobulin sequencing to investigate the clonality and composition of tumor-infiltrating B cells and antibody-secreting cells from an ovarian carcinoma biopsy of a Yo-PCD patient, and the specificities of tumor infiltrating B cell-derived monoclonal antibodies were tested against the CDR2 and CDR2L Yo antigens across different binding assays. I linked back the identified reactivities to features of the tumor infiltrating B cell repertoire to glean insight on autoimmune mechanisms that lead to the production of Yo autoantibodies. The epitope specificity of CDR2- and CDR2L-reactive antibodies were also examined by blocking ELISAs, which would help resolve fine epitope specificities of Yo autoantibodies, and identify candidate antibodies that facilitate the structural determination of CDR2 and CDR2L via cryo-EM in future experiments.

The direct contribution of these autoantibodies to anti-tumor immunity was assessed in vitro using an ovarian carcinoma model cell line, and the Purkinje cell uptake of antibodies was examined on primary Purkinje cells *in* vitro. Finally, the potential pathogenic role of mAbs to autoimmune-mediated Purkinje cell death were assessed *in vivo* by the intrathecal delivery of mAbs to mice and subsequent motor function assays.

2 Objectives

The overall goal of my dissertation is to extensively characterize tumor-infiltrating B cells in the context of paraneoplastic cerebellar degeneration, gain insights about the autoimmune responses they are involved in, and investigate their potential pathogenic role.

More specifically, my study had the following aims:

- To employ single-cell sorting and immunoglobulin sequencing to B cells isolated from tumor biopsies of patients with Yo-associated Paraneoplastic Cerebellar Degeneration.
- To look at the clonal composition and molecular features of tumor-infiltrating B cell clones by repertoire analysis at single-cell level
- To perform molecular and functional characterization of tumor-infiltrating B cell-derived monoclonal antibodies to glean insight on etiological and pathogenic mechanisms in Yo-associated Paraneoplastic Cerebellar Degeneration

3 Materials

Antibodies for ELISA

Product	Source
AffiniPure Goat Anti-Human IgG, Fcγ fragment specific	Jackson ImmunoResearch Laboratories, Cambridgeshire, United Kingdom.
Peroxidase AffiniPure Goat Anti-Human IgG, Fcγ fragment specific	Jackson ImmunoResearch Laboratories, Cambridgeshire, United Kingdom
IgG1, Kappa from human myeloma plasma	Sigma Aldrich, Steinheim, Germany

Antibodies and Reagents for Western Blot

Product	Source
AffiniPure Goat Anti-Rabbit IgG (H+L)	Jackson ImmunoResearch Laboratories, Cambridgeshire, United Kingdom.
Rabbit anti-CDR2 antibody	Sigma Aldrich Chemie GmbH, Steinheim, Germany
Rabbit anti-CDR2L antibody	Sigma Aldrich Chemie GmbH, Steinheim, Germany
Peroxidase AffiniPure Goat Anti-Human IgG, Fcγ fragment specific	Jackson ImmunoResearch Laboratories, Cambridgeshire, United Kingdom
Color Prestained Protein Standard, Broad Range (19–250 kDa)	New England Biolabs GmbH, Frankfurt am Main, Germany
Whattman Paper	Carl Roth GmbH & Co. KG, Karlsruhe, Germany
PVDF membrane	GE Healthcare Life Sciences, Freiburg, Germany
8-16%% Criterion™ TGX™ Precast Protein Gel	BioRad Laboratories GmbH, München, German

Antibodies Immunofluorescence Assays

Product	Source
Goat anti-human IgG – Alexa488	Invitrogen GmbH, Karlsruhe, Germany
Rabbit anti-calnexin	Cell Signaling Technologies, Massachusetts, USA
Mouse Anti-calbindin D28K	Thermo Fisher Scientific Inc., Darmstadt, Germany

Recombinant Control Antibodies

Product	Source

mGO53 (*non-reactive antibody)*	Produced in-house [40, 79, 80]
JB40 *(highly polyreactive antibody)*	Produced in-house [40]
ED38 *(weakly polyreactive antibody)*	Produced in-house [40]

Antigens for ELISA

Product	**Source**
CDR2 (Human) Recombinant Protein	Abnova, Taipei, Taiwan
CDR2L (Human) Recombinant Protein	Abnova, Taipei, Taiwan
Ovalbumin	Invivo Gen, San Diego, California
dsDNA sodium salt from salmon testes	Sigma Aldrich Chemie GmbH, Steinheim, Germany
Human recombinant insulin	Sigma Aldrich Chemie GmbH, Steinheim, Germany
Lipopolysaccharides	Sigma Aldrich Chemie GmbH, Steinheim, Germany

Antibodies for Flow Cytometry

Product	**Source**
Mouse Anti-CD19 – BV786, clone HIB19	BioLegend GmbH, San Diego, USA
Mouse Anti-CD20 – APC-H7, clone 2H7	BD Biosciences GmbH, Germany
Mouse Anti-CD27 – BV650, clone L128	BD Biosciences GmbH, Germany
Mouse Anti-CD38 – FITC, HIT2	BD Biosciences GmbH, Germany
Mouse Anti-CD3 – BV510, clone OKT3	BioLegend GmbH, San Diego, USA
Mouse Anti-IgG – BV421, clone HP6017	BioLegend GmbH, San Diego, USA
Mouse Anti-CD138 – PE, clone M15	BD Biosciences GmbH, Germany
Mouse Anti-IgD – Alexa647, clone IA6-2	BioLegend GmbH, San Diego, USA
Mouse Anti-CD45 – PE-Cy7, clone H130	BioLegend GmbH, San Diego, USA

Reagents for Flow Cytometry

Product	**Source**
7-Aminoactinomycin D (7-AAD)	Invitrogen GmbH, Karlsruhe, Germany
BD FACS™ Accudrop Beads	BD Biosciences GmbH, Heidelberg, Germany
UltraComp eBeads™ Compensation Beads	Invitrogen GmbH, Karlsruhe, Germany

Plasmids for Antibody Expression

Product	**Source**
Abvec2.0 IgHG1	Addgene # 80795
AbVec2.1-IGLC2	Addgene # 99575
Abvec1.1 IgkC	Addgene # 80796

Nucleic Acids and Nucleotides

Product	Source
1st PCR primers	Eurofins Genomics Germany GmbH, Ebersberg, Germany
100 bp DNA ladder	New England Biolabs GmbH, Frankfurt am Main, Germany
1 kb Plus DNA Ladder	New England Biolabs GmbH, Frankfurt am Main, Germany
Second PCR Primers	Sigma Aldrich Chemie GmbH, Steinheim, Germany
Deoxynucleotide Triphosphates (dNTPs)	Invitrogen GmbH, Karlsruhe, Germany
Oligonucleotides	Eurofins Genomics Germany GmbH, Ebersberg, Germany
Random Hexamer Primers	Roche Diagnostics GmbH, Mannheim, Germany

Enzymes

Product	**Source**
Calf Intestinal Alkaline Phosphatase (CIAP)	New England Biolabs GmbH, Frankfurt am Main, Germany
HotStar® Taq DNA polymerase	Qiagen GmbH, Hilden, Germany
Restriction endonuclease AgeI-HF®	New England Biolabs GmbH, Frankfurt am Main, German
Restriction endonuclease BsiWI-HF®	New England Biolabs GmbH, Frankfurt am Main, German
Restriction endonuclease SalI-HF®	New England Biolabs GmbH, Frankfurt am Main, German
Reverse Transcriptase SuperScript™ IV	Thermo Fisher Scientific Inc., Rosklide, Denmark
T4 DNA Ligase	New England Biolabs GmbH, Frankfurt am Main, Germany
Taq DNA Polymerase	Qiagen GmbH, Hilden, Germany

Bacteria

Product	**Source**
Escherichia coli DH10β	Clonetech Inc., Palo Alto, USA

Cell lines

Product	Source
FreeStyle™ 293-F cells.	Thermo Fisher Scientific Inc., Karlsruhe, Germany
OvCar3 cell line	American Type Culture Collection (ATCC), #HTB161

Culture medium

Product	Source
EX-CELL® 293 Serum-Free Medium	Thermo Fisher Scientific Inc., Karlsruhe, Germany
FreeStyle™ 293 Expression media	Thermo Fisher Scientific Inc., Karlsruhe, Germany
Gibco™ RPMI 1640	Life Technologies GmbH, Karlsruhe Germany
Lysogeny broth (LB) [25 g/L]	Sigma Aldrich Chemie GmbH, Steinheim, Germany
Lysogeny broth (LB) agar [35 g/L]	Sigma Aldrich Chemie GmbH, Steinheim, Germany
SOC medium	Sigma Aldrich Chemie GmbH, Steinheim, Germany
OvCar3 medium	RPMI, 20% FBS, 1% Pen-strep, 1% L-glutamine, 0.01 mg/mL of insulin from bovine pancreas

Commercial kits

Product	Source
KAPA Library Quant Kit	Roche Diagnostics GmbH, Mannheim, Germany
NucleoSpin® Gel and PCR Clean-up	Macherey-Nagel GmbH & Co. KG, Düren, Germany
NucleoSpin® Plasmid Kit	Macherey-Nagel GmbH & Co. KG, Düren, Germany
RNeasy Mini Kit	Qiagen AG, Hilden, German
SuperScript IV First-Strand Synthesis System	Invitrogen GmbH, Karlsruhe, Germany
TruSeq DNA Single Indexes Set A	Illumina, San Diego, CA, USA
TruSeq Nano DNA LT Library Prep Kit	Illumina, San Diego, CA, USA
Tumor Dissociation Kit, human	Miltenyi Biotec, USA
Pierce™ BCA Protein Assay Kits	Thermo Fisher Scientific Inc., Darmstadt, Germany
EZ-Link® NHS-Biotinylation Kit	Thermo Fisher Scientific Inc., Darmstadt, Germany
Slide-ALyzer® Mini Dialysis Kit	Thermo Fisher Scientific Inc., Darmstadt, Germany

Buffers

Product	Source
1 % BSA Buffer	1 % BSA in 1X PBS
2 % BSA buffer	2 % BSA in 1X PBS
5X First strand buffer (RT)	Invitrogen GmbH, Karlsruhe, Germany

ABTS buffer	0.1 M citric acid, 0.2 M disodium phosphate, 1 ABTS tablet/91 ml ABTS Buffer
IgG Conentration ELISA blocking buffer	0.05 % (v/v) Tween®20, 1 mM EDTA in 1 x PBS
Ag ELISA blocking buffer	10% SeaBlock Fish Serum in 1X PBS
1X PBST (Ag ELISA washing buffer)	0.05 % (v/v) Tween®20 in 1X PBS
FACS buffer	2 % FBS in 1X PBS
HotStar Taq buffer (10 x)	Qiagen GmbH, Hilden, Germany
NEBuffer™ 2.1	New England Biolabs GmbH, Frankfurt am Main, Germany
Qiagen Taq buffer (10 x)	Qiagen GmbH, Hilden, Germany
rCutSmart Buffer™ (10 x)	New England Biolabs GmbH, Frankfurt am Main, Germany
T4 DNA Ligase buffer (10 x)	New England Biolabs GmbH, Frankfurt am Main, Germany
TAE Buffer (50 x)	AppliChem GmbH, Darmstadt, Germany
RIPA+ Buffer	RIPA buffer + cOmplete™, Mini, EDTA-free Protease Inhibitor Cocktail (one tablet for every 10mL RIPA)
1X Lämmli buffer	5X Lämmli, diluted with RIPA buffer
1X SDS PAGE Running Buffer	10X SDS PAGE Running (0.25 M Tris HCl, 1.92 M Glycine and 1% (w/v) Sodium Dodecyl Sulfate (SDS); pH 8.3.) diluted with ddH_2O
1X Transfer Buffer	48 mM Tris base, 39 mM glycine, 20 % methanol in ddH_2O
Mild stripping buffer	25 mM glycine-HCl, 1% SDS, pH2.3 in ddH_2O
IF staining antibody dilution buffer	5%, 0.25% Tween20, diluted in 1X PBS
Western Blot blocking buffer	5% skimmed milk in 1X PBST
Western Blot antibody dilution buffer	5% BSA diluted in 1X PBST

Chemicals and Reagents

Product	**Source**
0.5 M Ethylenediaminetetraacetic acid (EDTA), pH 8.0	Carl Roth GmbH & Co. KG, Karlsruhe, Germany
10 x Phosphate-buffered saline (pH 7.4)	Fisher Scientific GmbH, Schwerte, Germany
2,2'-azino-bis (3-ethylbenzothiazole-6-sulfonic acid) diammonium (ABTS) substrate	Roche Diagnostics GmbH, Mannheim, Germany
8 M Sodium thiocyanate solution (NaSCN)	Sigma Aldrich Chemie GmbH, Steinheim, Germany
ABTS® Peroxidase Stop Solution Kit (5 x)	SeraCare, Milford, USA
Ampicillin (100 mg/ml)	Sigma Aldrich Chemie GmbH, Steinheim, Germany
Bovine serum albumin fraction V (BSA) (≥ 98 %)	Carl Roth GmbH & Co. KG, Karlsruhe, Germany
Calcium chloride dihydrate ($CaCl_2$ x 2 H_2O)	AppliChem, Darmstadt, Germany
Citric acid ($C_6H_8O_7$) (≥ 99.5 %, p.a)	Sigma Aldrich Chemie GmbH, Steinheim, Germany

cOmplete™, Mini, EDTA-free Protease Inhibitor Cocktail	Sigma Aldrich Chemie GmbH, Steinheim, Germany
Dimethyl sulfoxide (DMSO) for cell culture	AppliChem, Darmstadt, Germany
Disodium phosphate (Na_2HPO_4) (≥ 98 %, p.a)	Carl Roth GmbH & Co. KG, Karlsruhe, Germany
Dithiothreitol (DTT)	Life Technologies GmbH, Karlsruhe, Germany
Ethanol denatured, EMSURE® for analysis (denatured with 1 % MEK), Supelco®	Merck KGaA, Darmstadt, Germany
Ethanol, absolute	Merck KGaA, Darmstadt, Germany
Insulin from bovine pancreas	Sigma Aldrich Chemie GmbH, Steinheim, Germany
Gel Loading Dye, Purple (6 X)	New England Biolabs GmbH, Frankfurt am Main, Germany
GIBCO™ 10 x Phosphate-buffered saline (pH 7.4)	Life Technologies GmbH, Karlsruhe, Germany
GIBCO™ 1 x Phosphate-buffered saline (pH 7.4)	Life Technologies GmbH, Karlsruhe, Germany
GIBCO™ Fetal Bovine Serum (FBS)	Life Technologies GmbH, Karlsruhe, Germany
GIBCO™ L-glutamine	Life Technologies GmbH, Karlsruhe Germany
HRP-Streptavidin	BioLegend GmbH, San Diego, USA
Hydrogen peroxide solution (H_2O_2), 30 %	AppliChem, Darmstadt, Germany
Laemmli Buffer 5X	Bio-Rad Laboratories GmbH, Munich, Germany
Magnesium chloride-Hexahydrate (≥ 99.9 %, p.a)	Qiagen GmbH, Hilden, Germany
Methanol (CH_3OH) (≥ 99.9 %, p.a)	Carl Roth GmbH & Co. KG, Karlsruhe, Germany
NP-40	Sigma Aldrich Chemie GmbH, Steinheim, Germany
Nuclease free water	Eppendorf AG, Hamburg, Germany
Nucleic Acid Gel Stain SYBR™ Green I (10000 x)	Life Technologies GmbH, Karlsruhe Germany
PAP barrier pen	Sigma Aldrich Chemie GmbH, Steinheim, Germany
PBS+ (10X)	Pacheco, California, USA
peqGREEN, DNA/RNA Dye	Avantor, Radnor, USA
Pierce™ BCA Protein Assay Reagent A and B	Thermo Fisher Scientific Inc., Darmstadt, Germany
Pierce ECL Detection Reagent 1 and 2	Thermo Fisher Scientific Inc., Darmstadt, Germany
Polyethylenimine, branched (PEI)	Sigma Aldrich Chemie GmbH, Steinheim, Germany
Polysorbate,Polyoxyethylene-20-sorbitan monolaurate (Tween® 20)	Carl Roth GmbH & Co. KG, Karlsruhe, Germany
Protein G Sepharose™ Fast Flow	GE Healthcare Life Sciences, Freiburg, Germany
RIPA buffer	Thermo Fisher Scientific Inc., Darmstadt, Germany
Saponin	Sigma Aldrich Chemie GmbH, Steinheim, Germany
SeaBlock Fish Serum	Thermo Fisher Scientific Inc., Darmstadt, Germany
SeaKem® LE Agarose	Lonza, Rockland, ME, USA
Skimmed milk powder	Sigma Aldrich Chemie GmbH, Steinheim, Germany
Sodium chloride (NaCl) (≥ 99.5 %, p.a)	Fisher Scientific GmbH, Schwerte, Germany
Surface Decontaminant DNA AWAY™	Thermo Fisher Scientific Inc., Darmstadt, Germany
Surface Decontaminant RNase AWAY™	Thermo Fisher Scientific Inc., Darmstadt, Germany
Triton X-100	Sigma Aldrich Chemie GmbH, Steinheim, Germany

Trypsin-EDTA Gibco™	Thermo Fisher Scientific Inc., Darmstadt, Germany
Vectashield DAPI	BIOZOL Diagnostica Vertrieb GmbH, Eching. Germany

Consumables

Product	**Source**
125 ml Erlenmeyer cell culture flasks	Corning Inc., USA
40 µm Cell Strainer, nylon	Corning Inc., USA
96U dilution plate, untreated	Thermo Fisher Scientific Inc., Denmark
96-well semi-skirted PCR plate	4titude, Surrey, UK
Amicon® Ultra-0.5 Centrifugal Filter Unit, 50k	Merck-Millipore, Darmstadt, Germany
Assay Platte 384-well, high binding	Corning Inc., USA
Corning® 15 mL centrifuge tubes	Corning Inc., USA
Corning® 50 mL centrifuge tubes	Costar Inc., Corning, USA
Costar® Assay Platte 96-well, high binding	Corning Inc., USA
Costar® Stripette® serological pipettes 10 ml	Corning Inc., USA
Costar® Stripette® serological pipettes 2 ml	Corning Inc., USA
Costar® Stripette® serological pipettes 25 ml	Corning Inc., USA
Costar® Stripette® serological pipettes 5 ml	Corning Inc., USA
Costar® Stripette® serological pipettes 50 ml	Corning Inc., USA
CryoTube™ Vials, 1.8 ml	Thermo Fisher Scientific Inc., Darmstadt, Germany
Dualfilter 1000µl, PCR clean/sterile	Eppendorf AG, Hamburg, Germany
ep Dualfilter T.I.P.S.® 384, 0.1-2 0µl, PCR clean/sterile	Eppendorf AG, Hamburg, Germany
ep Dualfilter T.I.P.S.®, 2-10 0µl, PCR clean/sterile	Eppendorf AG, Hamburg, Germany
Eppendorf® Deepwell plates, standard, 96-wells, 1000µl	Eppendorf AG, Hamburg, Germany
epTIPS LoRetention Dualfilter, 20-300 µl, PCR clean/sterile	Eppendorf AG, Hamburg, Germany
Falcon® 14 mL Round Bottom High Clarity PP Test Tube, Graduated, with Snap Cap, Sterile	Corning Inc., USA
Falcon® 5 ml Polystyrene round bottom tube with cell strainer cap	Corning Inc., USA
FrameStar® 384 -well semi-skirted PCR plate	4titude, Surrey, UK
Injekt®-F syringe (1 ml)	Braun, Melsungen, Germany
Luna™ Cell Counting Slides	Aligned Genetics Inc., Gyeonggu-do, South Korea
Microvette® 200 Z-Gel	Sarstedt AG, Nümbrecht, Germany
Millicell® Disposable Hemocytometer	Merck-Millipore, Darmstadt, Germany
Multiply® - µStrip Pro 8-strip	Sarstedt AG, Nümbrecht, Germany
PARAFILM® M	Sigma Aldrich Chemie GmbH, Steinheim, Germany

PCR foil seal	4titude, Surrey, UK
Petri dishes (100 mm)	Greiner Bio-One GmbH, Frickenhausen, Germany
T75 Cell Culture Flask	Greiner Bio-One GmbH, Frickenhausen, Germany
Polyolefin peeling cover	HJ-Bioanalytik GmbH, Erkelenz, Germany
Polypropylene peeling cover film	Ratiolab, Dreieich, Germany
SafeSeal micro tube 1.5 ml	Sarstedt, Nümbrecht, Germany
SafeSeal micro tube 2 ml	Sarstedt, Nümbrecht, Germany
SafeSeal SurPhob Spitzen, 10 µl	Biozym Scientific GmbH, Hessisch Oldendorf, Germany
SafeSeal SurPhob Spitzen, 1250 µl	Biozym Scientific GmbH, Hessisch Oldendorf, Germany
SafeSeal SurPhob Spitzen, 20 µl	Biozym Scientific GmbH, Hessisch Oldendorf, Germany
SafeSeal SurPhob Spitzen, 200 µl	Biozym Scientific GmbH, Hessisch Oldendorf, Germany
SafeSeal SurPhob Spitzen, 300 µl	Biozym Scientific GmbH, Hessisch Oldendorf, Germany
SurPhob Spitzen EcoReload, 10 µl	Biozym Scientific GmbH, Hessisch Oldendorf, Germany
SurPhob Spitzen EcoReload, 1250 µl	Biozym Scientific GmbH, Hessisch Oldendorf, Germany
SurPhob Spitzen EcoReload, 200 µl	Biozym Scientific GmbH, Hessisch Oldendorf, Germany
SurPhob Spitzen EcoReload, 300 µl	Biozym Scientific GmbH, Hessisch Oldendorf, Germany
TubeSpin® Bioreactor 50 with Septum	TPP, Trasadingen, Switzerland
TubeSpin® Bioreactor 600	TPP, Trasadingen, Switzerland

Instruments

Product	**Source**
2100 Bioanalyzer	Agilent Technologies, Santa Clara, USA
The gentleMACS™ Octo Dissociator with Heaters	Miltenyi Biotec, USA
Automated Cell Counter Luna™	Aligned Genetics Inc., Gyeonggu-do, South Korea
Bacteria shaker Multitron Pro	Infors HT, Bottmingen, Switzerland
BD FACSAria™ III	BD Biosciences GmbH, Heidelberg, Germany
Centrifuge 5427 R (rotor FA-45-30-11)	Eppendorf AG, Hamburg, Germany
Centrifuge neoLabLine 3-1810	neoLab Migge GmbH, Heidelberg, Germany
Centrifuge Rotina 420R (rotor 4784-A)	Andreas Hettich GmbH & Co.KG, Tuttlingen, Germany
Centrifuge universal 320R (rotor 1689-A)	Andreas Hettich GmbH & Co.KG, Tuttlingen, Germany

CO_2 Incubator CB210	Binder, Tuttlingen, Germany
Compact Power Supply Owl™ EC300XL2	Thermo Scientific Inc., Rochester, NY, USA
Criterion™ cell PAGE tank	Bio-Rad Laboratories GmbH, München, Germany
Flake ice makers Flake-Line	WESSAMAT Eismaschinenfabrik GmbH, Kaiserslautern, Germany
Freedom Evo200 automation platform	Tecan, Crailsheim, Germany
Freezer MedLine (-20 °C)	Liebherr AG, Hefenhofen, Germany
Freezing container CoolCell™ FTS30	Corning Inc., USA
Fridge MedLine (4 °C)	Liebherr AG, Hefenhofen, Germany
Gel Doc™ XR+	Bio-Rad Laboratories GmbH, München, Germany
Gel Electrophoresis System Owl™ A3-1	Thermo Scientific Inc., Rochester, USA
Gel Electrophoresis System Owl™ EasyCast™ B3	Thermo Scientific Inc., Rochester, USA
Gel Electrophoresis Systems Owl™ EasyCast™ B1A Mini	Thermo Scientific Inc., Rochester, USA
Label Printer CL-S631	Citizen Systems Europe GmbH, Stuttgart, Germany
Leica CM 1950 cryostat	Leica, Wetzlar, Germany
Liquid nitrogen tank and level controller (N505CE-B)	MESSER SE & CO. KGAA, Bad Soden am Taunus, Germany and Taylor-Wharton Inc., Baytown, USA
Microplate reader infinite® M1000 pro	Tecan, Crailsheim, Germany
Microscope Primovert	ZEISS Microscopy, Oberkochen, Germany
Microwave Inverter	Sharp
Mixer Vortex-Genie® 2	Scientific Industries Inc., Bohemia, NY, USA
Multichannel pipets Research® plus 10	Eppendorf AG, Hamburg, Germany
Multichannel pipets Research® plus 100	Eppendorf AG, Hamburg, Germany
Multichannel pipets Research® plus 1200	Eppendorf AG, Hamburg, Germany
Multichannel pipets Research® plus 300	Eppendorf AG, Hamburg, Germany
Multichannel pipets xplorer® 1200, 40-1200 µl	Eppendorf AG, Hamburg, Germany
Multichannel pipets xplorer® 300, 15-300 µl	Eppendorf AG, Hamburg, Germany
Multipette® M4 pipette	Eppendorf AG, Hamburg, Germany
NanoQuant plate™	Tecan, Crailsheim, Germany
Notebook ThinkPad X1	Lenovo, Quarry Bay, Hong Kong
pH meter FiveEasy™	Mettler-Toledo GmbH, Giessen, Germany
Pipetman P1000, 100-1000 µl	Gilson S.A.S., Villiers-le-Bel, France
Pipette controller, PIPETBOY acu 2	Integra Biosciences GmbH, Fernwald, Germany
Pipette Pipetman P10, 1-10 µl	Gilson S.A.S., Villiers-le-Bel, France
Pipette Pipetman P2, 0.2-2 µL	Gilson S.A.S., Villiers-le-Bel, France
Pipette Pipetman P20, 2-20 µl	Gilson S.A.S., Villiers-le-Bel, France
Pipette Pipetman P200, 20-200 µl	Gilson S.A.S., Villiers-le-Bel, France
Precision balance PCB 1000-2	KERN & SOHN GmbH, Balingen, Germany
Safety Bench Hood Cabinet Class 2 HERAsafe KS12	Thermo Scientific Inc., Rochester, NY, USA

Thermocycler Mastercycler® epgradient S	Eppendorf AG, Hamburg, Germany
Thermocycler Mastercycler® Pro 384	Eppendorf AG, Hamburg, Germany
Thermomixer™ C	Eppendorf AG, Hamburg, Germany
Transblot SD Semi-dry Transfer Cell	BioRad Laboratories GmbH, München, Germany
Transilluminator DR-468	Clare Chemical Research, Dolores, USA
Ultra-Low Temperature Freezer (-80 °C)	Eppendorf AG, Hamburg, Germany
Vilber FUSION FX Chemiluminescence Detector	Vilber, Eberhardzell, Germany
Water bath with thermostat	Memmert GmbH + Co. KG, Schwabach, Germany
Zeiss LSM 710 ConfoCor3	Zeiss, Jena, Germany

Software and Webtools

Product	**Source**
BD FACSDiva™ software	BD Biosciences GmbH, Heidelberg, Germany
Dbeaver	https://dbeaver.io/
EndNote 21	Clarivate PLC, St. Helier, United Kingdom
FlowJo v10.7.2	Treestar Systems Inc., Ashland, USA
i-control™	Tecan, Crailsheim, Germany
Magellan™	Tecan, Crailsheim, Germany
Microsoft® Office Standard 2019	Microsoft Corporation, Redmond, USA
MySQL	Oracle Corporation, Austin, USA
NCBI IGBLAST	National Library of Medicine, Rockville Pike, USA
R version 4.3.2	RStudio, Inc., Boston USA
Rstudio version 2022.07.1+554	RStudio, Inc., Boston USA
Zen Blue 3.5 Microscopy Software	Zeiss, Jena, Germany
Qiagen IPA	Qiagen GmbH, Hilden, Germany

4 Methods

4.1 Sample Collection and Preparation

4.1.1 Sample Collection

Ovarian cancer tissue was collected from a patient with Yo-associated paraneoplastic cerebellar degeneration and an associated ovarian carcinoma from the Charité Hospital in Berlin in collaboration with Prof. Dr. Harald Prüß from the German Center for Neurodegenerative Diseases (DZNE) Berlin, Berlin, Germany. The sample was immediately placed on MACS Tissue Storage Solution at room temperature until further processing. The same procedures were done for a gastric carcinoma sample from a patient who also presented with Yo-associated paraneoplastic cerebellar degeneration, and acquired through the same collaboration

4.1.2 Tisssue Dissociation and Cryopreservation

Directly from the operating theater, the collected tissue was processed using the MACS human tissue dissociation kit (Mitenyi Biotec) and the gentleMACS™ Octo Dissociator with Heaters, a commercially available system and workflow that allows for the efficient dissociation of different tissue types into single-cell suspensions. First, the tissue was minced into 2-mm pieces. They were then transferred to the gentleMACS C Tube containing the enzyme mix (200 µL Enyzme H, 100 µL Enzyme R, 25 µL Enyme A all from the Tissue Dissociation Kit, into 4.7mL RPMI). The tube was then attached to the gentleMACS Dissociator, and the gentleMACS Program 37C_h_TDK_3 was run for the simultaneous mechanical and enzymatic digestion of the tissue. After the program, the sample was resuspended, and the suspension was applied to a 70µm MACS SmartStrainer placed above a 50mL tube. The strainer was additionally washed with 20mL of RPMI1640, and the resulting suspension was centrifuged at 300 x g, 4^{o}C for 7 minutes. Cells were then resuspended in FBS containing 10% DMSO and transferred to cryovials, which were then stored in a cooling container that was promptly transferred to a -80C freezer for cryopreservation.

4.1.3 Thawing of Cells

The cryopreserved cells were retrieved from liquid nitrogen storage and were rapidly thawed rapidly in a water bath at 37°C. Immediately after thawing, the cells were transferred to a 50-ml tube containing 30 ml of pre-warmed RPMI 1640 culture medium to dilute out the DMSO which is toxic to cells in liquid form at high concentrations. The cells were subsequently centrifuged at 400 x g, 4°C for 15 minutes. The supernatant was carefully removed and the cells were resuspended in 100 µL of FACS buffer (2% FBS in 1X PBS) and transferred to a 1.5 -mL tube. PBMC samples from healthy donor blood were thawed and processed in parallel.

4.2 Flow Cytometric Analysis

After resuspension in FACS buffer, the thawed cells were washed by filling the tube to 1 mL with FACS buffer, and centrifuging at 400 x g, 4°C for 7 mins. After centrifugation, the supernatant was removed, and the cells were resuspended in 100 µl of the staining cocktail (see Table 3 for the staining panel), and incubated for 1 hour at 4°C in the dark for immunofluorescence staining. During incubation, compensation beads were prepared by briefly pre-vortexing and subsequently adding one drop of OneComp eBeads Ultra into 1 mL of FACS buffer in a 1.5-mL tube. One tube of compensation beads was prepared for each fluorophore in the staining panel. The beads were then centrifuged at 12000 x g, 4C for 1 minute, and the supernatant was carefully removed. After washing, each compensation tube was stained with a 1:100 dilution of the respective single-color antibody from the staining cocktail panel, diluted in FACS buffer. These were incubated at 4C in the dark for 30 minutes. After incubation, the compensation beads were washed with 1mL of FACS buffer and centrifuged at 12000 x g, 4C for 1 minute. After washing, the beads were resuspended in 250 µL of FACS buffer and set aside on ice until flow cytometry analysis. After staining for 1 hour, the samples were washed with 1 mL of FACS buffer. To discriminate dead cells from live cells, the samples were subsequently stained with a 1:800 dilution of 7-amino-actinomycin D (7-AAD) diluted in FACS buffer, and was incubated in the dark at 4°C for 15 mins. After incubation with 7-AAD, the cells were washed with 1 mL of FACS buffer, and promptly resuspended in 100 µL of FACS buffer for flow cytometry analysis.

Compensation for each fluorophore was performed using each single-stained compensation beads. Right before measurement on the flow cytometer, each sample was briefly vortexed and passed through a 40-µm FACS strainer into a FACS tube. All data were acquired on the BD FACS AriaIII flow cytometer using the BD FACSDiva software. The data were analyzed using FlowJo v10.7.1 software.

Table 3. Fluorescently labeled anti-human antibodies used to analyze tumor-infiltrating lymphocytes and sort tumor-infiltrating B cells

Antibody	Fluorochrome	Clone	Source	Dilution
Anti-CD19	BV786	HIB19	BioLegend	1:10
Anti-CD20	APC-H7	2H7	BD Pharmingen	1:20
Anti-CD27	BV650	L128	BD Horizon	1:10
Anti-CD38	FITC		BD Pharmingen	1:20
7-AAD			Life Technologies	1:800
Anti-CD3	BV510	OKT3	BioLegend	1:100
Anti-IgG	BV421	HP6017	BioLegend	1:100
Anti-CD138	PE		BD Pharmingen	1:5
Anti-IgD	Alexa647	IA6-2	BioLegend	1:20
Anti-CD45	PE/Cy7	H130	BioLegend	1:100

4.3 Single-cell Sequencing and Analysis of the Ig-repertoire

4.3.1 Single-cell Index Sorting

For single-cell index sorting, the samples were stained using the same protocol described above. Approximately 10000 cells were initially acquired to establish the sort gates. The index sorting was carried out on all CD19positive B cells, pre-gated on single live cells that were CD45neg and CD3neg, using the BD FACS AriaIII flow cytometer and the BD FACSDiva software. The cells were sorted into 384-well plates containing 2 µl of the sort RHP mix (Table 4) that was pre-thawed directly before the sort, and the whole sorting procedure was maintained within 30 minutes per plate. After sorting, each plate was immediately placed on dry ice, and stored at -80°C until further processing.

Table 4. Composition of the sort mix containing random hexamer primers (RHP).

Reagent	Stock concentration	Volume (µl/well)
Nuclease free water	-	1.4813
PBS	10X	0.05
NP-40	10%	0.1375
DTT	100 mM	0.1
RNasin	40 U/µl	0.0938
RHP	300 ng/µl	0.1375
Total		2.0

4.3.2 Synthesis of cDNA by RT-PCR

Frozen 384-well sort plates (containing RHP mix) were thawed on ice and subsequently incubated at 68°C for 60 seconds. Afterward, 2 µl of an RT master mix was added to each well, and reverse transcription-PCR was carried out (Table 5). Julia Gärtner (DKFZ, Heidelberg, Germany) kindly carried out the cDNA synthesis.

Table 5. Composition of the reverse transcription (RT) mix for cDNA synthesis from single-cell derived mRNA.

Reagent	Stock concentration	Volume (µl/well)
Nuclease free water	-	0.6375
RT buffer	5 x	0.80
DTT	100 mM	0.300
dNTP	25 mM each	0.1375
RNasin	40 U/µl	0.0563
SuperScript IV	200 U/µl	0.0688
Total		2.0

Table 6. PCR program for reverse transcription of single cell derived mRNA into cDNA.

Step	Temperature	Time	Cycles
RNA denaturation	42 °C	5 mins	1
Annealing of hexamers	25 °C	10 mins	1
Reverse transcription	50 °C	60 mins	1
Final denaturation	94 °C	5 mins	1
Cooling	4 °C	-	1

4.3.3 Human immunoglobulin gene transcript amplification

After successfully transcribing the mRNA into cDNA, immunoglobulin gene transcripts were amplified by semi-nested PCR. Here, immunoglobulin genes of the heavy, kappa, and lambda loci were amplified separately in two rounds of PCR amplifications. In the first PCR, 3 µl of diluted cDNA was used as template to amplify either immunoglobulin heavy, kappa, or lambda locus genes and mixed with 7 µl of the primary PCR-reaction mixture (.). Each reaction contained a 5’ primer binding to the leader region (5´primer) and a 3`primer binding to the constant region of each corresponding locus. The forward primer contains overlapping sequences that serves as a binding site for the forward primer of the second PCR. For heavy locus encoded immunoglobulin genes, the process was done on a second plate in order to increase the yield of the PCR product. One microliter of first PCR product was used as template for the second PCR and was added to 9 µl of the secondary PCR reaction mix (Table 7). The secondary PCR primers were uniquely barcoded based on the 384-well plate column and row positions, and the unique combination of column and row barcodes were used link back each sequence to the corresponding well position after sequencing. The reverse primers used here were designed to bind to the constant region of the immunoglobulin heavy, kappa, or lambda gene. See Table 8 for PCR program of the first and second PCR. Gel electrophoresis on a 2% agarose gel was used to assess whether the heavy and light genes were successfully amplified. Immunoglobulin gene transcript amplification was kindly carried out by Julia Gärtner (Heidelberg, German Cancer Research Center).

Table 7. Composition of the first and second PCR reaction mix

Reagent (1st PCR)	Stock concentration	Volume [µl/well]
Nuclease free water	-	5.79
PCR-reaction buffer	10 x	1.0
5' primer mix	50 µM	0.0325
3' primer mix	50 µM	0.0325
dNTP-mix	25 mM each	0.10
cDNA template	-	3.0
HotStarTaq DNA Polymerase	5 U/µl	0.045
Total		10.0
Reagent (2nd PCR)	**Stock concentration**	**Volume [µl/well]**
Nuclease free water	-	5.855
PCR-reaction buffer	10 x	1.0
5' primer mix	1.67 µM	1.0
3' primer mix	1.67 µM	1.0
dNTP-mix	25 mM each	0.10
cDNA template	-	1.0
HotStarTaq DNA Polymerase	5 U/µl	0.045
Total		10.0

Table 8. Thermocycler program for the firstand secondary PCRs.

Step	**Temperature**			**Time**	**Cycles**
	Heavy	Kappa	Lambda		
Initial Denaturation	94 °C	94 °C	94 °C	15 min	1
Denaturation	94 °C	94 °C	94 °C	30 sec	50
Annealing	56 °C	50 °C	58 °C	30 sec (1° PCR)	
	60 °C	45 °C	58 °C	30 sec (2° PCR)	
Elongation	72 °C	72 °C	72 °C	55 sec (1° PCR)	
				45 sec (2° PCR)	
Final elongation	72 °C	72 °C	72 °C	10 min	1

4.3.4 Next-generation sequencing (NGS)

From each heavy, kappa, and lambda 384-well plate after the second PCR, 1 µl of the secondary DNA product was taken from each well, and were pooled together. The pooled PCR products were then purified using the NucleoSpin Gel and PCR Clean-up Kit according to the kit instructions. To further purify and isolate PCR products around the correct size range, the samples were loaded on a 4 % agarose gel which was run for 6 hours at 80 V. Bands containing the amplicons of around 400 bp were sliced out, and purified using the NucleoSpin Gel and PCR

Clean-up Kit according to the kit instructions. Afterward, the DNA concentrations and purities were measured by performing a PicoGreen measurement and by comparing the OD_{260}/OD_{280} and OD_{260}/OD_{230} ratios on obtained after measurements with the Tecan M1000 Pro plate reader. After DNA isolation and purification, 1 µg of DNA from each of the loci was ligated with adaptors using the TruSeq DNA Single Indexes Set A, and libraries were prepared using the TruSeq Nano DNA LT Library Prep Kit. To assess the efficiency of the adaptor ligation, automated capillary electrophoresis was performed using the 2100 Bioanalyzer. To measure the concentration of the purified DNA that were successfully ligated with adapters, qPCR was carried out using the KAPA Library Quant Kit. The final libraries were sent to the Functional Genomics Center, ETH Zurich, Switzerland, for Illumina MiSeq300 sequencing. The Library preparation was kindly performed by Julia Gärtner (DKFZ, Heidelberg, Germany).

4.3.5 Sequence analysis of human Ig genes

The paired-end reads received from Illumina sequencing were assembled using Pandaseq [81-84]. (Pandaseq parameters: t=0.8, maximum length=550, and minimum length = 300). PhiX sequences were then filtered out by aligning the assembled sequences to the PhiX bacteriophage genome. PhiX sequences are usually added to the libraries before sequencing to ensure a balanced composition of bases. After filtering, the sequences were processed by using the sciReptor bioinformatics analysis pipeline [85] (version 8.0.1, github.com/b-cell-immunology/sciReptor). The reads were linked back to the corresponding 384-well plate position and consensus sequences were built into contigs from the reads linked to each well. The assembled contigs were aligned using the IgBLAST tool to annotate V, D, J segments, framework regions (FRWs), constant segments, somatic hypermutations and CDR3 information [86]. Additionally, the flow cytometry index sort information, containing the flow cytometry marker intensities of each sorted cell and the metadata of the samples, were assigned to the corresponding sequences and stored in the DBeaver database. Subsequent sequence analyses and visualization were carried out using the programming language R in Rstudio (R version 4.3.2).

4.4 Ig Gene Cloning and Antibody Expression

4.4.1 Specific PCR and Purification

The specific PCR amplification of immunoglobulin genes was carried out to amplify the heavy and light genes of B cell clones of interest for subsequent gene cloning and antibody expression. A detailed pipetting scheme was prepared to facilitate the distribution of correct forward and reverse specific PCR primers corresponding to the V and J genes of the heavy and light chains of each well. All work was done under sterile RNAse-free conditions by treating all surfaces and cleaning all materials with RNase Away, DNAse Away, and ethanol prior to use. The preparation of the master mixes and distribution of primers and mixes were performed on ice. Specific PCR primers (50 µM stock) were diluted to a final concentration of 3.3 µM with nuclease-free water. A primer plate was prepared by adding 2.1 µl of each forward and reverse primer to the corresponding well. A template plate was prepared afterward by transferring 2 µl of each template from the respective 384-well plate to their assigned well on a 96-well PCR plate. The PCR master mix was then prepared (Table 9). A volume of 35.7 µl of the master mix was distributed to each well of the primer plate. From the combined mix in the primer plate, 3µl was transferred to the correponding well of the template plate. The plates were sealed and specific PCR was ran using the PCR program in (Table 10). Successful PCR amplification was assessed by agaroase gel electrophoresis. Two microliters of the PCR product pre-diluted with with 1 µl of 6X gel loading dye and 3µl of nuclease-free water. Four microliters of the mix were then loaded on a 2 % agarose gel. The expected size for IgH amplicons is ~500bp and for IgK/IgL amplicons is ~300-400bp. The PCR products were then purified using the NucleoSpin Gel and PCR Clean-up Kit and eluted with 75 µl of pre-warmed (65°C) elution buffer, with a final yield of approximately ~43 µl.

Table 9. Composition of the specific PCR mix for the amplification of Ig genes

Reagent	Volume per reaction (x 1.05) [µl]
Nuclease-free water	30.87
10 x HotStar Taq buffer	4.20
dNTPs [25µM each]	0.42
HotStar Taq	0.21
Total	35.70

Table 10. PCR program for specific PCR amplification.

Temperature	Duration	Cycles
94 °C	15 min	1
94 °C	0.5 min	50
60 °C	0.5 min	
72 °C	0.75 min	
72 °C	10 min	1
4 °C	hold	1

4.4.2 Restriction Digestion of Vectors and PCR products

Stocks of digested AbVec2.0-IGHG1, AbVec1.1-IGKC and AbVec2.1-IGLC2 vectors were first prepared by restriction enzyme (RE) digestion with the appropriate restriction enzymes (Table 11). One hundred micrograms of the vector were combined with 10X Cut-Smart buffer, 100U of each of the corresponding restriction enzymes, topped up to 400 µl with nuclease-free water. The plasmids were digested at 37^{o}C for 24 hours. After RE digestion, 25 U of calf intestinal alkaline phosphatase (CIAP) was added to the reaction mix to remove 5' end phosphate groups and prevent spontaneous relegation, and this was for 1 hour at 37 °C. Afterward, the digested plasmids were purified using the NucleoSpin Gel and PCR Clean-Up Kit, according to the kit instructions. Fifty microliters of pre-warmed elution buffer were added to each column for elution. The DNA concentration was measured on a NanoQuant Plate and the Tecan Infinite M1000 plate reader. The digested plasmids were diluted to 25ng/µl with elution buffer and stored at -20 °C in 100µl- aliquots.

The specific PCR products were subjected to RE digestion after the preparation of double RE-digested vectors. Forty microliters of the specific PCR product was mixed with 4.45 µl of 10X Cut-Smart buffer, and the corresponding volumes of restriction enzymes were added. Heavy chain amplicons were digested with 1U of AgeI-HF and 1U SalI-HF; Kappa chain amplicons with 1U AgeI-HF and 1U of BsiWI-HF; Lambda chain amplicons with 1U AgeI-HF and 1U of XhoI. These were digested overnight at 37 °C. After digestion, the digested PCR products were purified using the NucleoSpin Gel and PCR Clean-Up Kit. Each sample was eluted with 50 µL of pre-warmed elution buffer. DNA concentrations were measured on a NanoQuant Plate with the Tecan Infinite M1000 plate reader.

Table 11: Overview of RE combinations used for digestion

Plasmid / Ig locus	RE 1	RE 2
Abvec2.0 IgHG1/Heavy chain	AgeI-HF	SalI-HF
AbVec1.1-IGKC/ Kappa chain	AgeI-HF	BsiWI-HF
AbVec2.1-IGLC2/Lambda chain	AgeI-HF	XhoI

4.4.3 Ligation

The specific PCR products were ligated to the respective double-digested expression vectors. A mix of 1 µl of 10X ligation buffer, 1 µl of the corresponding double-digested vector and 0.5 µl DNA Ligase (Stock concentration: 400U/µl) was combined with 7.5µl of the specific PCR product. The ligation reaction then incubated at 16 °C overnight.

4.4.4 Transformation

The ligation reaction mixes were transformed into chemically competent E. coli DH10β by heat shock transformation. The competent cells were thawed on ice, and 10 µl of the E. coli suspension was distributed to each well of a 96-well plate. Three microliters of plasmid DNA was added to each mix and incubated for 30 minutes on ice. Heat shock transformation was performed by transferring the 96-well plate to a plate incubator at 42 °C, and was incubated for

45 sec. The samples were then immediately placed back on ice for 2 minutes. One hundred microliters of SOC medium was then added the transformation mix, and incubated at a 37 °C, shaking at 225 rpm for 60 minutes. After incubation, 100 µl of the heat-shocked bacteria were plated on the Lysogeny broth (LB) agar plates and incubated overnight at 37 °C.

4.4.5 Colony PCR

Successful insertion of the DNA into the expression plasmid and subsequent transformation into competent bacteria was assessed by colony PCR screening. Twenty-five microliters of the colony PCR master mix (Table 12) was added to each well in a 96-well plate kept on ice. Using 10 µl pipette tips, three single colonies were picked from each transformation plate. And streak-plated on an LB agar plate containing 0.1 µg/ml of ampicillin. Immediately after streak plating, each tip was dipped into corresponding wells containing the PCR mix to inoculate the remaining bacteria. The tips were allowed to stand on each well for 10 minutes and were then taken out. A PCR was then ran to amplify products correctly ligated to the corresponding expression vector (Table 13). Successful ligation and transformation were then assessed by gel electrophoresis. Two microliters of each sample were mixed with 4 µl of 1.5X loading dye, and were separated on 2 % agarose gels. The expected sizes of correctly inserted fragments are ~650 bp for the heavy-chain, and ~700 bp for the light chain.

Table 12: Colony PCR reaction mix for insert screening.

Component	Volume (µl)
Nuclease-free water	21.825
10X Qiagen Taq buffer (Qiagen)	2.500
dNTPs [25 mM each]	0.125
Forward primer (Absense) [50 µM]	0.200
Reverse primer (AbVec2.0-IGHG1: IgG-internal, AbVec1.1-IGKC: hIGKC-172-rv, AbVec2.1-IGLC2: hIGLC-057-rv) [50 µM]	0.200
Taq (Qiagen)	0.150
Total	25

Table 13. Colony PCR Program

Step	Temperature	Duration	Cycles
Initial Denaturation	94 °C	5 min	1
Denaturation	94 °C	0.5 min	27
Annealing	58 °C	0.5 min	
Elongation	72 °C	1 min	
	4 °C	hold	1

4.4.6 Sanger sequencing

Successful cloning of Sequences of DNA with correct sequences into in each expression vector was verified by Sanger sequencing. Three microliters of colony PCR products from the first colony of each sample were diluted to 15 µl with nuclease-free water, and shipped together with the Absense primer (10 µM) to Eurofins Scientific. Sequencing results were obtained and IgBLAST was ran on each resulting sequence, and compared with the respective reference sequence from the single-cell sequencing. The inserted sequences were checked for presence of stop-codons, frameshift mutations, proper alignment with the origin of replication in the plasmid, correct insert lengths of 350-380 bp, and the presence of a leader sequence. Clones with correct sequences were then identified as candidates for transfection, while the remaining colony PCR products were sent for further sequencing for samples with incorrect sequences. Candidate clones were excluded from expression in case all three colony PCR products contained no correct sequence for either of the respective Ig chain.

4.4.7 Plasmid mini preparation

Bacterial colonies with successfully cloned constructs were inoculated into 5 ml of LB medium with 0.1 µg/ml of ampicillin. The cultures were incubated overnight for 16 hours at 37°C with shaking (200 rpm). The plasmid DNA from each sample was isolated using the NucleoSpin Plasmid kit, following the manufacturer's instructions. Ethanol was further removed before elution by heating the plasmid isolation columns at 65 °C for 1 minute. Seventy-five microliters

of pre-warmed elution buffer was then used to eluted the plasmid from the column into 1.5 mL tubes. The DNA concentrations were measured using the Tecan Infinite M1000 plate reader

4.4.8 Expression of recombinant monoclonal antibodies (mAbs)

FreeStyle™ 293-F cells were seeded to a 50-mL bioreactor tubes (TPP) at a seeding density of 1.5 x 10^6 cells/ml in 5 ml FreeStyle™ 293 Expression Medium (Gibco). This was incubated in a shaker at 180 rpm, 37 °C and 8% CO2 for 24 hours before transfection. The following day, 7.5 µg of heavy and light chain plasmids were added to the cells, and the tubes were incubated in a shaker at 180 rpm, 37 °C and 8% CO2 for 5 minutes, for homogenous distribution of the DNA. After incubation, 75 µl of sterile 0.6 mg/ml polyethyleneimine (PEI), a cationic polymer that complexes with DNA and is readily endocytosed by cells, was added to each culture and incubated overnight at 37 °C, 8 % CO2 with shaking (180 rpm). The following day, 5 ml of pre-warmed serum-free EX-CELL® 293 medium containing 800 M L-glutamine was added to the cells and further incubated for 6 days in the same incubation conditions. After six days, the bioreactor tubes were centrifuged at 4000 rpm, 4 °C for 20 minutes. The supernatant was carefully transferred to a fresh 15-ml tube and stored at 4 °C until use.

4.4.9 Recombinant mAb purification

To purify the expressed mAbs for use in *in vitro* or *in vivo* assays requiring cleaner preparations of antibody, mAb purification was performed. Prior to purification, a small aliquot of the mAb supernatant was stored in a separate 1.5-mL tube. An appropriate volume of Protein G beads was then transferred to a fresh 50-mL tube, and 45 mL of 1X PBS was added to wash the beads. After washing, the beads were centrifuged at 1024 x g at 4°C for 20 minutes. The supernatant was then removed, leaving 5 mL for bead resuspension. The appropriate amount of beads were then added to each mAb supernatant, and incubated overnight at 4°C on rotating shakers. After overnight incubation, the samples were centrifuged at 1024 x g at 4°C for 20 minutes. During the centrifugation, biospin chromatography columns were equilibrated by applying 1 mL of 1X PBS, and letting it empty by gravity flow. After centrifugation, the

supernatants were removed from each sample, leaving only 1 mL to resuspend the bead pellets. This remaining volume was transferred to the pre-equilibrated column, and was allowed to run through the column. One milliliter of 1X PBS was further applied to the column to wash down the beads remaining on the column walls. Each column was then transferred on top of a collection tube containing 20 µL of 1M Tris, and samples were eluted from the column by adding 200 µL of 0.1M Glycine (pH3) to the column. This was repeated for a total of five times per sample to ensure complete elution of the sample from the column. Antibody concentrations were measured in each eluate fraction using the Tecan Infinite M1000 plate reader, and fractions with high protein concentration values were pooled for use in binding assays. After purification, the antibodies were further dialyzed in PBS using the Slide-ALyzer® Mini Dialysis Kit (Thermo Scientific) according to the manufacturer's instructions, for use in *in vivo* assays.

4.4.10 IgG Concentration Measurement

To measure the concentration of IgG's that were recombinantly expressed as mAbs, an IgG ELISA was employed, wells are coated with anti-IgG Fc antibodies to capture IgG antibodies for quantification, in a sandwich ELISA format. One day before the ELISA, wells on a 96-well clear flat-bottom plate (Corning) were coated with a 1:500 dilution of goat anti-human IgG-Fc (Jackson, JIR 109-005-098), diluted in 1X PBS. The coated plates were spun down briefly to collect the entire volume at the bottom of the well, sealed and incubated at 4^{o}C overnight. After coating, the plates were washed thrice with ddH_2O, and tapped dry, before adding 100µL of blocking buffer (0.05% Tween20 and 1 mM EDTA in 1X PBS) in each well. The plates were incubated at RT for 1 hour. During the blocking incubation period, an 8-well 2.5-fold serial dilution series of each test sample was prepared on a low-binding 96-well plate. The highest concentration in the dilution series was prepared by making 1:30 predilutions of each sample, diluted with 1X PBS. Two 8-well, 2.5-fold dilution series of the human IgG1, κ-isotype control (Sigma, I5154-1MG), were also prepared, at starting concentrations of 1 µg/ml and a 3 µg/ml, to establish standard curves for relative quantification. After the blocking step, the plates were washed thrice with ddH_2O. Fifty microliters of the samples and standards, which were prepared in the described dilution series,

were transferred to the coated 96-well plate, and incubated at RT for 1 hour. After incubation, the plates were washed thrice with ddH_2O, and 50µL of a 1:1000 dilution of HRP-conjugated mouse anti-human IgG-Fc (Jackson Immuno Research, 115-035-008) diluted in 1X PBS was added to each well, and was incubated for 1 hour. After incubation with HRP-conjugated secondary antibody, the plates were washed six times with ddH_2O, and 100 µL of H_2O_2 diluted in ABTS (1:1000) was added in each well for chromogenic development. Absorbance at 405 nm was measured using a Tecan M1000 Pro plate reader, and antibody concentrations were calculated based on the human IgG κ-isotype control standard curves.

4.5 Plate-based Immunoassays

4.5.1 Antigen ELISA

To assess reactivities to recombinant CDR2 and CDR2L antigens, antigen ELISAs were performed. Clear flat-bottom 384-well plates (Corning) were coated with 25 µL of the Yo antigens CDR2 or CDR2L, or an irrelevant antigen from chicken egg white, ovalbumin (OVA), at a concentration of 0.5 µg/mL. Plates were sealed, briefly centrifuged to ensure that the entire volume is at the bottom of the well, and stored at 4^oC overnight for coating. After overnight incubation, the coated plates were then washed with 1X PBST (0.05% Tween in 1X PBS) three times. The plates were subsequently blocked with 50 µL of blocking buffer (10% Sea Block Fish Serum in 1X PBS) and incubated for 1.5 hours at RT. During the incubation period, a 4-well 4-fold dilution series of each sample was prepared in 96-well low-binding plates, diluted in 1X PBS. Each sample was prediluted to 1 µg/mL as the highest starting dilution. After the blocking step, the plates were washed thrice with 1X PBST, and 15 µL of each sample prepared in the dilution series was added per well, and was incubated for 1.5 hours at RT. After incubation, the plates were washed thrice with 1X PBST, and 15 µL of a 1:1000 dilution of HRP-conjugated mouse anti-human IgG-Fc (Jackson Immuno Research, 115-035-008) diluted in 1X PBS was added to each well, and was incubated for 1 hour. After incubation with HRP-conjugated secondary antibody, the plates were washed six times with 1X PBST, and 20 µL of H_2O_2 diluted in ABTS (1:1000) was added in each well for chromogenic development. Absorbance at 405 nm was measured using a Tecan M1000 Pro

plate reader, and areas under the curve (AUC) from the resulting reactivity profiles were calculated in RStudio as an indirect measure of binding affinity.

4.5.2 Polyreactivity ELISA

To test for non-specific reactivity to structurally distinct antigens, polyreactivity ELISAs were performed. Clear flat-bottom 384-well plates (Corning) were coated with 25 µL per well of double-stranded DNA (dsDNA; 10 µg/mL Sigma Aldrich), insulin (5 µg/mL, Sigma Aldrich), or lipopolysaccharide (LPS; 10 µg/mL, Sigma Aldrich) diluted in 1X PBS. Plates were sealed, briefly centrifuged to ensure that the entire volume is at the bottom of the well, and stored at 4^{o}C overnight for coating. After coating, the plates were washed thrice with ddH_2O, and tapped dry. The plates were subsequently blocked with 100µL of blocking buffer (0.05% Tween20 and 1 mM EDTA in 1X PBS) in each well, and incubated for 1 hour at RT. During the incubation period, a 4-well 4-fold dilution series of each sample was prepared in 96-well low-binding plates, diluted in 1X PBS. Each sample was prediluted to 1 µg/mL as the highest starting dilution. After the blocking step, the plates were washed thrice with ddH_2O, and 15 µL of each sample prepared in the dilution series was added per well, and was incubated for 1 hour at RT. After incubation, the plates were washed thrice with ddH_2O, and 15 µL of a 1:1000 dilution of HRP-conjugated mouse anti-human IgG-Fc (Jackson Immuno Research, 115-035-008) diluted in 1X PBS was added to each well, and was incubated for 1 hour. After incubation with HRP-conjugated secondary antibody, the plates were washed six times with ddH_2O, and 20 µL of H_2O_2 diluted in ABTS (1:1000) was added in each well for chromogenic development. Absorbance at 405 nm was measured using a Tecan M1000 Pro plate reader, and areas under the curve (AUC) from the resulting reactivity profiles were calculated in RStudio as an indirect measure of binding affinity.

4.5.3 High-sensitivity cross-linking ELISA

To assess reactivities with higher sensitivity and be able to identify weak-binding antibodies, a high-sensitivity cross-linking ELISA was performed. In this assay, primary test antibodies are pre-complexed with secondary antibodies to allow for higher avidity-based recognition of coated wells, leading to greater sensitivity to detect weak-binding mAbs. Clear flat-bottom 384-well plates (Corning) were coated with 25 µL of recombinant CDR2 or CDR2L. Plates were sealed, briefly centrifuged to ensure that the entire volume is at the bottom of the well, and stored at 4^{o}C overnight for coating. After overnight incubation, the coated plates were then washed with ddH_2O six times. The plates were subsequently blocked with 50 µL of blocking buffer (10% Sea Block Fish Serum in 1X PBS) and incubated for 1.5 hours at RT. During the incubation period, each sample was prediluted to 1 µg/mL with 1X PBS containing 1% BSA, and was combined with an equal volume of a 1:1000 dilution of HRP-conjugated mouse anti-human IgG-Fc (Jackson Immuno Research, 115-035-008) diluted in 1X PBS with 1% BSA. This primary – secondary antibody mixture was allowed to complex in a low-binding 96-well plate for 1 hour at RT. After the blocking step, the plates were washed six times with ddH_2O, and 15 µL of each the pre-complexed primary-secondary antibody mixture was added to each well, and was incubated for 1 hour at RT. After incubation, the plates were washed six times with ddH_2O, and 20 µL of H_2O_2 diluted in ABTS (1:1000) was added in each well for chromogenic development. Absorbance at 405 nm was measured using a Tecan M1000 Pro plate reader, and single-well OD readings were taken as an indirect measure of binding avidity.

4.5.4 Blocking ELISA

To be able to assess whether two antibodies share the same epitope on recombinant CDR2 and CDR2L antigens, a variation of a competitive ELISA, termed blocking ELISA was performed. In this assay, un unlabeled antibody is applied to the coated antigen, and a biotinylated antibody is sequentially added. Shared epitope specificities would render the second biotinylated body blocked from its binding site by the first unlabeled antibody, leading to attenuated signal upon addition of HRP-conjugated streptavidin (BD Biosciences). Biotinylation of mAbs was done using the EZ-Link® NHS-Biotinylation protocol, following the manufacturer's

instructions. Clear flat-bottom 384-well plates (Corning) were then coated with 25 µL of recombinant CDR2 or recombinant CDR2L at a concentration of 0.5 µg/mL. Plates were sealed, briefly centrifuged to ensure that the entire volume is at the bottom of the well, and stored at 4^{o}C overnight for coating. After overnight incubation, the coated plates were then washed with 1X PBST (0.05% Tween in 1X PBS) three times. The plates were subsequently blocked with 50 µL of blocking buffer (10% Sea Block Fish Serum in 1X PBS) and incubated for 1.5 hours at RT. During the incubation period, an 8-well 2-fold dilution series of the unlabeled mAb was prepared in 96-well low-binding plates, diluted in 1X PBS. Each sample was prediluted to 64 µg/mL as the highest starting dilution. After the blocking step, the plates were washed thrice with 1X PBST, and 15 µL of each unlabeled sample prepared as a dilution series, was added per well, and was incubated for 1.5 hours at RT. After the 1.5-hour incubation period, and without washing, 8µg of the biotinylated antibody was added to the each well, and was incubated for an additional 15 minutes. After incubation, the plates were washed thrice with 1X PBST, and 15 µL of a 1:1000 dilution of HRP-conjugated streptavidin (BD Biosciences) diluted in 1X PBS was added to each well, and was incubated for 1 hour. After incubation with HRP-conjugated streptavidin, the plates were washed six times with 1X PBST, and 20 µL of H_2O_2 diluted in ABTS (1:1000) was added in each well for chromogenic development. Absorbance at 405 nm was measured using a Tecan M1000 Pro plate reader, and areas under the curve (AUC) from the resulting reactivity profiles were calculated in RStudio as an indirect measure of the extent of blocking by the blocking antibody.

4.6 Immunoprecipitation Assays and Western Blot

4.6.1 Maintenance of OvCar3 cells

OvCar3 cells were expanded and maintained for immunoprecipitation experiments. OvCar3 cells were maintained at 37°C, 5% CO_2 in OvCar3 medium (RPMI 1640, 20% FBS, 1% Pen-strep, 1% L-glutamine, 0.01 mg/mL insulin). Cells were seeded at a seeding density of 0.5 x 10^6 cells/mL in a T75 culture flask (Greiner), and filled to 6mL with OvCar3 medium. When 80% confluence is reached, cells were subcultured by removing the OvCar3 medium, and washing the cells carefully with 6 mL of sterile 1X PBS. After washing, 1X PBS was removed, and 6 mL of trypsin-EDTA solution (Sigma Aldrich) was added. The flask was incubated in the incubator at 37°C for 2 minutes. After incubation, the sides of the flask were gently tapped to completely detach the cells, and 6 mL of OvCar3 medium was added to deactivate the trypsin. The entire volume was transferred to a 15-mL tube, and centrifuged at 500 x g for 5 minutes. After centrifugation, the supernatant was removed, and the cells were resuspended in 2 mL of OvCar3 medium. A cell count was performed using the Luna™ automated cell counter, and cells were reseeded at a seeding density of 0.5 x 10^6 cells/mL, onto a fresh T75 culture flask containing 6 mL of OvCar3.

4.6.2 RIPA Lysis Extraction of OvCar3 Lysates

RIPA (RadioImmunoPrecipitation Assay) buffer is a lysis buffer that contains a combination of detergents (such as Triton X-100 or NP-40), salts, commonly used for cell lysis. To extract the cytoplasmic content of OvCar3 cells, RIPA lysis was performed. RIPA buffer was supplemented with protease inhibitors by adding one tablet of cOmplete™, Mini Protease Inhibitor Cocktail (Sigma Aldrich) to 10 mL of RIPA buffer. Medium was removed from T75 flasks containing OvCar3 cells at 90% confluence, and was carefully washed with 1X PBS. PBS was removed, and 350 µL of RIPA was added to the flask. The flask was incubated on ice for 15 minutes, with occasional swirling to ensure the even distribution of RIPA buffer. After incubation, the cells were mechanically detached by scraping with a pre-chilled cell scraper. The detached lysates were promptly transferred to a 1.5 mL tube, and centrifuged at 12000 x g for 30 minutes

to clarify the lysate. After centrifugation, the clarified lysate was transferred to a fresh 1.5 mL tube. BCA quantification of the protein amount was carried out using the Pierce™ BCA Protein Assay Kits, following the manufacturer's instructions. Lysates were stored at -80 ^{o}C until use.

4.6.3 Immunoprecipitation of OvCar3 Lysates

To detect mAb specificity against antigens in their native state, immunoprecipitation against OvCar3 lysates were performed. OvCar3 lysates were first pre-incubated with the immunoprecipitating antibody (IP Ab) by adding 1 µg of the IP Ab to 500µg of OvCar3 lysate. This was incubated in a rotating shaker for 5 hours at 4^{o}C. Fifteen microliters of pre-washed Protein G Sepharose 4 Fast Flow beads were then added to each sample, and further incubated in a rotating shaker at 4^{o}C overnight. After incubation, the samples were centrifuged for 30 seconds at 4^{o}C, 2000 rpm, and the supernant was subsequently removed. The pellet was washed three times with 500 µL of RIPA buffer, and resuspended in 40 µL of RIPA buffer supplemented with protease inhibitors.

4.6.4 Western Blot Assay of IP Products

To detect whether CDR2 and CDR2L were immunoprecipitated by the immunoprecipitating mAbs, a western blot assay was performed. Lämmli denaturing buffer was added to the immunoprecipitated samples to make a 1X Lämmli solution. These were then heated for 10 minutes at 95^{o}C. During incubation, an 8-16% gradient pre-cast PAGE gel (Bio Rad) was assembled onto the PAGE tank, and filled with 1X SDS Running buffer. After incubation, the heated samples were centrifuged at 400 rpm at RT for 1 minute. The supernatant was directly loaded on the PAGE gel, alongside the Color Prestained Protein Standard (NEB). The gel was run at 120V for 3.5 hours to achieve good size resolution of proteins between 25-75 kDA. During the PAGE run, PVDF membrane was activated by soaking in methanol for 1 minute, rinsing in distilled water, and transferring in Transfer Buffer (48 mM Tris base, 39 mM glycine, 20 % methanol). After the run, the PAGE gel was carefully removed from the cassette and casing, and assembled

into the transfer sandwich. The transfer sandwich was assembled, by placing the PVDF membrane on top of six pre-cut Whatman papers. The PAGE gel was then carefully placed on top of the PVDF membrane, finally topped with six more pre-cut Whatman papers to complete the sandwich. Bubbles were gently rolled out of the the transfer sandwich was then, was placed on the Transblot SD Semi-dry Transfer Cell. The blot was run at 10V constant voltage for up to 45 minutes. After the blot, the membrane was carefully taken out, and blocked with 5% skimmed milk in PBST (0.05% Tween20 in 1X PBS). This was incubated for 1 hour at RT. After blocking, the blots were incubated with 5mL of rabbit anti-CDR2 (Sigma Aldrich) or rabbit anti-CDR2L (Sigma Aldrich) primary antibodies at 1:500 dilutions, diluted in PBST with 5% BSA, overnight at 4^{o}C with gentle rotation. After primary antibody incubation, the membrane was washed thrice in PBST, incubating for 5 minutes with gentle rotation per wash. After washing, 10mL of anti-rabbit HRP-conjugated secondary antibody, diluted to 1:10000 with PBST was then added, and incubated for 1 hour at RT. After incubation, the membrane was washed thrice in PBST. A freshly prepared a 1:1 mixture of Pierce ECL Detection Reagent 1 and 2 was then added drop-wise to the blot. The blot was then imaged on the Vilber FUSION FX Chemiluminescence Detector using the Captain Edge software. To confirm that the heavy chain of the immunoprecipitating antibody emitted faint non-specific signals, the membrane was incubated with mild stripping buffer (25 mM glycine-HCl, 1% SDS, pH2.3) with shaking, at RT for 10 minutes. The buffer was decanted and fresh stripping buffer was added, and incubated with shaking at RT for 10 minutes. The membrane was subsequently washed twice with 1X PBS, 10 minutes per wash. The membrane was washed further with PBST three more times, 5 minutes per wash. The membrane was then re-probed with HRP-conjugated anti-human IgG-Fc (Jackson Immuno Research, 115-035-008) for 1 hour at RT. The same procedure was then followed with the WB Captain Edge software and Vilber FUSION FX Chemiluminescence Detecto for WB imaging.

4.6.5 Western Blot Assay of Linear Epitopes

To assess whether expressed mAbs can detect linear epitopes on recombinant CDR2 and CDR2L, a western blot assay was carried out using generated mAbs as detection antibodies. Lämmli denaturing buffer was added to 0.13µg of recombinant CDR2 or CDR2L, and was diluted in RIPA buffer to a final volume of 25 µL. These were then heated at 95^{o}C for 10 minutes. During incubation, an 8-16% gradient pre-cast PAGE gel (Bio Rad) was assembled onto the PAGE tank, and filled with 1X SDS Running buffer. The same PAGE running procedure and Western Blotting procedure was carried out as in the Western Blot – IP protocol. The blots were then blocked with 5% skimmed milk in PBST (0.05% Tween20 in 1X PBS), and incubated for 1 hour at RT. After blocking, 5mL of of mAbs (5 µg/mL), diluted in PBST with 5% BSA were added to the blot, and incubated overnight at 4^{o}C with gentle rotation. After primary antibody incubation, the membrane was washed thrice in PBST, incubating for 5 minutes with gentle rotation per wash. After washing, 10mL of anti-human IgG HRP-conjugated secondary antibody (Jackson Immuno Research, 115-035-008) diluted to 1:10000 with PBST was then added, and incubated for 1 hour at RT. After incubation, the membrane was washed thrice in PBST. A freshly prepared a 1:1 mixture of Pierce ECL Detection Reagent 1 and 2 was then added drop-wise to the blot. The blot was then imaged on the Vilber FUSION FX Chemiluminescence Detector using the Captain Edge software.

4.7 Mass Spectrometry

To identify potential binding partners of the cognate antigen targeted by the mAbs, mass spectrometry (MS) was performed by the Genomics and Proteomics Core Facility (GPCF) of the German Cancer Research Center (DKFZ), Heidelberg. Immunoprecipitated products from lysates of OvCar3 cells using one of the high-binding monoclonal antibodies, and immunoprecipitated products from OvCar3 lysates treated with empty Sepharose G beads, were sent to the GPCF for Mass Spectrometry. Subsequent processing of the MS results, and a list of immunoprecipitated proteins and their associated p-values and peptide quantifications were provided by Martin

Schneider from the GPCF. A basic analysis of potential protein networks formed by the identified proteins was done using the Qiagen IPA software.

4.8 Surface Plasmon Resonance

To measure the fine affinities of monoclonal antibodies to recombinant CDR2 and CDR2L, Surface Plasmon Resonance was carried out in cooperation with Opeyemi Ernest Oludada, German Cancer Research Center. The method has been previously employed and described in detail in his published study [87].

4.9 Immunofluorescence Assays and Confocal Microscopy

4.9.1 Immunofluorescence staining of OvCar3 cells

To assess the subcellular localization of targets of expressed mAbs, immunostaining on fixed permeabilized OvCar3 sections was carried out. Four-well chamber slides (Thermo Fischer) were seeded with 20,000 OvCar3 cells per well in 500 µL of OvCar3 medium. Two days after seeding, the media was taken out and the cells were washed with 200 µL of PBS. Four-hundred microliters of freshly-prepared 2% paraformaldehyde in 1X PBS was then added per well, and incubated for 15 minutes at RT for fixation. After fixation, the wells were washed thrice with 200 µL of 1X PBS, incubating for 5 minutes per wash. The PBS was then taken out, and the cells were permeabilized with 100 µL of 0.1% Saponin, and incubated for 5 minutes. This stepped was skipped staining in unpermeabilized conditions. After permeabilization, the cells were washed thrice with 200 µL of PBS, incubating for 5 minutes per wash. The fixed permeabilized cells were then blocked with 10% SeaBlock in 1X PBS for 30 minutes at RT. After blocking, the cells were washed thrice with 1X PBS, incubating for 5 minutes per wash. Monoclonal antibodies were then added as primary antibodies at a concentration of 5 µg/mL, diluted in antibody dilution buffer (5%, 0.25% Tween20, diluted in 1X PBS). This was incubated for 1.5 hours at RT. After primary antibody incubation, the cells were washed thrice with 1X PBS. Subsequent steps were then carried out in the dark. Two hundred microliters of AF488-conjugated anti-human IgG secondary

antibody, diluted to 1:250 with dilution buffer was then added to each well, and was incubated for 1.5 hours at RT. The cells were then washed thrice, and the walls of the 4-well chamber that partitioned the cells on the slide were detached from the slide. The slide with fixed permeabilized and stained cells was then mounted with two drops of VectaShield DAPI. A cover slip was layered over the slides, and sealed with nail polish. Imaging of the slides was done on the Zeiss LSM 710 ConfoCor3 confocal microscope, and image analysis was performed using the Zeiss Zen Blue 3.5 software.

4.9.2 Immunofluorescence staining of Primary Ovarian Carcinoma Sections

To assess the whether mAbs will recognize antigens expressed in ovarian carcinomas that is not associated with any neurological disorders, cryosections of primary ovarian carcinoma sections from a neurologically normal patient was obtained from the NCT Tissue Bank, Heidelberg, Germany (Antragsnummer: 190089) and stored at -80°C.

On the day of the experiment, cryosections were equilibrated at RT for 30 minutes. They were then rehydrated by dipping in ddH_2O, and briefly allowed to dry. A circular perimeter around the carcinoma section was marked with a hydrophobic barrier pen to prevent solutions applied to the cryosections from spilling out of the area of interest. The slides were then fixed with 2% formaldehyde diluted in 1X PBS and incubated for 10 minutes at RT. After fixation, the slides were washed with 1X PBS+ (BioCare Medical), a 1X PBS solution supplemented with calcium and magnesium ions, always incubating for 5 minutes in between washes. The cryosections were then permeabilized by adding 75 µL of 0.5% Triton-X 100 diluted in 1X PBS, and was incubated for 5 minutes. The slides were washed three times with 1X PBS+. The slides were the blocked with 75 µL Blocking Solution (2% BSA and 5% goat serum in 1X PBS), and incubated for 1 hour at RT. After blocking, the slides were gently tapped on a paper towel to remove excess solution, and were washed thrice with 1X PBS+. After incubation, 75 µL of mAb diluted to 5 µg/mL in blocking solution was applied to the cryosections, and incubated overnight at 4^{o}C. Slides were enclosed in a light-proof container and surrounded with moist paper towels to prevent drying of the primary antibody solution. After incubation, the slides were dipped in ddH_2O, washed thrice with 1X PBS+, and dipped in ddH_2O for a final wash before the application of secondary antibody. Subsequent steps were done in the dark. AlexaFluor488-conjugated anti-human IgG was diluted 1:500 with

5% goat serum in 1X PBS, and 75 µL was applied to the cryosection and incubated for 1.5 hours at RT. After secondary antibody staining, the slides were washed with 1X PBS+, and dipped in ddH_2O. Excess water from the slides were removed by gently dabbing the slides on a paper towel. The slides were then mounted with two drops VectaShield DAPI. A cover slip was layered over the slides, and sealed with nail polish. Imaging of the slides was done on the Zeiss LSM 710 ConfoCor3 confocal microscope, and image analysis was performed using the Zeiss Zen Blue 3.5 software.

4.9.3 Immunofluorescence staining of Rat Cerebellar Sections

To assess the binding of mAbs to antigens expressed by Purkinje cells in the rodent cerebellum, the mAbs were applied to rat cerebellar sections for immunofluorescence assays. Frozen whole brains from Sprague-Dawley rats in TissueTekt were obtained as a kind gift from Dr. Christin Glowa (German Cancer Research Center, Heidelberg). Prior to the experiment, transverse 8 µM cryosections of the cerebellum were prepared on glass microscope slides using the Leica CM 1950 cryostat, and were stored at -80°C. On the day of the experiment, cryosections were equilibrated at RT for 30 minutes. They were then rehydrated by dipping in ddH_2O, and briefly allowed to dry. A circular perimeter around the transverse section was marked with a hydrophobic barrier pen to prevent solutions applied to the cryosections from spilling out of the area of interest. The slides were then fixed with 2% formaldehyde diluted in 1X PBS and incubated for 10 minutes at RT. After fixation, the slides were washed with 1X PBS+ (BioCare Medical), a 1X PBS solution supplemented with calcium and magnesium ions, always incubating for 5 minutes in between washes. The cryosections were then permeabilized by adding 75 µL of 0.5% Triton-X 100 diluted in 1X PBS, and was incubated for 5 minutes. The slides were then washed three times with 1X PBS+. Subsequently after washing, the slides were the blocked with 75 µL Blocking Solution (2% BSA and 5% goat serum in 1X PBS), and incubated for 1 hour at RT. After blocking, the slides were gently tapped on a paper towel to remove excess solution, and were washed thrice with 1X PBS+. After incubation, 75 µL of mAb diluted to 5 µg/mL in blocking solution was applied to the cryosections, and incubated overnight at 4°C. Anti-calbindin (Thermo Fisher Scientific) were also used as a positive control for Purkinje cell staining. Slides were enclosed in a

light-proof container and surrounded with moist paper towels to prevent drying of the primary antibody solution. After incubation, the slides were dipped in ddH_2O, washed thrice with 1X PBS+, and dipped in ddH_2O for a final wash before the application of secondary antibody. Subsequent steps were done in the dark. AlexaFluor488-conjugated anti-human IgG was diluted 1:500 with 5% goat serum in 1X PBS, and 75 µL was applied to the cryosection and incubated for 1.5 hours at RT. After secondary antibody staining, the slides were washed with 1X PBS+, and dipped in ddH_2O. Excess water from the slides were removed by gently dabbing the slides on a paper towel. The slides were then mounted with two drops VectaShield DAPI. A cover slip was layered over the slides, and sealed with nail polish. Imaging of the slides was done on the Zeiss LSM 710 ConfoCor3 confocal microscope, and image analysis was performed using the Zeiss Zen Blue 3.5 software.

4.9.4 Immunofluorescence staining of Mouse Cerebellar Sections

Immunofluorescence staining of mouse cerebellar sections were performed by Dr. César Cordero-Gomez from the German Center for Neurodegenerative Diseases (DZNE) Berlin, Berlin, Germany and by Prof. Dr. Markus Höltje from the Institute of Integrative Neuroanatomy in Charité, Berlin, Germany in independent collaborations, using established protocols in their respective laboratories [88]; [89]. Purified, dialyzed monoclonal antibodies were shipped to their respective institutions in dry ice.

4.9.5 Immunofluorescence staining of Primary Purkinje cells

Immunofluorescence staining of mixed cerebellar primary cultures containing purkinje cells and established from embryonic mouse brain, were performed by Prof. Dr. Markus Höltje from the Institute of Integrative Neuroanatomy in Charité, Berlin, Germany, through a collaboration. Purified, dialyzed monoclonal antibodies were shipped to their institution in dry ice. Monoclonal antibodies, diluted to 5 µg/mL, were applied either on fixed and permeabilized cerebellar primary cultures, to confirm quality of Purkinje cell binding, or were applied in the

same concentration to the media of the cerebellar primary cultures and incubated for 24 hours, to assess uptake of the mAbs by Purkinje cells.

4.10 *In vivo* Intrathecal mAb Delivery and Motor Assays

Intrathecal delivery of monoclonal antibodies and subsequent motor dysfunction analysis by rotarod assays were performed by Dr. César Cordero-Gomez in collaboration with Prof. Dr. Harald Prüß from the German Center for Neurodegenerative Diseases (DZNE) Berlin, Berlin, Germany. Monoclonal antibodies are intrathecally delivered directly to the CNS through the surgical implantation of monoclonal antibody-containing osmotic pumps, and has been described in detail in their published study [50]. Latency time to stay and balance on a rotating rod were then measured as a readout of motor function. Four mice per treatment group were evaluated, and mGO53 was intrathecally delivered as a control antibody.

4.11 Statistical Analysis

Data analysis was carried out using RStudio (version 4.2.1). Plots were generated using the ggplot2 package in R, and stastical analysis using non-parametric tests were carried out using the ggsignif package. P-values where applicable (*P < 0.05; **P < 0.01; ***P < 0.001) are indicated in the graphs and figure legends.

5 Results

5.1 Tumors from Patients with Yo-associated Paraneoplastic Cerebellar Degeneration

5.1.6 Tissue preparation of Yo-associated Tumors into Single-cell Suspension

A

Patient	Diagnosis	Associated Cancer	Samples Available
1	Yo-PCD	Ovarian Carcinoma	Tumor
2	Yo-PCD	Gastric Carcinoma	Tumor

B

C

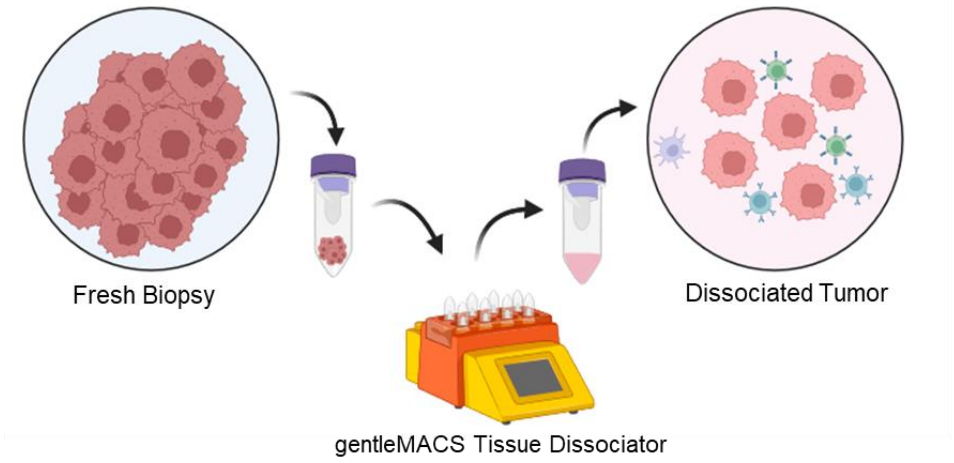

Figure 4. Sample overview and preparation of Yo-associated tumors into single-cell suspensions. A) Summary of tumor samples collected from patients with Paraneoplastic Cerebellar Degeneration. B) Ovarian carcinoma biopsy from patient 1, collected fresh from the surgery room. C) Experimental workflow to obtain single-cell suspensions from patient-derived tumor biopsies.

Fresh tumor biopsies were collected from two patients through a collaboration with Prof. Dr. Harald Prüß from the Center of Neurodegenerative Diseases in Berlin. These patients were diagnosed with Yo-associated Paraneoplastic Cerebellar Degeneration, and co-presented with tumors (Figure 4A). Patient 1 had an associated ovarian carcinoma that presented with their neurological complications (Figure 4B), and Patient 2 had a co-occurring gastric carcinoma. A

biopsy from each tissue was promptly collected during the scheduled surgical removal, and I immediately processed the samples into single-cell suspension (Figure 4C).

5.1.7 Single-cell suspensions from Yo-associated tumors have varied viabilities

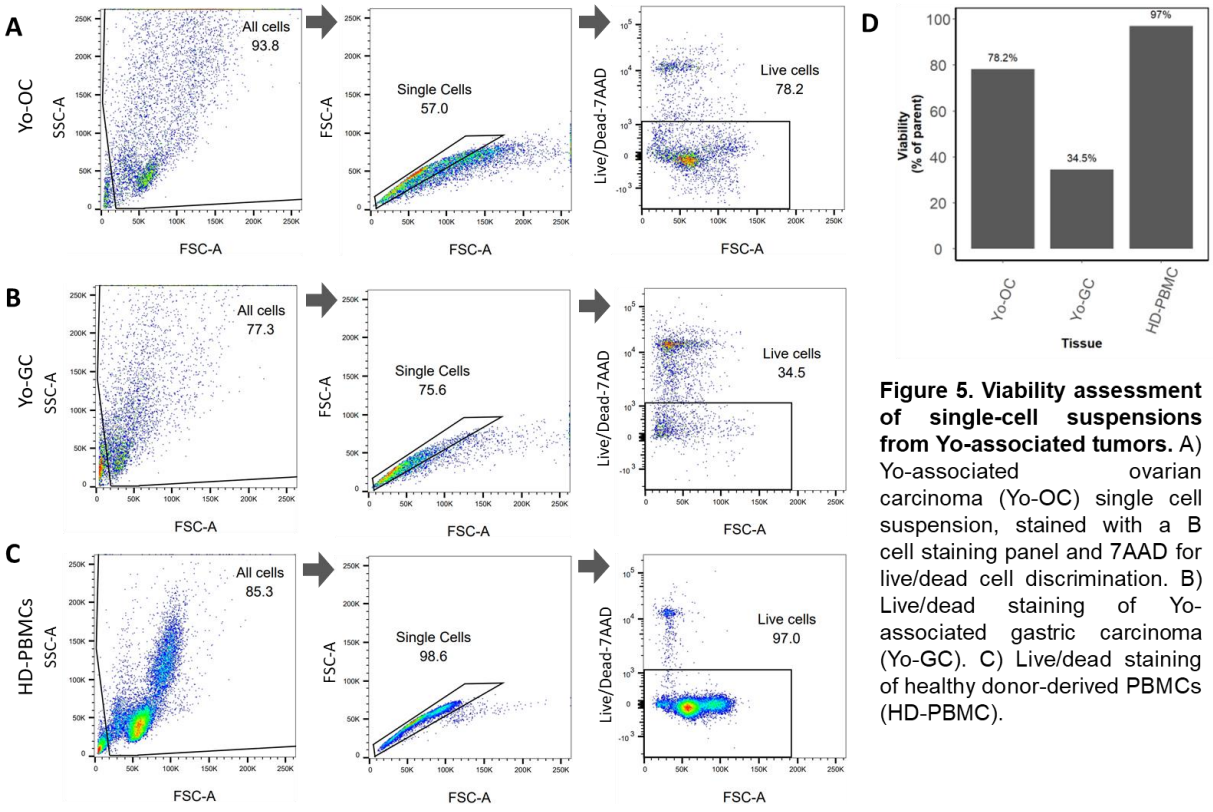

Figure 5. Viability assessment of single-cell suspensions from Yo-associated tumors. A) Yo-associated ovarian carcinoma (Yo-OC) single cell suspension, stained with a B cell staining panel and 7AAD for live/dead cell discrimination. B) Live/dead staining of Yo-associated gastric carcinoma (Yo-GC). C) Live/dead staining of healthy donor-derived PBMCs (HD-PBMC).

To assess the viability of the cells isolated from each of the tumor biopsies, I stained the collected samples with a B cell panel that included a viability marker 7-AAD, which stains for DNA on all non-viable cells via perfusion through their leaky plasma membrane (Figures 5A and 5B). I also stained Peripheral Blood Mononuclear Cells (PBMCs) isolated from a healthy donor unrelated to the study with the same panel for comparison (Figure 5C), and analyzed them by flow cytometry. The viability of the cells isolated from each of the tumor samples varied greatly. The ovarian carcinoma biopsy obtained from the patient with Yo-associated Paraneoplastic Cerebellar Degeneration, hereafter referred to as Yo-OC, had a viability of 78.2%, while the biopsy from the patient with gastric carcinoma, subsequently referred to as Yo-GC, had a much lower viability at 34.5% (Figure 5D). The viability of PBMCs from the healthy donor, concurrently

stained with the tumor samples, remained high at 97%, insinuating that the lower viability of the tumor samples was related to the conditions during collection and processing, and not during downstream handling.

5.1.8 Yo-associated tumors are infiltrated by B and T cells

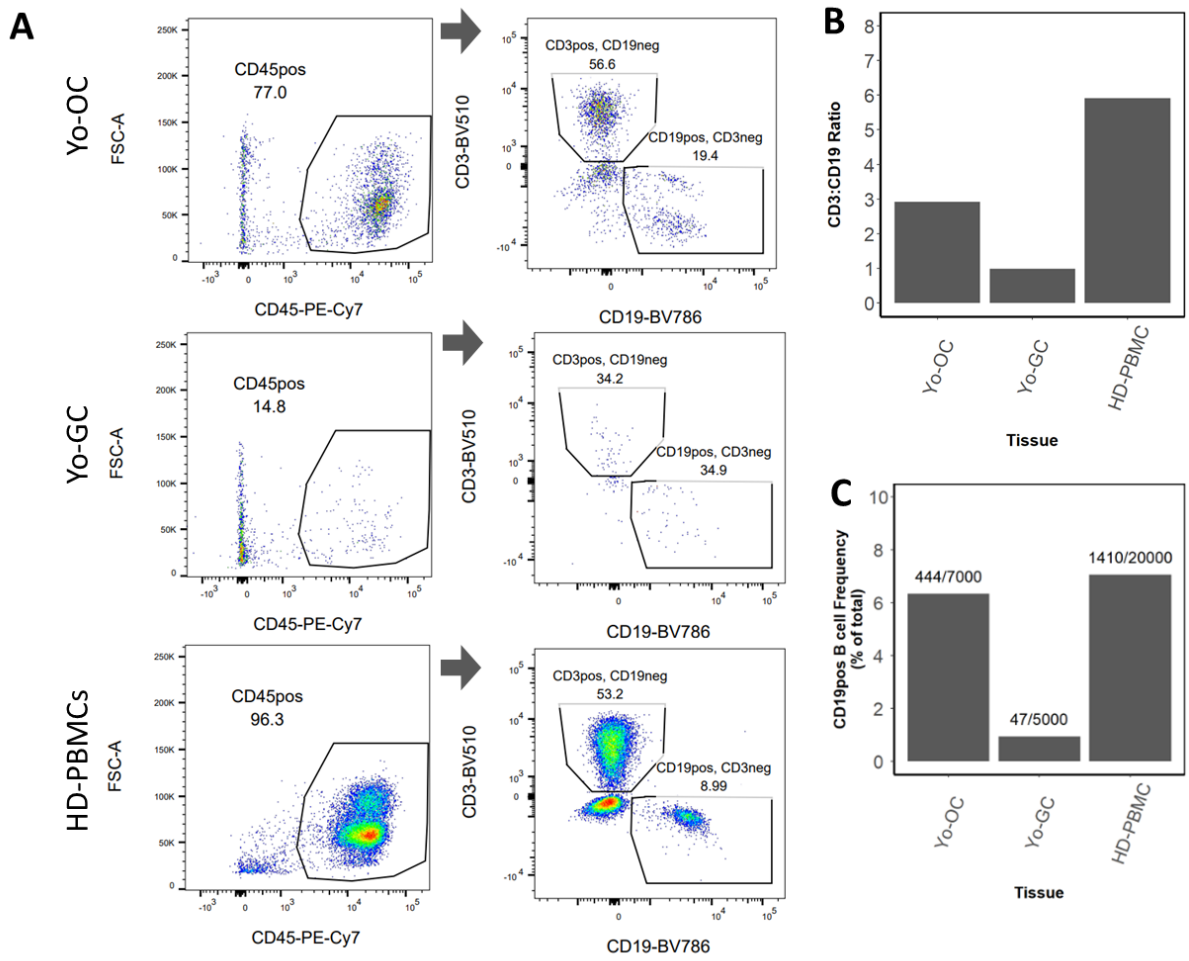

Figure 6. Determination of Yo-tumor-infiltrating immune cell numbers by flow cytometry. A) CD3 and CD19 staining on lymphocytes across tissues, gated on viable (7AADneg), CD45-positive cells. B) CD3pos T cell to CD19pos B cell ratios calculated from the CD3pos and CD19pos lymphocyte frequencies. C) Quantification of CD19pos B cell counts over total number of cells analyzed per sample.

To determine if Yo-associated tumors are infiltrated by lymphocytes and to what extent, I examined the frequencies of CD3-positive T cells and CD19-positive B cells isolated from the tumor (Figure 6A). The CD3-positive T cells and CD19-positive B cells were pre-gated on CD45-positive, viable (7AADneg) cells. I determined the relative proportions of T cells to B cells from each sample, by getting ratios of CD3-positive to CD19-positive cells among the CD45-positive lymphocytes. The ratio of T- to B cells in the Yo-OC sample and the Yo-GC were 2.91 and 0.98 respectively (Figure 6B). The healthy donor PBMCs had a ratio of 5.92 – at least three-fold higher than the T- to B cell ratios in Yo tumor samples. I also calculated the CD19-positive B cell frequencies compared to the total number of cells recorded per sample. For the Yo-OC tumor, B cell frequencies were comparable to the B cell frequencies recorded from the healthy donor, at 6.34% in the Yo-OC tumor compared to 7.0% from the healthy donor PBMCs (Figure 6C). The number of B cells were much lower for the Yo-GC sample, at 0.94%. The similar frequencies of B cells between the Yo-OC tumor and healthy PBMCs imply that the difference in the T- to B cell ratios between the two samples could be because of less T cells infiltrating the Yo-OC compared to healthy donor blood. Across the board, T-B ratios and B cell frequencies were lowest for the Yo-GC sample, which was also the sample with the much lower viability.

5.1.9 Antibody-secreting cells predominate the humoral response in Yo-tumors

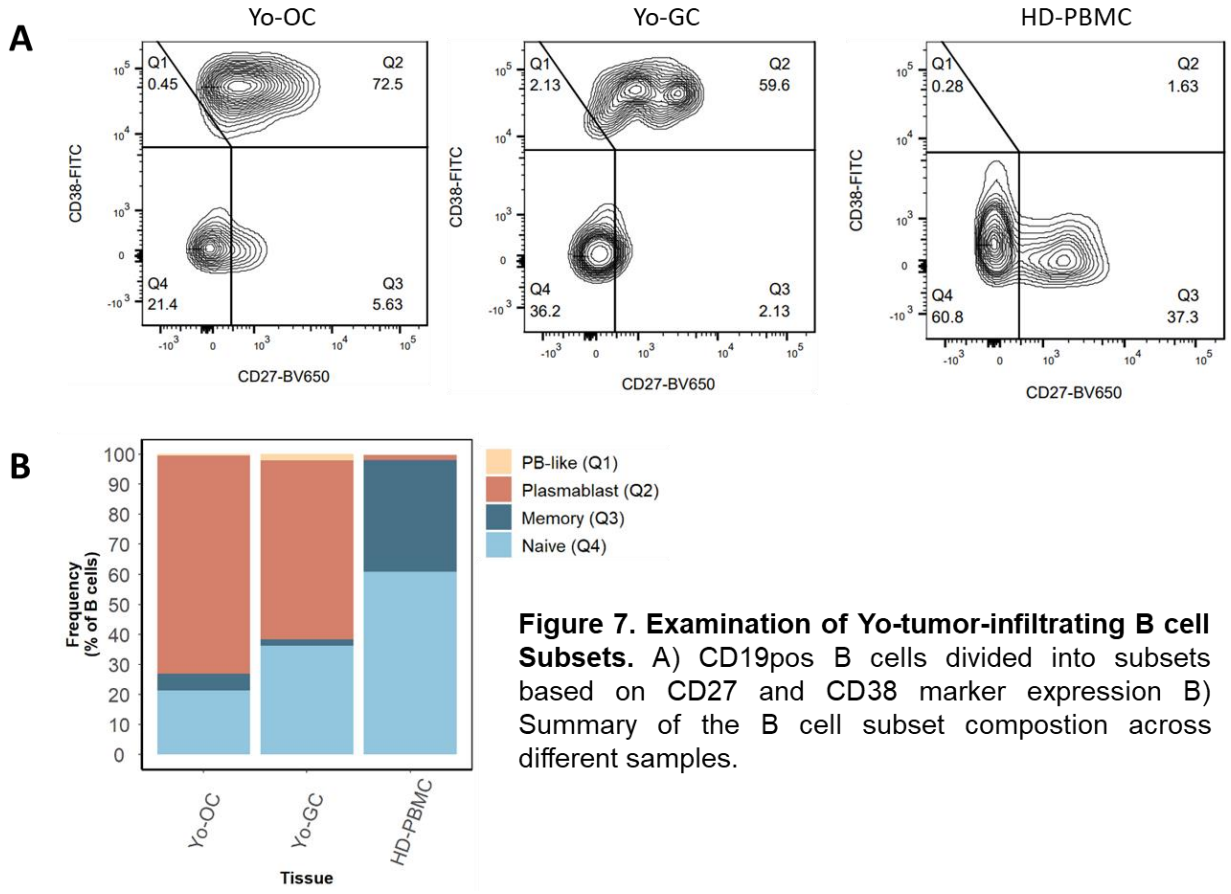

Figure 7. Examination of Yo-tumor-infiltrating B cell Subsets. A) CD19pos B cells divided into subsets based on CD27 and CD38 marker expression B) Summary of the B cell subset compostion across different samples.

To determine the subsets that comprise the CD19-positive B cell population in the Yo-tumor samples, I classified the CD19-positive B cells based on their CD27 and CD38 expression. CD27 is typically a marker for memory B cells and is essential for their maintenance, while high levels of CD38 indicate activation, and the combination of the two can broadly discriminate between most major B cell subsets. B cells highly-expressing CD38, and were positive for CD27 were classified into the plasmablast subset (Q2), which represents antibody-secreting cells that have been activated but have not terminally differentiated into plasma cells. Absence of the plasma cell marker CD138 in this subset (Supplementary Figure 1.) confirms their plasmablast

phenotype. An adjacent subfraction of cells (Q1) was termed plasmablast-like (PB-like). These few cells cluster with the CD27pos CD38hi plasmablasts signifying their antibody-secreting phenotype, but remained below the threshold for CD27 expression to be strictly classified as plasmablasts. Similar to the plasmablast subset (Q2), these plasmablast-like cells (Q1) highly express CD38, and were negative for IgD expression, (Supplementary Figure 2.) indicating that they have undergone a similar course of activation.

B cells that were positive for CD27 but do not express CD38 were defined as the memory B cell subset (Q3), while B cells that were negative for both markers were designated as naïve B cells (Q4), further confirmed by the retention of IgD expression in majority of the cells in this subpopulation (Supplementary Figure 3.). In both Yo-associated tumor samples, B cells were predominantly of the plasmablast phenotype, comprising as much as 72.5% of B cells in the Yo-OC tumor, and 59.6% in the Yo-GC tumor (Figure 7A). The plasmablasts in the Yo-GC sample in particular further appeared to consist of two subpopulations of CD27-expressing fractions, although due to the very low cell numbers, might not reflect meaningfully distinct phenotypes. These two CD38hi, CD27-positive clusters did not vary in the expression levels of any of the other markers included in the panel, such as CD19 and CD20. Notably, only a very low number of cells from each of the samples fall in the plasmablast-like compartment (Q1), further supporting the notion that these few cells may merely be an outcrop of conventionally-defined plasmablasts, and still likely belong in the same phenotypic cluster. B cells in the naïve compartment were the next highest in frequency at 21.4% for the OC tumor, and 36.6% for the Yo-GC tumor – both lower than the naïve B cell frequency of healthy donor PBMCs at 60.8%. A small number of memory B cells were also present, at 5.63% for the OC tumor and 2.13% for the Yo-GC tumor – both much less compared to memory B cells from the healthy donor PBMCs at 37.3%. The high frequencies of plasmablasts in the Yo-tumors, and the lower frequencies of other subsets such as memory and naïve B cells compared to those in healthy donor PBMCs, indicate that the humoral response in these tissues is predominated by antibody-secreting cells that have been highly-activated (Figure 7B).

5.2 Single-cell Immunoglobulin Sequencing of Yo-tumor B cells

5.2.1 *Ig* genes from Yo-tumor B cells were successfully amplified

To examine the clonal composition and cellular features of tumor-infiltrating B cells at monoclonal resolution, the tumor-infiltrating B cells from the Yo-associated tumor biopsies were subjected to single-cell immunoglobulin gene amplification and sequencing. I sorted live CD19-positive B cells from the Yo-OC and Yo-GC tumors, after staining with the same B cell panel as in Figure 4. The CD19-positive B cells were pre-gated on non-doublet, live, CD45-positive cells, CD3-negative cells (Supplementary Figure 4). The phenotypic information of the sorted cells was linked to the cell's position on the plate using the index sorting function, to able to trace back the phenotypic features from flow cytometry to each individual cell. A total of 1,131 CD19-positive B cells were sorted from the Yo-OC sample, and 131 CD19-positive B cells were sorted from the Yo-GC sample (Figure 8A). Immunoglobulin transcripts were amplified from each well using a platform that was established for the high-throughput analysis of human antibody repertoires at single cell level [82], and the resulting libraries were sent for Next-generation Sequencing. The resulting reads were processed using Scireptor [85], a processing and analysis pipeline that combines bioinformatics tools for the annotation of immunoglobulin sequences in a relational database, and further integrates the cell surface marker expression from the index sorting to every sorted cell.

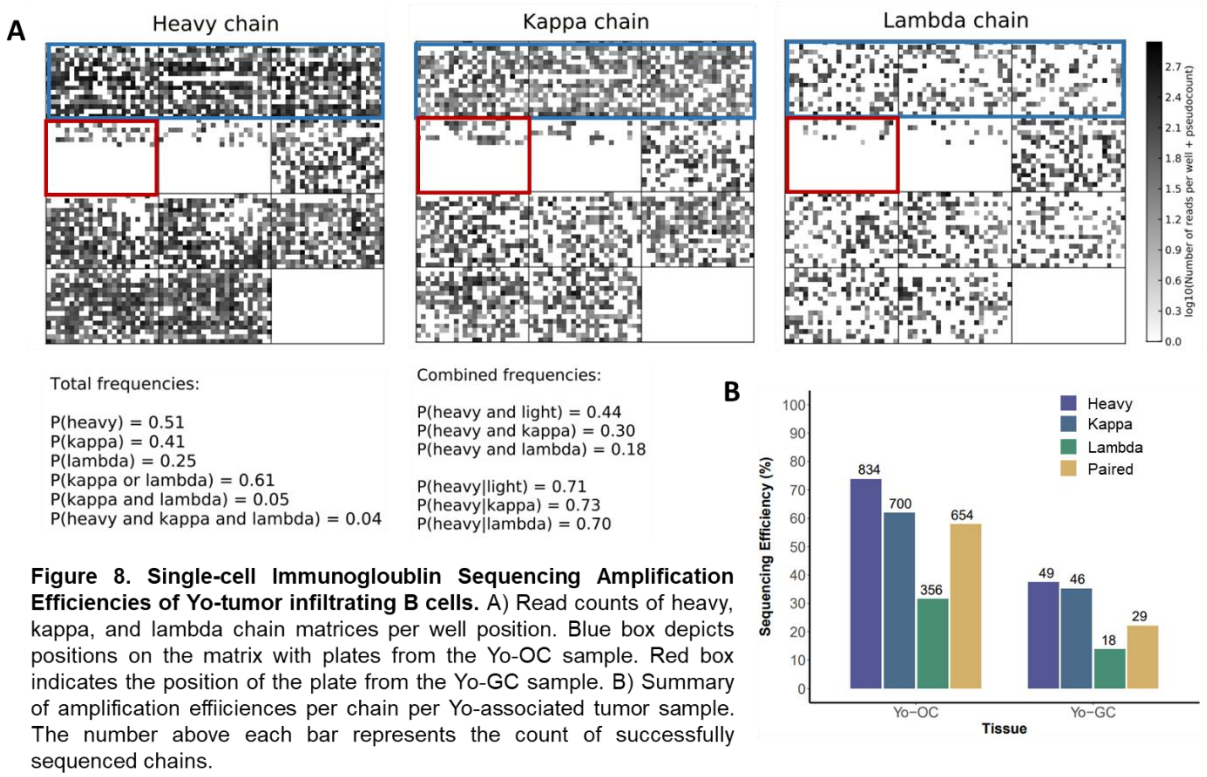

Figure 8. Single-cell Immunogloublin Sequencing Amplification Efficiencies of Yo-tumor infiltrating B cells. A) Read counts of heavy, kappa, and lambda chain matrices per well position. Blue box depicts positions on the matrix with plates from the Yo-OC sample. Red box indicates the position of the plate from the Yo-GC sample. B) Summary of amplification effiiciences per chain per Yo-associated tumor sample. The number above each bar represents the count of successfully sequenced chains.

High sequencing efficiencies of *IGH* and *IGK/IGL* gene sequences were obtained from B cells sorted from the Yo-OC sample. Out of 1,131 cells sorted, 834 heavy chain sequences were amplified, and paired *IGH and IGK/IGL* gene sequences could be mapped to 654 cells, resulting in a paired-chain amplification efficiency of 57.82% (Figure 8B). A small fraction of paired sequences with one pair having PCR-induced mutations that resulted in non-productive open reading frames, were further filtered out as these would not be viable candidates for downstream characterization, and 637 paired chain sequences were left in the end.

On the other hand, only 29 paired IGH and IGK/IGL gene sequences were successfully amplified out of 131 sorted B cells from the Yo-GC sample (Figure 8B). Due to the low amplification efficiency for this sample, presumably as a consequence of the low viability of the tissue sample, subsequent repertoire analyses and investigations were focused on the Yo-OC B cells.

5.2.2 The Yo-associated ovarian carcinoma Ig repertoire is primarily composed of diverse, highly-mutated, IgG1-switched plasmablasts

I first analyzed the distribution of Ig heavy, kappa, and lambda chain gene usages from the sequenced B cells of the Yo-OC sample to examine whether the immunoglobulin repertoire of the Yo-OC sample was predominated by B cell clones that have a specific gene usage, which might indicate shared specificities. Genes from the *IGVH3* family constituted 49.8% of heavy chain sequences, followed by *VH4* genes at 27.8%, *VH1* genes at 21.8% and *VH5* genes at 1.1% (Figure 9A). For the kappa chain sequences, 48.5% belonged to the *VK1* family, 37% to the *VK3*, 9.41% to *VK2* and 5.02% to *VK4 (*Figure 9B). Lambda chain sequences were composed of 28.58% VL3 family genes, followed by an equal frequency from the *VL1* and *VL2* families at 26.3%. *VL7* comes next at 14.1%, followed by *VL4*, *VL6*, *VL9* genes at 2.75%, 1.18%, and 0.784% respectively (Figure 9C). All in all, the gene usage distributions for both V Heavy and V Light genes entail that the Yo-OC is populated by B cells expressing diverse Igs/specificities.

To examine the clonal diversity of the B cells in the Yo-OC in more detail, B cells belonging to the same clonal ancestry were defined and clustered together based on having identical *VH* and *JH* genes, identical *VK* or *VL* and *JK* or *JL* genes, and the same CDR3 lengths for both the respective Ig heavy and light chains. From the 637 B cells, 335 mapped to 92 expanded clonal lineages with at least 2 clonal members (Figure 9D). The rest of the 301 B cell clones were singletons and were relegated to the non-expanded compartment.

I calculated different measures of diversity based on the number of clones identified and their abundance (Figure 9E). The Shannon Diversity Index was calculated at 5.667, where higher values are indicative of a high diversity and evenness across clones. Another measure of diversity, the Simpson Index, was also calculated, and the Inversed Simpson (1-Simpson Index) was 0.9945, where values closer to 1 indicate a high clonal diversity.

I also calculated the frequency of Ig V heavy and V light chain combinations to assess if certain V gene pairings are selected for in the repertoire of Yo-OC B cells (Figure 9F). No extraordinary usage of certain combinations was observed, and the high counts of *IGHV4-4* to

IGKV3-11, *IGHV3-48* to *IGKV1-39*, and *IGHV4-59* to *IGKV3-11* is attributable to the number of clones that make up the expanded clusters with those *V* gene combinations.

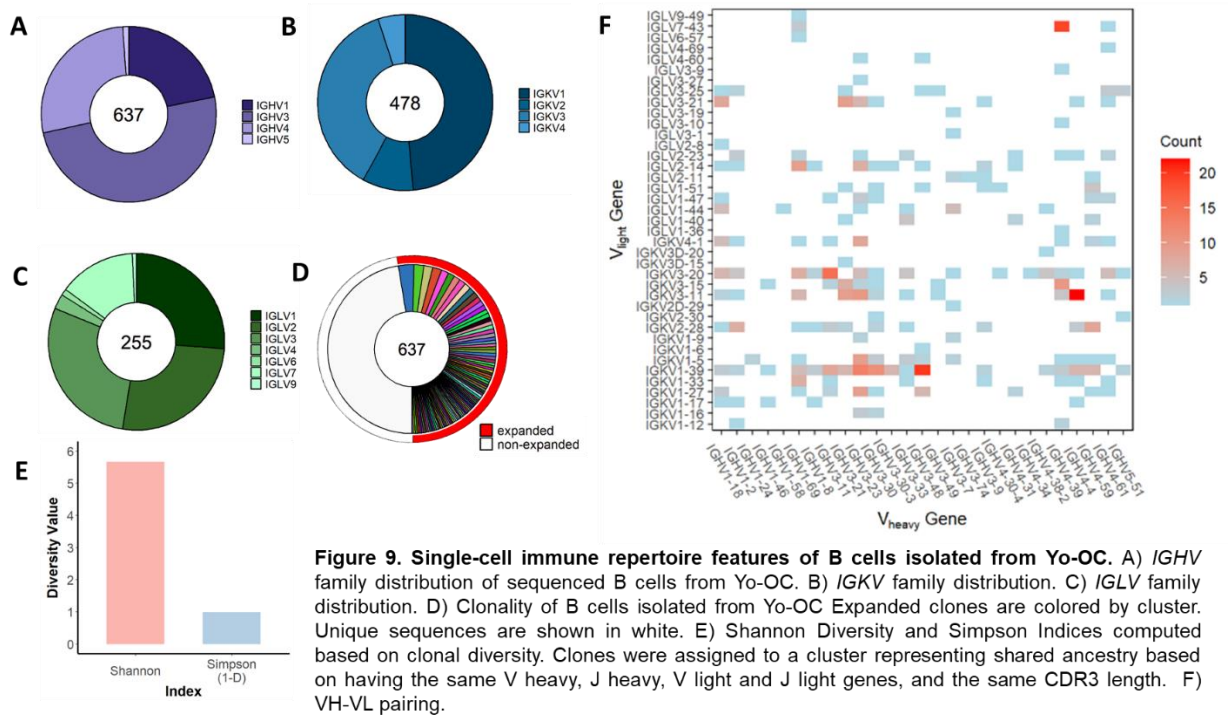

Figure 9. Single-cell immune repertoire features of B cells isolated from Yo-OC. A) *IGHV* family distribution of sequenced B cells from Yo-OC. B) *IGKV* family distribution. C) *IGLV* family distribution. D) Clonality of B cells isolated from Yo-OC Expanded clones are colored by cluster. Unique sequences are shown in white. E) Shannon Diversity and Simpson Indices computed based on clonal diversity. Clones were assigned to a cluster representing shared ancestry based on having the same V heavy, J heavy, V light and J light genes, and the same CDR3 length. F) VH-VL pairing.

To assess the composition of the sequenced B cells based on phenotype, and examine it against other features of the repertoire, such as isotype distribution and SHM counts, I analyzed the marker expression of CD27 and CD38 of the sequenced Yo-OC B cells, and linked it to the *IG* isotype (Figure 10A) and SHM status. As observed in the initial flow cytometry analysis of the tumor cell suspension, about three quarters of the B cells (523/637) had a plasmablast phenotype (Figure 110), and almost all of them were class-switched to IgG1 (Figure 10B), which was the predominant isotype in the repertoire. An analysis of the total somatic hypermutation counts of each B cell subset shows that except for the B cells in the naïve compartment, the average total SHM lie between 20-22 mutation counts, and do not vary greatly among plasmablasts, memory B cells, and the PB-like subset (Figure 10D).

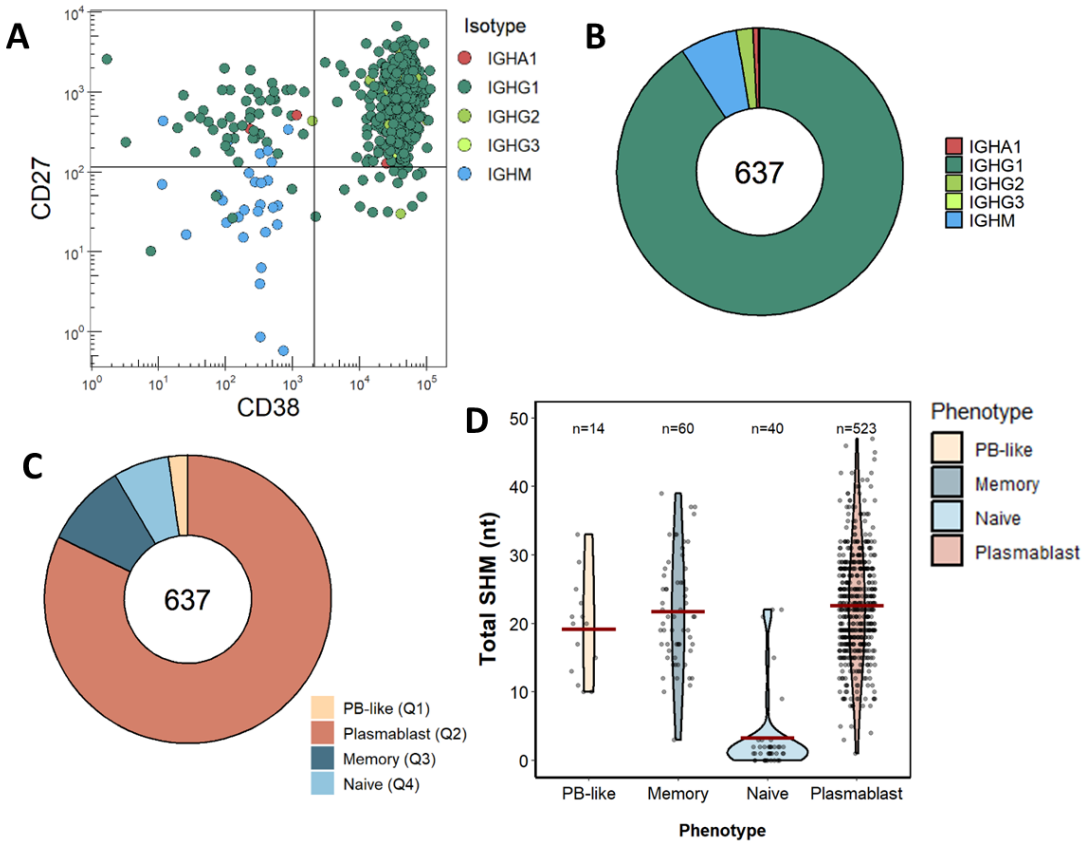

Figure 10. B cell subset and isotype distribution, and somatic hypermutation counts of Yo-tumor-infiltrating B cells. A) CD27 and CD38 expression based on flow index data, colored by Ig isotype. B) Isotype distribution of Yo-tumor-infiltrating B cells. C) Phenotypic distribution of Yo-tumor-infiltrating B cells. D) Total somatic hypermutation counts of different Yo-tumor-infiltrating B cell subsets.

5.2.3 Selection Criteria for Antibody Cloning and Expression

Based on salient features of the Yo-tumor B-cell-infiltrating (Yo TIL-B) repertoire, where majority of these highly-diverse clones were class-switched to IgG1 and differentiated to plasmablasts (Figure 11A), I formulated selection criteria to downselect clones for gene cloning and mAb expression. I focused on the expanded compartment, and selected the clone from each B cell cluster that presumably had undergone the most affinity maturation. To this end, I chose the IgG1-switched clone with a plasmablast phenotype and the had the highest total SHM count among its clonal relations from each cluster (Figure 11B).

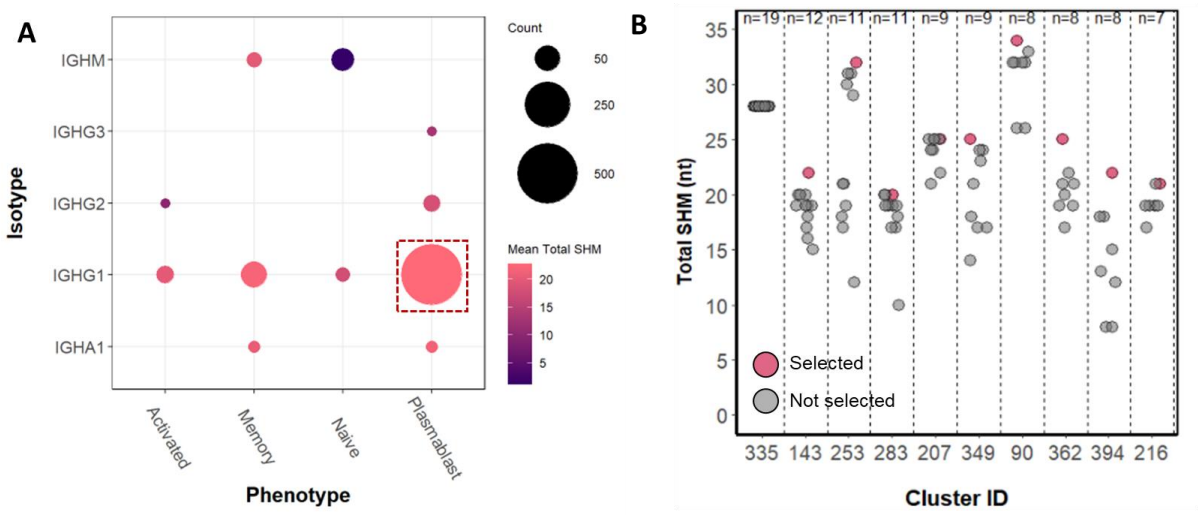

Figure 11. Repertoire features that inform the selection criteria for antibody cloning and expression. A) Overview of prominent repertoire features and the associated counts and average total SHMs of B cell clones with succesfully sequenced paired chains. Red box represents features that comprised the primary selection criteria for cloning. B) Total SHM of different clones that comprise the top 10 most clonally-expanded clusters. Points colored red represent the clones that were selected for cloning.

5.3 Reactivity Profiling of Yo tumor-derived Monoclonal Antibodies

5.3.1 Yo tumor-derived mAbs mainly target CDR2L

From the 92 clones that were selected from each cluster, I successfully cloned and expressed 65 as monoclonal antibodies. To determine the reactivities of these antibodies, I performed antigen ELISA against the two Yo antigens, CDR2 and CDR2L (Figure 12A). Majority of the mAbs (52/65) bound to CDR2L (Figure 12B). Thirty-eight of those mAbs bound to CDR2L only, and were ascribed CDR2L-specific (Figure 12C). The fourteen mAbs that bound to CDR2 also cross-bound CDR2L (Figure 12D), and were designated as Yo cross-reactive mAbs. Only a small fraction (13/65) did not bind to either of these Yo antigens, nor an irrelevant antigen ovalbumin (OVA).

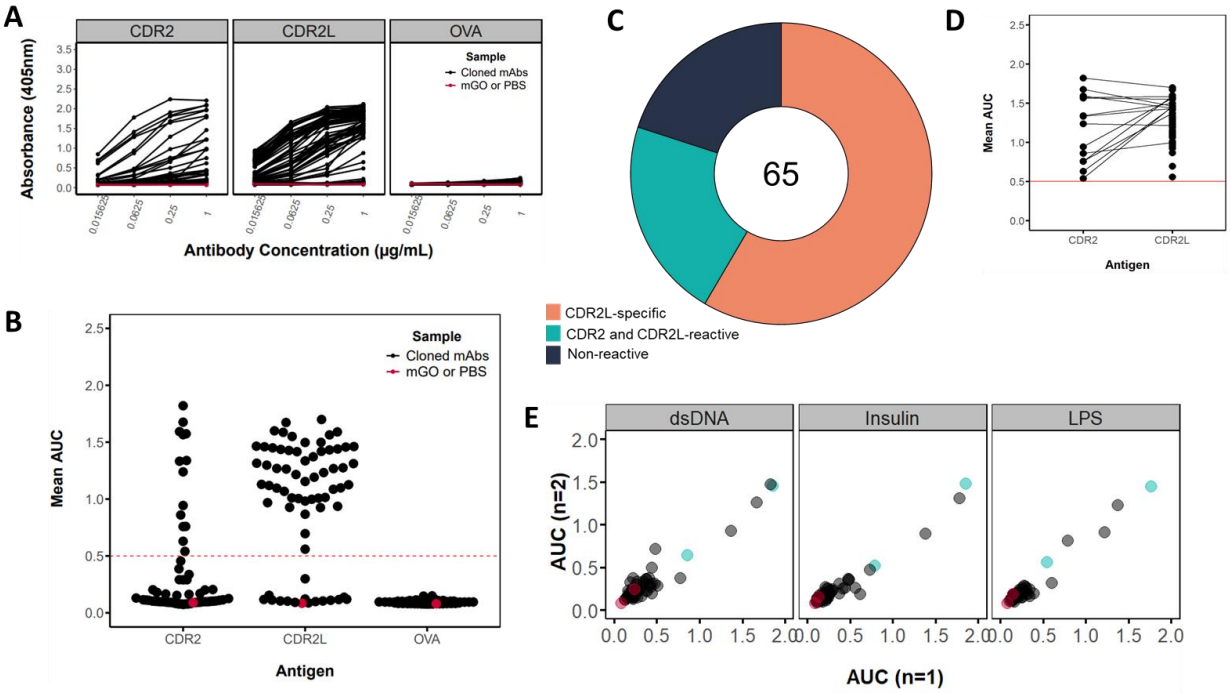

Figure 12. ELISA binding profiles of Yo-tumor-derived mAbs. A) ELISA profiles of antibodies tested against the Yo antigens CDR2 and CDR2L, and an irrelevant protein, Ovalbumin. B) Calculated areas under the curve (AUC) from the ELISA binding profiles in *A*. Dashed red line at 0.5 depicts the AUC cutoff used to define reactive antibodies. C) Distribution of antibody reactivity to CDR2 and CDR2L. D) Association between CDR2 reactivity and CDR2L reactivity. E) Calculated AUCs from Polyreactivity ELISA binding profiles to other unrelated antigens.

To assess whether the binding to Yo antigens was specific, I performed a polyreactivity ELISA on the mAbs to test their binding to double-stranded DNA, insulin, and lipopolysaccharide – unrelated and structurally different antigens. Only two out of the 65 mAbs displayed overt polyreactivity, with calculated AUCs for all three antigens lying between the AUCs of the weakly-polyreactive mAb JB40 and the highly-polyreactive mAb ED38 (Figure 12E). These suggest that the binding was rather specific to the Yo antigens, and the higher frequency of antibodies that target CDR2L suggest its relevance over CDR2 as the main target of Yo antibodies.

5.3.2 Yo antigen reactivity is not linked to particular *V* genes, SHM count, nor clonal expansion

To determine what features of the repertoire are linked to Yo antigen reactivity I revisited other features of the repertoire which were not deliberately selected for during cloning, but may be linked to Yo reactivity. One aspect that was remarkable among the sequenced B cells was the immense diversity of clones. I plotted the frequency of all the tested mAbs to their corresponding V heavy and V light genes, in comparison to the rest of the untested clones, and found that Yo antigen reactivity does not seem to be biased by the usage of any specific *IGHV* nor *IGKV* nor *IGLV* gene, and that the V usage of Yo-reactive clones is spread across the different IGH and IGKV/IGLV gene families (Figure 13A and 13B).

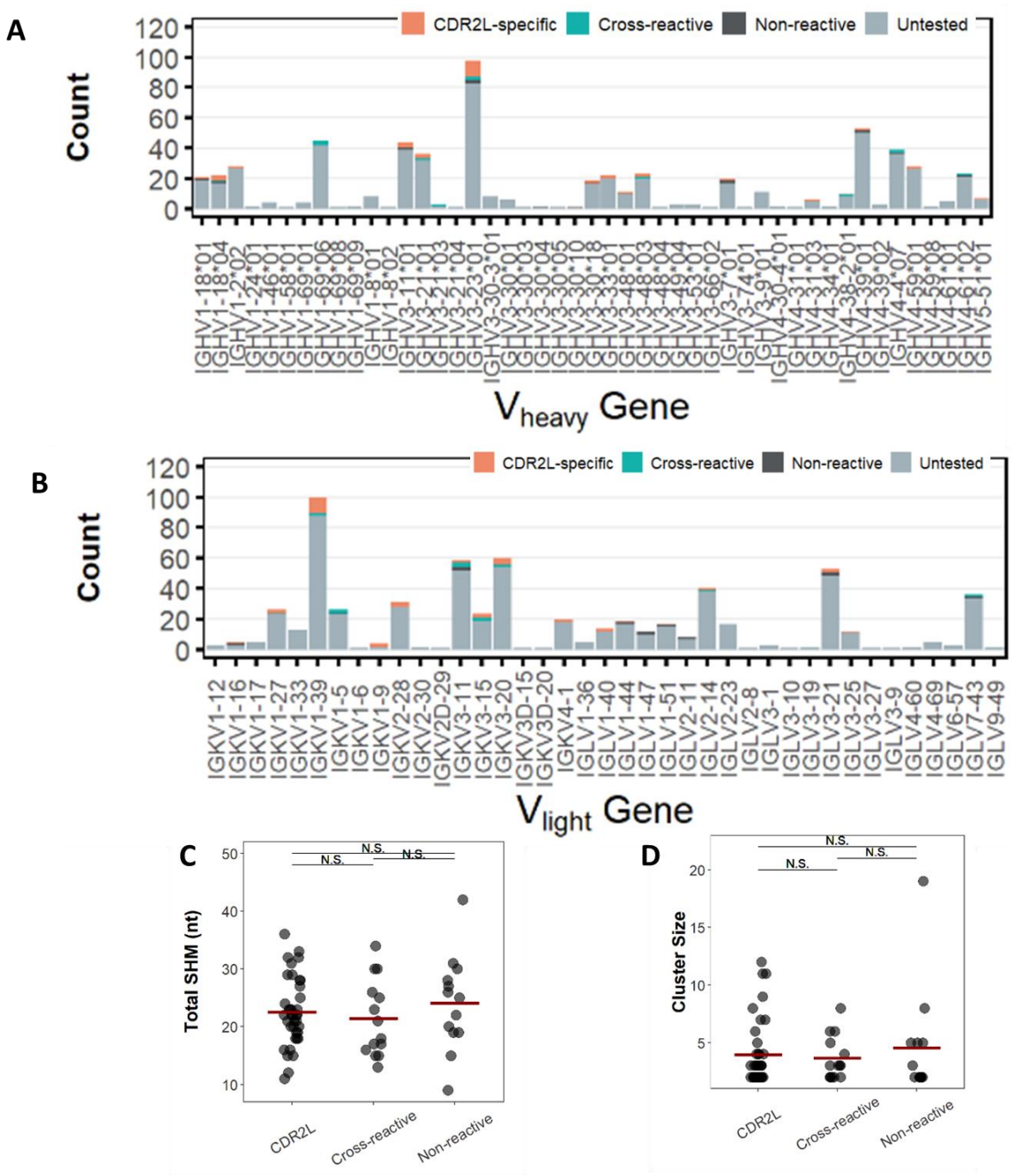

Figure 13. Repertoire features in relation to Yo antigen reactivity. A) Frequencies of V heavy gene usage of Yo-OC B cells and tested mAbs. B) Frequencies of V light gene usage of Yo-OC B cells and tested mAbs. C) Total SHM counts of tested Yo-tumor mAbs separated by Yo-antigen reactivity defined by the Yo antigen ELISA. D) Clone count of clusters linked to the reactivites of Yo-tumor mAbs defined by Yo antigen ELISA. Red bars in *C* and *D* indiciate calculated mean per group. Pairwise wilcoxon rank tests were performed for the statistical analysis.

The average somatic hypermutation counts and mean cluster sizes among CDR2L-specific, Yo cross-reactive, and Yo non-reactive mAbs also do not differ significantly (Figure 13C and 13D), implying that B cells with other specificities are able to participate in germinal center reactions as much as Yo autoreactive clones.

5.4 Specificity of Yo-reactive Monoclonal Antibodies

5.4.1 Yo tumor-derived mAbs immunoprecipitate Yo antigens in an ovarian carcinoma model cell line

To confirm the specificity of Yo-reactive mAbs to CDR2 and CDR2L, I selected the two high-binding cross-reactive mAbs P2_290, and P2_1125, and two CDR2L-specific mAbs P2_235 and P2_363, and used them in immunoprecipitation assays. OvCar3 cells are models of ovarian cancer that have been reported to express both CDR2 and CDR2L, and I used the selected mAbs to immunoprecipitate OvCar3 lysates.

Immunoprecipitation with the Yo-cross-reactive mAbs, and subsequent detection of CDR2L and CDR2 on western blot shows that both CDR2L, which runs at 55kDa, and CDR2 which runs at 62kDa, were pulled down by P2_290 and P2_1125 from the OvCar3 lysate (Figure 14A). The band intensity was more prominent for CDR2L in both IP conditions, suggesting that either it is preferentially immunoprecipitated by the cross-reactive antibodies, or CDR2L and CDR2 have different expression levels in OvCar3 cells, or that the CDR2L detection antibody binds very efficiently to CDR2L on the blot compared to the CDR2 detection antibody.

The CDR2L-specific mAbs also immunoprecipated CDR2L (Figure 14B, left blot). On the other hand, detection of a weak signal for CDR2 in the lane of the CDR2L-specific mAb P2_363, (Figure 14B, right blot), as in the lane for P2_1125 in the CDR2 blot, suggests a very weak degree of cross-reactivity that was not discernable in the Yo antigen ELISAs.

A non-Yo-reactive antibody P2_050 was also used for comparison in all immunoprecipitation conditions, which was not able to immunoprecipitate either of the Yo antigens. The faint bands that appear below 55kDa were confirmed to be due to the non-specific detection by the secondary antibody, of the Ig heavy chain fragments of the respective antibodies used for immunoprecipitation. This was confirmed by stripping and re-probing the blots with anti-human IgG (Supplementary Figure 5).

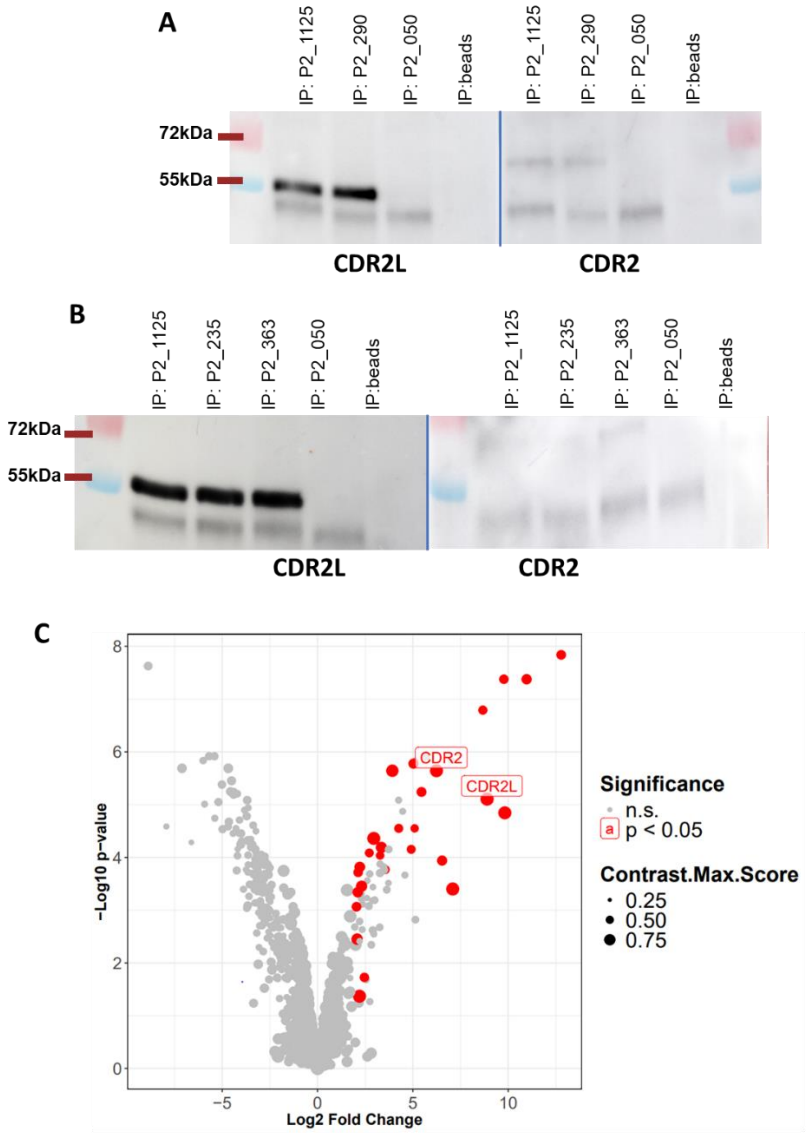

Figure 14. Immunoprecipitation of ovarian cancer cell line lysates using select Yo-reactive mAbs. A) Western blot profiles of CDR2L and CDR2 of immunoprecipitated from OvCar3 lysates u sing Yo-antigen cross-reactive mAbs, and the non-reactive mAb P2_050. B)) Western blot profiles of CDR2L and CDR2 of immunoprecipitated from OvCar3 lysates using CDR2L-specific mAbs, side-by-side with the cross-reactive mAb P2_1125 and non-reactive mAb P2_050. C) Mass Spectroscopy analysis of proteins immunoprecipated from OvCar3 lysates by the P2_1125 mAb.

I also performed immunoprecipitation with the high-binding cross-reactive mAb P2_1125, followed by Mass Spectrometry analysis. Rankings were based on the fold-change difference in abundance compared to the beads-only IP and on the Constrast Max Score, a scoring algorithm developed by the MS facility in-house to more reliably identify hits. These rankings show that CDR2 and CDR2L were the top proteins that were immunoprecipitated by the P2_1125 mAb (Figure 14C). Fragments that exceed the calculated fold-change in abundance of CDR2 and CDR2L but had a much lower Contrast Max Score, were identified to be from peptides of the immunoglobulin chains of P2_1125 that was used for immunoprecipitation. Other proteins that were identified after immunoprecipitation with P2_1125 are potential interactors of CDR2 and CDR2L.

To explore potential pathways or gene networks associated with CDR2 or CDR2L, I performed Ingenuity Pathway Analysis from genes identified by Mass Spectrometry, that were at least 2-fold more abundant in the P2_1125-IP condition, had a p-value of less than 0.05, and a Contrast Max Score of at least 0.6, making up a list of 53 proteins (Supplementary Table 1). From this list, I performed a basic core analysis using the Qiagen IPA software, to be able to infer pathways and functional networks that the proteins could be involved in. As the function of CDR2 and CDR2L are undefined to date, no definite pathways identified involved the two proteins (Supplementary Figure 6).

From these experiments, I conclude that the Yo-reactive mAbs are able to bind to their cognate antigens CDR2 and CDR2L, in an ovarian carcinoma model expressing these Yo antigens. Further insight regarding the nature of Yo-antigens however warrant a proper elucidation of their function.

5.4.2 CDR2L-specifc mAbs harbor weak cross-reactivity to CDR2

To examine whether CDR2L-specific mAbs do indeed harbor weak cross-reactivity to CDR2, and to assess whether non-Yo-reactive mAbs also carry weak reactivities to Yo antigens that were not discernible in the conventional antigen ELISA, I screened thirty-seven CDR2L-specific and the 13 non-Yo-reactive mAbs using a cross-linking high-sensitivity ELISA. In this ELISA format, coated antigens are incubated with a pre-crosslinked mix of test primary antibodies and HRP-labelled anti-human IgG, to increase binding avidity towards the coated antigen. Together with detergent-free washing conditions, this facilitates increased sensitivity to detect antibody binding.

After testing all the CDR2L-specific and non-reactive mAbs, I mathematically determined a threshold for considering reactivity to an antigen by calculating the second derivative of the frequency distribution of the tested antibodies, and taking the first point of inflection (Supplementary Figure 7). This represents the point in which antibodies demonstrating significant binding (higher absorbance) are separated from those that do not, thereby providing a data-driven basis for classification. Majority of the CDR2L-specific mAbs (23 out of 37), including P2_235 and P2_363 used in the immunoprecipitation assays, harbored cross-reactivity to CDR2 (Figure 15 A and B), which exhibited absorbance values (405nm) above the threshold. A few mAbs (5 out of 13) that were originally defined as Yo non-reactive from the Yo antigen ELISA also harbored weak cross-reactivities to both Yo antigens in the high-sensitivity format (Figure 15A and B). Despite falling below the threshold to qualify as reactive antibodies in the Yo antigen ELISA, their weak reactivities to Yo antigens may have already been indicated by their marginally higher calculated AUCs in that conventional ELISA format compared to bona fide Yo non-reactive mAbs. The weak binding strengths that led to weak cross-reactivities, especially of CDR2L-specific mAbs to CDR2, was appraised by Western blot analysis (Figure 15C), using two of the CDR2L-specific mAbs, P2_363 and P2_295, which both exhibited CDR2 cross-reactivity on the crosslinking high sensitivity ELISA. While a corresponding band for the recombinant CDR2L antigen after incubation with either the two antibodies was immediately appreciable after a short exposure of five seconds, the detection of recombinant CDR2 took a much longer exposure (5

minutes) to obtain a corresponding signal. In summary, this substantiates that weak cross-reactivity to CDR2 for the CDR2L-specific mAbs, and weak Yo-antigen cross-reactivities for a few non-reactive mAbs exist, and that the weak reactivities were likely below the detection limit of the conventional Yo antigen ELISA. And while weak cross-reactivities to CDR2 were observed, readily-observable binding to CDR2L still corroborates CDR2L as the main target of the CDR2L-specific mAbs.

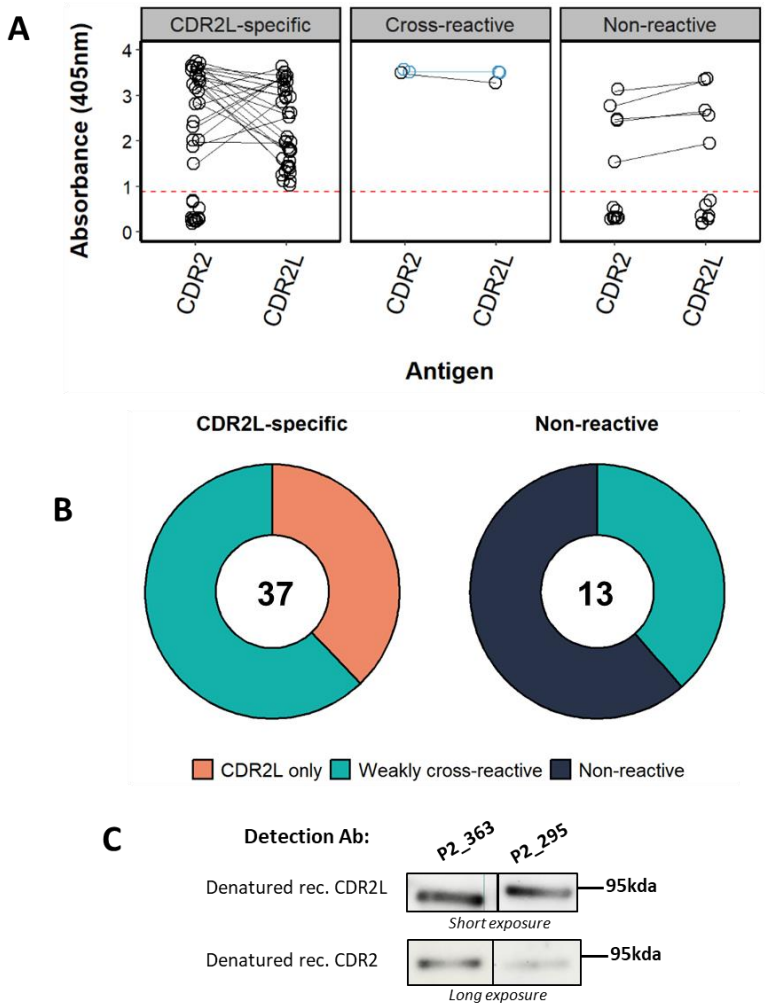

Figure 15. Detection of weak Yo antigen reactivity from CDR2L-specific and Yo non-reactive mAbs. A) Absorbance profiles of CDR2L-specific and Yo-non-reactive mAbs against CDR2 and CDR2L from a high-sensitivity cross-linking ELISA. Antibodies are separated by Yo-antigen ELISA reactivites, and cross-reactive mAbs P2_290 (blue) and P2_504 were included for comparison. Dashed red line depicts calculated threshold for binding vs non-binding. B) Summary of the proportion of weakly-cross-reactive mAbs to the mAbs that retained their original specificities. C) Western blot profiles of two of the identified CDR2L-specific mAbs with weak cross-reactivities to CDR2. CDR2L blot was taken with a short exposure time (5 secs), while the CDR2 blot was taken after a long exposure time (5 mins).

5.5 Binding Modes of Yo-reactive Monoclonal Antibodies

5.5.1 Two high-binding Yo cross-reactive mAbs target the same linear epitopes on CDR2 and CDR2L

CDR2 and CDR2L share around 45% sequence homology at the amino acid level, and most of this similarity is contained in the first third of their sequences (Figure 16A). To interrogate potential binding configurations to CDR2 and CDR2L, and to infer the shared epitopes that explain the antibody cross-reactivity to both Yo antigens, I performed blocking ELISAs using the high-binding Yo cross-reactive mAbs P2_290 and P2_1125, which were among the mAbs that depicted strong binding to CDR2L and CDR2 from the antigen ELISAs. In this variation of a competition ELISA, pre-incubation with an unbiotinylated antibody will block the binding of a second biotinylated antibody if both target the same epitope on an antigen, and provided they have similar relative binding affinities. In this format, biotinylated P2_1125 was used as the second antibody, and unbiotinylated P2_290 was used as the blocking antibody.

Addition of biotinylated P2_1125 after blocking with an unlabeled version of the same mAb (self-blocking condition) resulted in a dose-dependent decrease in absorbance as higher concentrations of unlabeled P2_1125 increasingly block epitope access to either CDR2 or CDR2L. This represented perfect blocking conditions, as the biotinylated mAb is in competition with its unbiotinylated self for the same epitope (Figure 16B). When unbiotinylated P2_290 was used as the blocking antibody, the same dose-dependent decrease was observed, which did not hold for the negative control conditions when blocking with the non-binding antibody mGO or PBS only. This suggests that epitopes of P2_290 and P2_1125 overlap, resulting in epitope blocking by P2_290 that mimics self-blocking conditions. The similarity of the blocking profiles between CDR2 and CDR2L further suggests that, consistent with observations from binding assays, the same epitope is likely being targeted on both Yo antigens.

To examine if the shared epitope between P2_1125 and P2_290 was a linear or conformational epitope, I performed a western blot analysis using P2_1125 and P2_290 as detection antibodies to detect denatured (linearized) CDR2L and CDR2. The detection of a signal in both the CDR2L and CDR2 blots using either of the two antibodies suggests that the shared

epitope that P2_1125 and P2_290 on both CDR2L and CDR2 are linear epitopes, and are likely located in the first 125 amino acids of their sequence which CDR2 and CDR2L share with high similarity (Figure 16C).

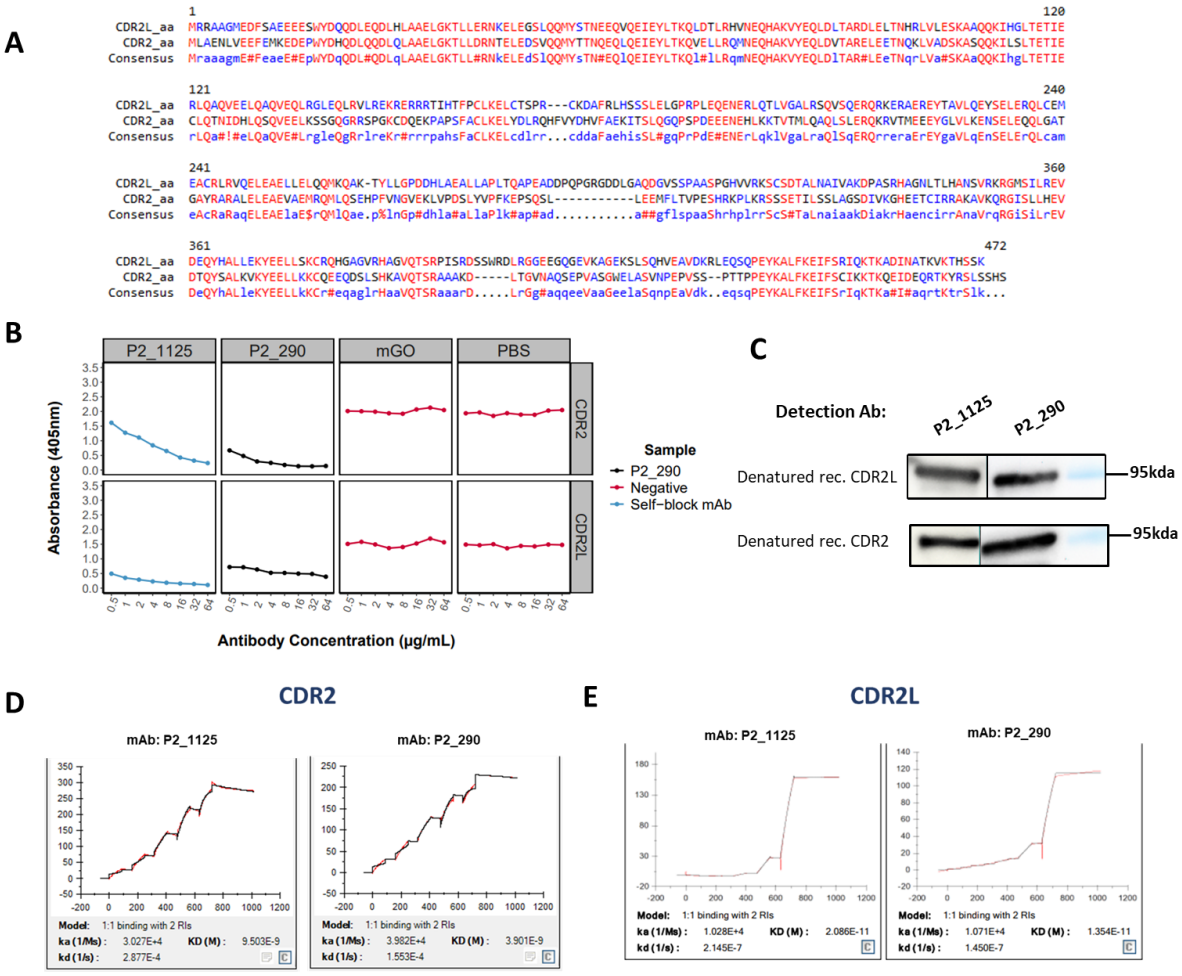

Figure 16. Fine analysis of binding properties of two Yo cross-reactive mAbs to CDR2 and CDR2L. A) Protein sequence comparison between human CDR2 and CDR2L. B) Blocking ELISA profiles of biotinylated P2_1125 against unbiotinylated P2_1125 and unbiotinylated P2_290 on CDR and CDR2L. C) SPR affinity profiles of P2_1125 and P2_290 to CDR2. D) SPR affinity profiles of P2_1125 and P2_290 to CDR2L. *Data in D and E generated by Ernest Oludada*

Despite potentially targeting the same epitopes on both Yo antigens, affinity measurements by Surface Plasmon Resonance (SPR) show that there is still preference for binding to CDR2L, with both P2_290 and P2_1125 mAbs having affinities in the range of 10^{-11} for CDR2L, compared to affinities only in the range of 10^{-9} for CDR2 (Figure 16D and 16E; Table 14).

Table 14. Summary of KD (M) Affinities to Yo antigens.

mAb	Affinity (KD)	Antigen
P2_290	3.901E-09	CDR2
P2_1125	9.503E-09	CDR2
P2_290	1.354E-11	CDR2L
P2_1125	2.086E-11	CDR2L

5.5.2 Yo-reactive mAbs display varied of binding modes to CDR2 and CDR2L

To examine the assortment of binding configurations to Yo antigens, I also comprehensively assessed other potential binding modes to CDR2 and CDR2L in relation to P2_1125 by performing blocking ELISAs with the other 63 Yo tumor-derived mAbs. This paints a more complete picture of different binding modes, and helps infer the diversity of epitopes on the Yo antigens that are targeted by antibodies. In this round of blocking ELISAs, P2_1125 was kept as the biotinylated competitor, and AUCs of the blocking curve profiles were calculated.

Firstly, I determined an AUC threshold for both antigens, to define mAbs that are able to effectively block P2_1125 binding, and those that do not (Figure 17A). The threshold for CDR2 was determined to be 82, while the threshold for CDR2L was determined to be 96. These thresholds were calculated from the second derivatives of the density curves, where the point of inflection that occurs before the absolute maximum was taken as the threshold. Mathematically, this defines a stringent threshold at the cusp of where the frequency of antibodies exponentially increases. Antibodies that fall below the threshold are the ones that potentially block the P2_1125 epitope, resulting in a decreased AUC from biotinylated P2_1125; while antibodies above the threshold represent non-competitive binding conditions.

I separated the AUC blocking profiles into bins based on Yo antigen ELISA reactivities, and observed that most of the cross-reactive mAbs are the ones that efficiently block the binding of

P2_1125 on both antigens, and that CDR2L-specific mAbs and non-reactive mAbs unsurprisingly are not able to interfere with P2_1125 binding on both antigens (Figure 17B). In the CDR2L-specific compartment, two binding modes seem to exist – one that interferes with the binding of P2_1125 on CDR2L only, leaving binding to CDR2 unaffected; and one that does not seem to block the binding of P2_1125 on both Yo antigens, suggesting that they may target a different epitope altogether.

I further segregated the mAbs into quadrants based on the bins defined by the thresholds, and plotted them against the original AUCs from the Yo antigen ELISAs. These different quadrants represent competitive or non-competitive conditions for epitopes in CDR2 and CDR2L. Antibodies that fall in Q3 can be qualified to be those that block the epitopes of P2_1125 on both Yo antigens. Q2 represents non-competitive conditions. While antibodies that fall in Q1 and Q4 represent antibodies that interfere with the binding of P2_1125 on its epitope either on CDR2 or CDR2L respectively (Figure 17C).

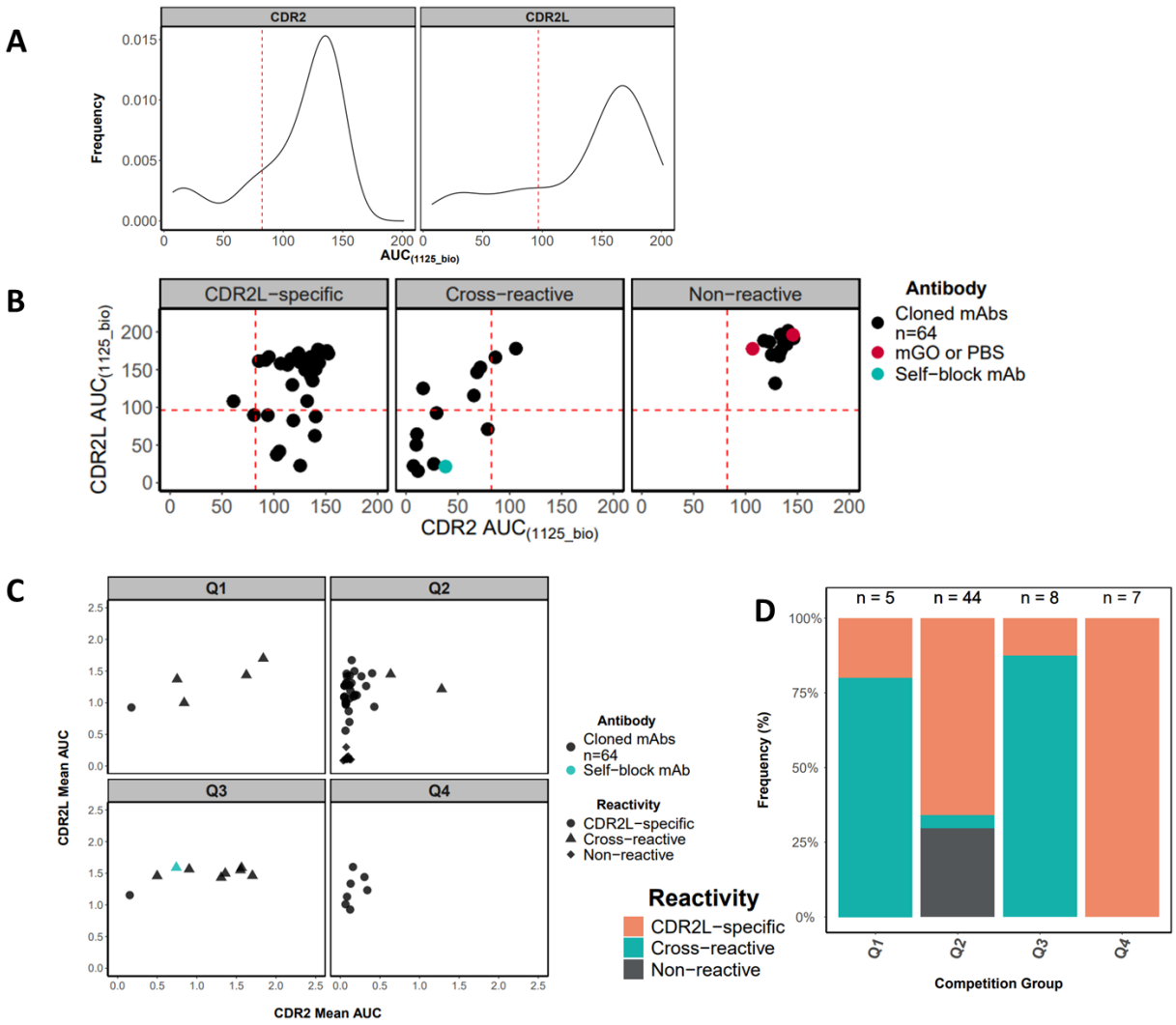

Figure 17. Epitope binding modes of Yo-tumor mAbs vis-à-vis biotinylated P2_1125. A) Frequency distribution of Yo-tumor mAbs in relation to calculated P2_1125 AUCs after blocking ELISAs. Dashed red line indicates mathematically-determined cutoff for classifying blockers and non-blockers of the P2_1125 epitope. B) AUCs from blocking ELISA profiles of Yo-tumor mAbs against biotinylated P2_1125. mAbs were separated based on Yo antigen ELISA reactivities C) Yo-tumor mAbs separated to Q1-Q4 based on blocking profiles against P2_1125. Mean AUC here are derived from Yo antigen ELISA binding profiles. D) Proportion of mAbs by their Yo-antigen reactivity in each category epitope blocking category.

Expectedly, antibodies in Q4 were all CDR2L-specific (Figure 17D). That they caused diminished binding of biotinylated P2_1125 suggest that they target the same or overlapping epitopes. Antibodies in Q3 were all cross-reactive, except for one CDR2L-specific mAb, suggesting that these antibodies may share the same epitope on both CDR2 and CDR2L with P2_1125. Antibodies in Q2 on the other hand were mostly CDR2L-specific (29/44), however two were cross-reactive, and the rest were non-reactive mAbs (13/44), and mAbs in Q1 corollarily were mostly

cross-reactive (4 out of 5), all suggesting an assortment of binding modes toward CDR2 and CDR2L with reference to P2_1125.

Altogether, while some cross-reactive antibodies potentially target the same epitope as P2_1125, the diversity of other binding modes in reference to P2_1125 hint at other modes of binding and binding affinities of Yo-reactive antibodies to both CDR2 and CDR2L.

5.5.3 Yo antigens are localized intracellularly

To further get insight on the binding context of Yo antibodies and determine the location of binding to Yo antigens, I stained OvCar3 cells with the high-binding Yo cross-reactive mAbs P2_290 and P2_1125 and evaluated the staining patterns via confocal microscopy. The staining pattern was predominantly cytoplasmic, but also marginally intensified around the nucleus (Figure 18A and 18B). This binding is something that occurs only when OvCar3 cells were permeabilized, and flow cytometry analysis of OvCar3 cells stained with P2_290 and P2_1125 only show signal under permeabilized conditions (Figure 18D and 18E). This confirms that Yo antigens are localized intracellularly.

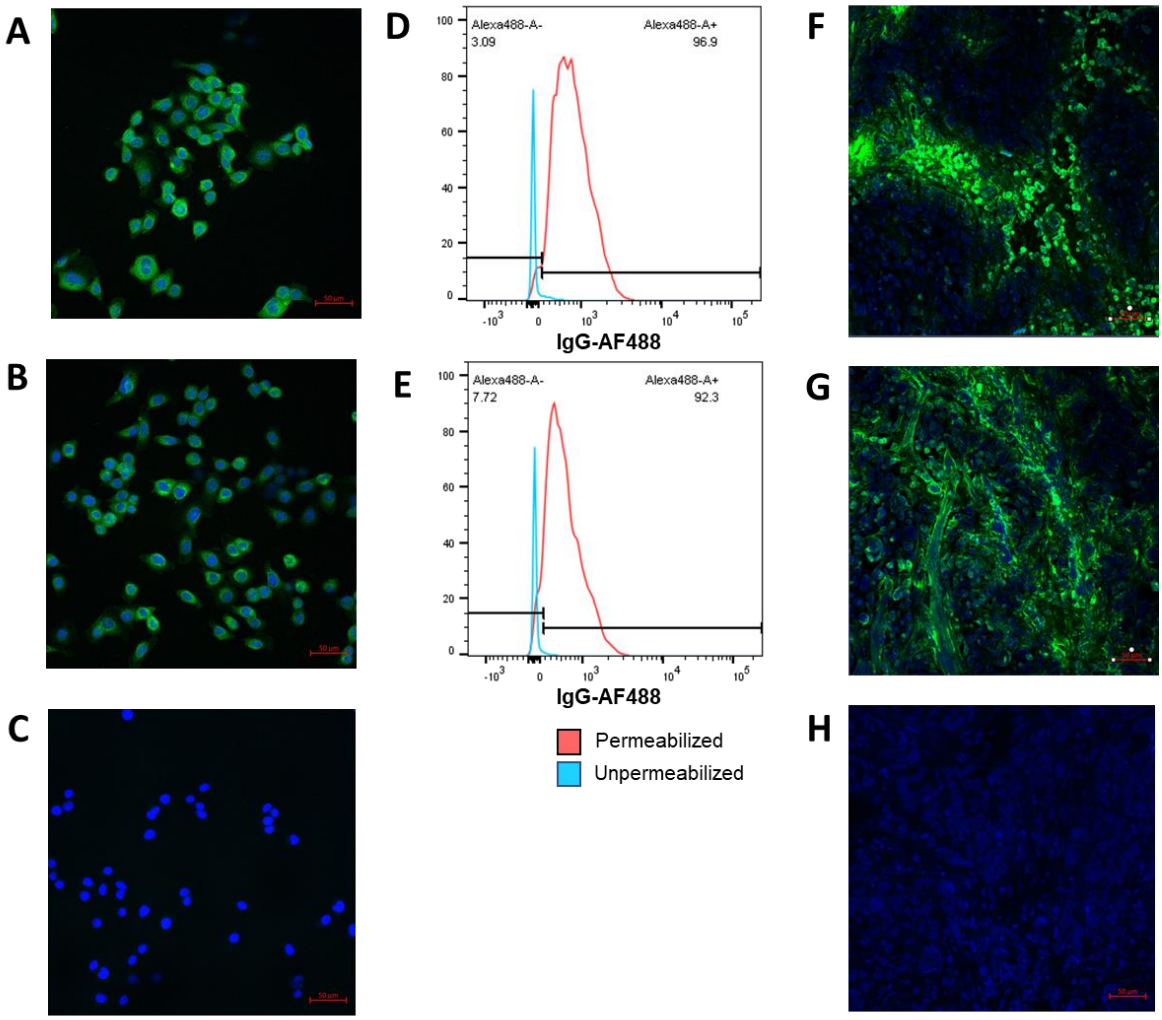

Figure 18. Binding context of high-binding cross-creactive Yo-mAbs. A) Permeabilized OvCar3 cells stained with P2_290 mAb. B) Permeabilized OvCar3 cells stained with P2_1125 mAb. C) Permeabilized OvCar3 cells stained only with anti-IgG secondary Ab. D) Quantification of P2_290 staining of permeabilized and unpermeabilized OvCar3 cells. E) Quantification of P2_1125 staining of permeabilized and unpermeabilized OvCar3 cells. F) Staining of an ovarian carcinoma primary section with P2_290 mAb. G) Staining of an ovarian carcinoma primary section with P2_1125 mAb. H) Staining of ovarian carcinoma primary section with secondary anti-IgG Ab only (Green fluorescence = anti-IgG ; blue fluorescence = DAPI).

This intracellular binding was also tested for a few other Yo-reactive mAbs on immunofluorescence assays (Supplementary Figure 8). Intracellular binding of all mAbs was further comprehensively quantified by flow cytometry staining of permeabilized OvCar3 cells, and mean MFIs for Yo cross-reactive mAbs and CDR2L-specific mAbs were 2-fold and 1.5-fold higher respectively, compared to the mean MFIs of Yo non-reactive mAbs, which gave minimal

fluorescence intensities (Supplementary Figure 9.), indicating that Yo-reactive antibodies bind strongly to antigens, presumably CDR2 and/or CDR2L, in OvCar3 cells. Interestingly, one Yo non-reactive mAbs displayed a markedly high MFI value as well, implying that it targets a separate antigen that was present from the original Yo ovarian carcinoma and is also expressed on OvCar3 cells.

Finally, binding of the P2_290 and P2_1125 was also tested on ovarian carcinoma sections from a neurologically normal cancer patient. Staining of the ovarian carcinoma sections by P2_290 and P2_1125 depict diffuse cytoplasmic staining of some of the cells in the section, suggesting that expression of Yo antigens is not limited to tumors associated with neurological complications only (Figure 18F-H).

5.6 Neuronal Binding of Yo-reactive mAbs

5.6.1 High-binding Yo cross-reactive mAbs bind to Yo antigen in the neuronal context

To be able to assess whether Yo tumor-derived mAbs also recognize the Yo antigens in the neuronal setting, I stained rodent cerebellar transverse sections with the high-binding Yo cross-reactive mAbs P2_290 and P2_1125, and with the CDR2L-specific mAbs P2_235 and P2_363. The P2_1125, P2_290, and P2_363 mAbs show strong staining of Purkinje cells in the Purkinje cell layer, reminiscent of staining patterns obtained with the Purkinje cell marker calbindin (Supplementary Figure 10.), while P2_235 only shows moderately weak staining (Figure 19A-D). In all cases, the staining pattern is predominantly cytoplasmic. However, upon closer inspection in mouse sections at higher magnification, the staining by cross-reactive mAbs P2_1125 and P2_290 also marginally intensifies around the nucleus (Figure 19E-F).

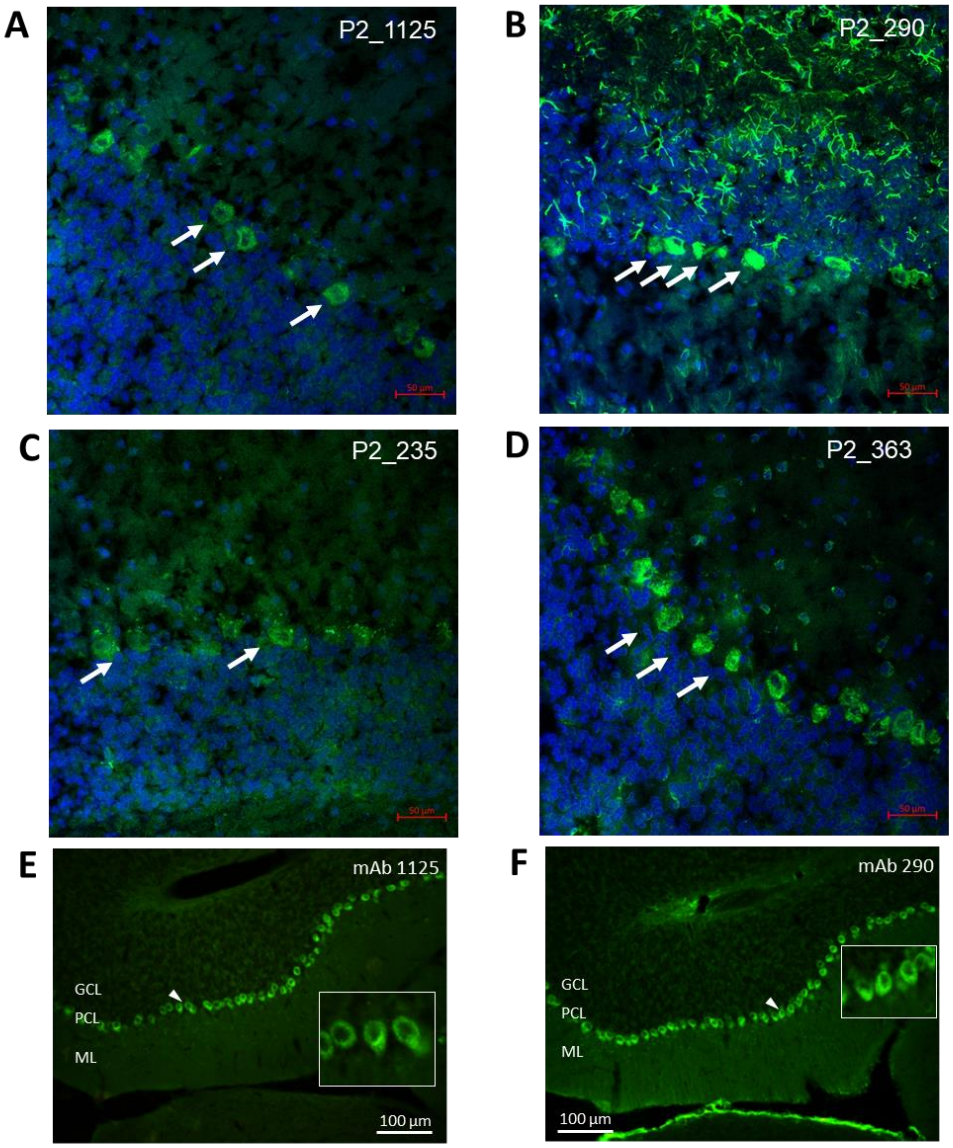

Figure 19. Staining of rodent cerebellar sections with Yo-tumor mAbs. A) Rat cerebellar section stained with the Yo-cross-reactive P2_1125 mAb. B) Rat cerebellar section stained with Yo-cross-reactive P2_290 mAb. C) Rat cerebellar section stained with CDR2L-specific P2_235 mAb. D) Rat cerebellar section stained with CDR2L-specific P2_363 mAb. E) Mouse cerebellar section stained with P2_1125. F) Mouse cerebellar section stained with P2_290. White arrows in A-D point to Purkinje cells. White arrows in E-F refer to the magnified area in the in-lay. GCL = Granule cell layer, PCL = Purkinje cell layer, MCL = mMolecular layer. *Green = anti-IgG, Blue = DAPI. Data from E and F were generated by Prof. Dr. Markus Höltje*

5.6.2 A high-binding Yo-reactive mAb exhibits cross-reactivity to Glial Cells

Aside from the intense staining on Purkinje cells, I also observed that the high-binding Yo cross-reactive P2_290 mAb stained other structures on the rat cerebellar transverse section (Figure 20B). Upon panning to a nearby glia limitans structure, a barrier structure composed of astrocytic endfeet, I observed an even more remarkable staining of astrocytes (Figure 20A). This is also true for astrocytes identified from *in vitro* cerebellar cultures, and stained sections of mouse cerebellum upon panning to the molecular layer, by collaborators (Figure 20B and 20C). This indicates that either Yo antigens are also expressed by cell types outside of Purkinje cells, and that it takes a high-affinity mAb to detect such low expression. Alternatively, it could be the case that P2_290 cross-binds other antigens expressed by astrocytes.

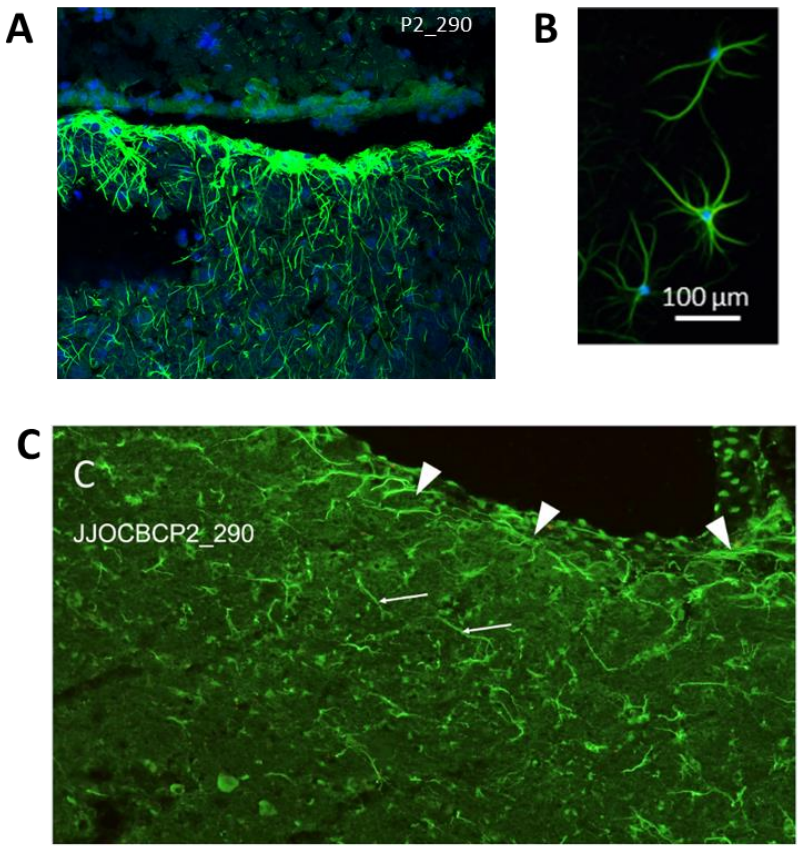

Figure 20. Staining of astrocytes by the high-binding, cross-reactive P2_290 mAb. A) Glia limitans bordering the rat cerebellar section, stained with P2_290 mAb. B) *In vitro*-cultured astrocytes, stained with P2_290 mAb. C) Mouse molecular cell layer of the cerebellum, stained with P2_290 mAb. *Green = anti-IgG, Blue = DAPI. Data from C was generated by César Cordero-Gomez. Data from B was generated by Prof. Dr. Markus Höltje.*

5.6.3 Purkinje cells take up of Yo-reactive mAbs *in vitro*

In the absence of commercially-available Purkinje cell lines, I teamed up with Prof. Dr. Markus Höltje from the Institute for Integrative Neuroanatomy (Charité), in Berlin, who established *in vitro* cerebellar mixed cultures, to assess whether Purkinje cells can take up the Yo-reactive antibodies in culture simply by their addition to the culture medium. After 24 hours of incubation with medium containing either P2_290 or P2_1125, and imaging of Purkinje cells identified by their morphology and expression of Calbindin, an intense staining of the Purkinje cell body was evident (Figure 21A and 21B). This confirms reports by other studies of the ability of Purkinje cells to take up Yo antibodies.

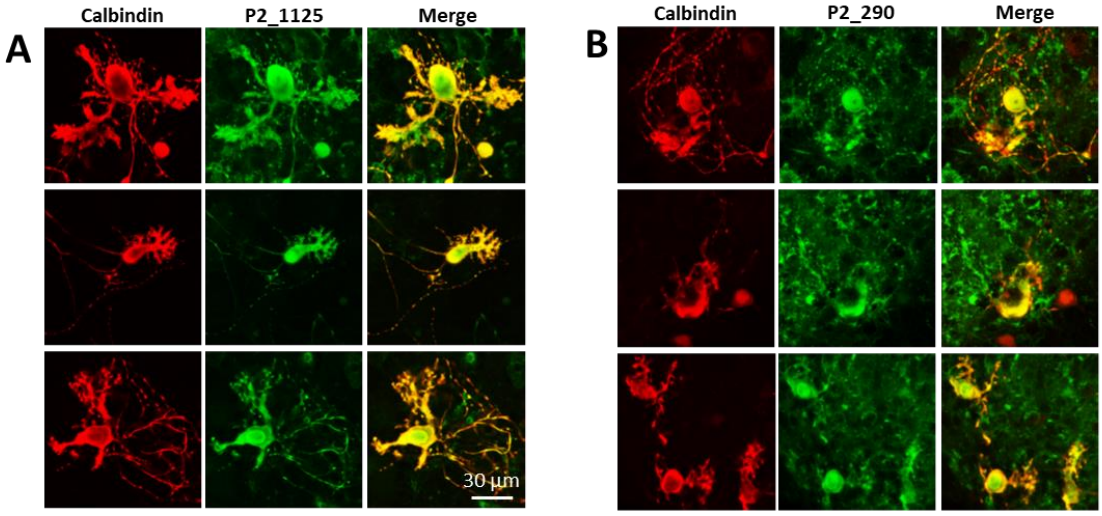

Figure 21. Incubation of Purkinje cells *in vitro* with Yo cross-reactive mAbs. A) Purkinje cells 24h after incubation with P2_1125 mAb. Left panels in red depicts staining with Calbindin. Middle panels in green depict IgG staining. Right panels depicts merged channels of the Calbindin and IgG staining. B) Purkinje cells 24h after incubation with P2_290 mAb. Lefts panel in red depicts staining with Calbindin. Middle panels in green depict IgG staining. Right panels depicts merged channels of the Calbindin and IgG staining. *Data generated by Prof. Dr. Markus Höltje.*

5.7 *In vivo* Assessment of Pathogenic Potential

5.7.1 High-binding Yo cross-reactive mAbs affect motor function in mice

To investigate whether the uptake of Yo-reactive antibodies contribute to motor dysfunction, which is a hallmark of cerebellar degeneration, I teamed up with another collaborator who has a system that enables the continuous intrathecal delivery of mAbs through surgically-implanted osmotic pumps in mice. Using their intrathecal delivery system, they delivered P2_290 and P2_1125 directly to the central nervous system. Ten and fourteen days after continuous intrathecal delivery, they subjected the mice to a rotarod assay (Figure 22A), and measured the length of time each mouse is able to hold on to a rotating rod. In animals continuously injected with P2_1125 and P2_290 mAbs, a decreased capability to hold on, reflected by the smaller amount of time on the rod, was seen compared to mice intrathecally injected with an irrelevant antibody mGO53. This trend was already apparent as early as 10 days after continuous delivery (Figure 22B), and mice injected with the P2_1125 mAb displayed significant motor incompetence up to 14 days (Figure 22C). The mice injected with the P2_290 mAb also still displayed decreased motor competence up to 14 days of continuous intrathecal delivery, albeit variably. These however suggest that the high-binding Yo cross-reactive mAbs do disrupt normal motor function in mice, after direct and continuous intrathecal delivery.

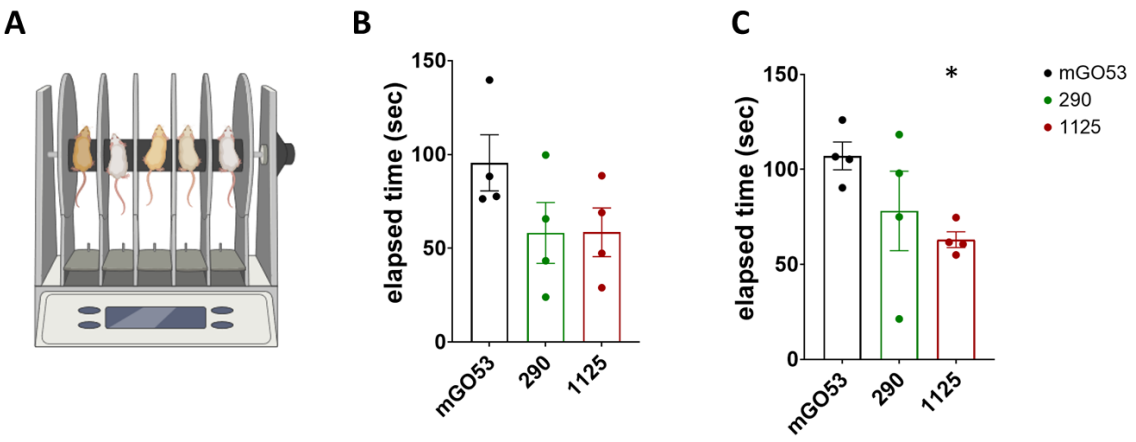

Figure 22. Intrathecal delivery of Yo-mAbs. A) Cartoon representation of Rotarod assay on mice. *Image generated in BioRender.* B) Rotarod assay results 10 days after continuous intrathecal delivery of high-binding Yo-cross-reactive mAbs. C) Rotarod assay results 14 days after continuous intrathecal delivery of high-binding Yo-cross-reactive mAbs. A Wilcoxon rank-sum test was performed, comparing each sample to mGO-treated controls for statistical analysis, α=0.05. *Data generated by César Cordero-Gomez.*

6 Discussion

In Yo antibody-associated paraneoplastic cerebellar degeneration, the identity of the major Yo antigen and the relevant epitopes of Yo autoantibodies are is still a subject of contention [59, 60, 66, 75, 90]. Furthermore, Yo-PCD has been widely regarded as a T-cell mediated autoimmune disorder, and Yo antibodies produced by B cells are only considered as biomarkers ([1, 55, 66, 91]. Although the notion of a pathogenic role of B cells has been put forward, definitive proof is scant, and evidence hitherto presented have been limited to the polyclonal setting [92, 93]. The data in this dissertation, represent first insights into Yo autoantibody specificities, binding characteristics and functional effects at monoclonal resolution by utilizing single-cell immunoglobulin sequencing and mAb expression to examine B cells infiltrating Yo-associated tumors.

The paucity of studies analyzing tumor-infiltrating lymphocyte repertoires of patients with paraneoplastic cerebellar degeneration however reflects the rarity of the disorder and the difficulty in obtaining good-quality patient-derived samples. Sample quality is a particularly important consideration, as it greatly affects the quality of DNA and RNA that is subsequently isolated, especially in single-cell sequencing approaches that involve next-generation sequencing [94, 95]. Several extraneous factors might affect sample quality in actual practice, such as length of time between surgical removal, transport from the operating room, and tissue processing, all of which can reduce cell viability and invariably affect DNA and RNA quality [96, 97]. The variation in the observed viabilities between the Yo-GC and Yo-OC tumor samples in this study, as well as the differences in downstream PCR amplification efficiencies indirectly portray the effects from these extraneous conditions. A relatively good sample viability for the Yo-OC sample however allowed me to examine the tumor-infiltrating T and B cells in the context of Yo-associated ovarian carcinoma, and amplify paired immunoglobulin chains from the tumor-infiltrating B cells for further investigation.

Tumor-infiltrating lymphocytes are recruited to the site of the tumor and the surrounding stroma, and are frequently associated with improved clinical outcomes [98-101]. CD8+ cyotoxic

T cells (CTL) in the tumor microenviroment (TME) can directly recognize and kill tumor cells, through T cell-mediated cytotoxicity via release of perforin and granzyme directly to the tumor [102, 103]. CD4+ T helper (Th) cells on the other hand are essential in supporting CTL expansion and B cell maturation and clonal expansion, through the secretion of various cytokines [104-106]. One hallmark of tumors associated with PCD is intense immune cell infiltrates, usually T cells and plasma cells [57, 107]. The presence of CD3+ T cells identified in both Yo-associated OC and GC in this study potentially signify anti-tumor responses. What proportion of those T cells are CD8+ T cells, and what the frequencies of the subsets of CD4+ T cell are have yet to be explored.

Tumour-infiltrating B cells and plasma cells (PCs), collectively referred to as tumor-infiltrating B lymphocytes (TIL-Bs), have also been linked to antitumor responses. Their presence in several cancer types has been associated with an improved clinical prognosis [37, 108]. Indeed, high densities of intra-epithelial CD8+ T cells have been extensively shown to be associated with improved survival of ovarian cancer patients, but recent studies revealed that their prognostic value is restrained to the presence of other TILs, particularly B cells [109-111]. Early studies in human cancer also show that TIL-B subsets include naïve B cells, activated and memory B cells, GC B cells, and antibody-secreting cells [112, 113]. In Yo-PCD tumors, immune cell infiltrates have been found to be enriched for IgG-secreting plasma cells and plasmablasts, with memory B cells and naïve B cells present only to a lesser extent [114]. This is consistent with the pronounced infiltration of plasmablasts observed in both the Yo-OC and Yo-GC B cell subsets. Furthermore, I found that these plasmablasts were IgG1-switched and highly mutated, suggesting antigen-driven isotype switching and differentiation.

Class switch recombination to IgG1 was observed for virtually all the sequenced plasmablasts from the Yo-OC. IgG antibodies, versus IgM, are functionally more versatile as they can engage in different effector functions such as phagocytosis, antibody-dependent complement deposition (ADCD), antibody-dependent cellular cytotoxicity (ADCC), and FcγR-mediated engagement of innate immune effector cells. Their flexible hinge region compared to IgM antibodies also allows them to navigate more freely, and bivalently bind to their cognate antigens. The predominance of isotype switching to IgG is typically a hallmark of late germinal

centers in response to immunization [115]. The extent of IgG1 class switching observed herein is likely indicative of similar protracted GC responses.

In terms of ontogeny, the high somatic hypermutation loads observed in the plasmablasts from the Yo-OC point to a GC-driven maturation process. However, whether these plasmablasts represent cells on their way to long-lived plasma cell differentiation as end-products of on-going GC reactions, or are rather short-lived plasma cell precursors is uncertain. The absence of CD138 expression, a plasma cell surface marker, in all the cells suggests that they are confined to the plasmablast subset. While it is conceivable that these PBs may be on their way to becoming long-lived plasma cells, the absence of a continuum of CD138 expression that might suggest asynchronous but persistent differentiation towards the PC state, makes it tempting to speculate an alternative ontogeny – that rather than cells on their way to becoming long-lived plasma cells, they may be products of the reactivation of GC-derived IgG-switched memory B cells which have been produced from earlier GC reactions [116] and that the plasmablasts observed herein are merely short-lived plasma cell precursors. This is under the assumption that CD138 on its own is a faithful marker for plasma cells [117, 118], however the expression of other bona fide markers of plasma cells, such as the transcription factors BLIMP1, XBP1, and IRF4, remains to be examined [119]. A pre-existing memory B cell-derived ontogeny however may also be supported by the extent of IgG-switching in the memory B cells from the Yo-OC, with comparable SHM loads to the plasmablast subset.

Earlier studies have described that the plasma cell fate is restricted only to the highest affinity clones, and that the assortment of lower affinity clones get consigned to the memory subset, which maintains high clonal diversity. However, it has been recently shown that germinal centers can also output clonally diverse plasma cells regardless of their affinity [120]. Thus, the immense clonal diversity of TIL-Bs observed in the Yo-OC sample does not offer any further insight with regards to their ontogeny. Nevertheless, the clinical experience that tumor removal, treatment with rituximab, and plasma exchange all result in clinical benefit in some patients without relapse, might support a short-lived plasma cell trajectory for the antibody-secreting cells found in these Yo-PCD patients [53, 121-123]. Not all people who receive antibody-depleting treatments experience the same clinical benefit, however, and it is likely that the clinical picture

spans the two conceptual frameworks, where patients who have not harbored long-lived plasma cell responses are the ones for whom antibody depletion is effective. Single-cell transcriptomic analysis and RNA velocity analyses are recently-established technologies, that when applied to the B cell subsets infiltrating Yo-tumors, may shed light on the true differentiation trajectories of these plasmablasts. The continuum of clinical benefits achieved by antibody depletion likely is confounded by several other factors as well, such as the stage of the disorder and extent of neuronal damage to the cerebellum, and incomplete removal of the antigenic stimulus causing autoantibody production.

In parallel to the predominance of an IgG1-switched plasmablast phenotype, the high levels of SHM highlight antigen-driven GC responses, and is reminiscent of the SHM levels achieved by antigen-specific B cells after vaccination [124] [125, 126]. Where these GC responses primarily occur in Yo-PCD is not yet resolved. Tertiary lymphoid structures are de novo aggregations of lymphocytes – particularly B cells, T cells and follicular dendritic cells – whose organization resembles that of lymph nodes, but are found outside of conventional secondary lymphoid organs [34, 112]. These structures have also been identified in the stroma of tumors, and they house ectopic GCs, which can serve as sites of affinity maturation towards antigens diffusing through the tumor microenvironment.

In ovarian cancers and various other solid tumors, TLSs have been associated with increased tumor-infiltrating antibody-secreting cells and better prognosis [6, 110, 127, 128]. In Yo PCD-associated tumors, even higher levels of immune infiltrates of CD8+ T cells and antibody-secreting cells have been reported, and TLS have been detected in several of these tumors [114]. Whether the highly-mutated plasmablasts and memory B cells observed in our Yo-PCD sample were derived from surrounding tumor-draining lymph nodes or are products of TLS GC reactions, remains to be explored, although it is plausible that both sites of maturation have synergistic contributions. Applying single-cell transcriptomic sequencing on the tumor tissue suspension could reveal transcriptional signatures, such as Bcl-6 expression in tumor-infiltrating B cells, in addition to the presence of DC-LAMP+ dendritic cell and Tfh cell subpopulations, that might hint at GC reactions localized to the TME, and would support the presence of TLSs in the Yo-OC sample. In addition, multiplex immunofluorescence and spatial transcriptomics and spatial

proteomics are recently-developed approaches that could provide image-based confirmation of the presence of these structures and provide further insights into their architectural organization at high resolution [129-133]. The non-capsular structure and proximity of TLSs to tumor cells may also facilitate the presentation of antigens that are minimally abundant or highly context-dependent [112]. Whether this is indeed the case, and the nature of the antigens being taken up in tertiary lymphoid structures – whether tumor-associated antigens, neoantigens or autoantigens – are also open questions. Together with deciphering the differentiation fates of antibody-secreting cells observed in Yo-PCD, understanding the sites where autoantibodies are generated may likely improve therapeutic approaches and help tailor treatment decisions.

Humoral responses to a single antigen generally tend to be mirrored by structural similarities between antibodies to that antigen, and this may be reflected by the predominant usage of specific V genes. Convergent antibody gene features have been observed in some infection or vaccination settings, which have been linked to protection [134-137]. In autoimmune disorders increased frequencies in the usage of certain *VH* genes, such as *IGHV4-34* in RA and SLE, have been observed [138-140]. This can be accompanied by the notable expansion of specific B cell clones, primarily identified by their unique CDR3 amino acid sequence and heavy gene and light gene combinations [141, 142]. With the immense clonal diversity observed in the TIL-Bs sequenced from the Yo ovarian tumor, and with gene usage frequencies not too different from those observed in steady-state peripheral blood immunoglobulin repertoires [143], it may be difficult to conceive that a single antigen is driving these humoral immune responses. The use of single-cell approaches that preserve paired-chain information allows for the interrogation of antibody specificities at monoclonal resolution. Many workflows have been developed to achieve this, each with their advantages and disadvantages [81, 82, 144-148], but all practicable in resolving antibody specificities at single-cell level.

In Yo-PCD, two proteins have been considered as the relevant Yo antigens and targets of Yo autoantibodies. CDR2 was the first Yo antigen to be identified through screening patient sera with HeLa phage libraries [149], while subsequent studies implicate CDR2L as another important Yo antigen [75] [60, 76]. That majority of the antibodies expressed from diverse highly-activated and highly-mutated clones bound to these Yo antigens, was remarkable and unexpected. Despite

the high clonal diversity, convergent reactivity towards Yo antigens among the highly-activated, highly-mutated clones are reminiscent of recall responses from clonally diverse memory B cells after vaccination booster regimens. This supports the prior theory that the Yo OC-infiltrating plasmablasts originated from antigen-experienced memory B cells.

Most of the Yo antigen-specific mAbs tested were not polyreactive, and did not bind to structurally unrelated antigens, highlighting their specificity. Nevertheless, if they originated from polyreactive precursors, which are typically retained at very low frequencies in the mature naïve B cell repertoire [22, 40], is unclear. This could be addressed by reverting these Yo-reactive antibodies to their germline configuration, and reassessing their autoreactivity and polyreactivity. Understanding the origin of Yo-reactive B cells is important, as it allows us to glean where the defects in tolerance might be in Yo-PCD, and where high frequencies of Yo antigen reactivity or polyreactivity even after germline reversion might indicate defects in the pre-immune tolerance checkpoints.

Despite only a small fraction of clones not binding to either Yo antigens, the similarity in the degree of SHM and clonal expansion with Yo-reactive antibodies suggests that B cells with other specificities, presumably towards other tumor-associated antigens, can still undergo GC reactions, and that GC responses are not completely dominated by Yo antigens.

In terms of preferred target of Yo autoantibodies, CDR2L has been put forward as the more relevant antigen by studies that have found higher specificity and sensitivity towards CDR2L in *in vitro* binding assays using Yo-PCD patient-derived polyclonal serum or CSF [60, 75, 76]. Consistent with this notion, majority of the monoclonal antibodies tested in this study by Yo antigen ELISA also targeted CDR2L specifically, and the smaller fraction which displayed detectable CDR2 reactivity were all CDR2L-binders.

The relative abundances of Yo antigens in Yo tumors with respect to each other could directly influence the frequencies of CDR2L-reactive and CDR2-reactive B cells. Absolute quantities of CDR2L and CDR2 in Yo-tumors have not been studied, however a study reporting on gains in CDR2L gene copy numbers but not CDR2 copy numbers in Yo-tumors might imply higher protein levels of CDR2L than CDR2 [114]. The high proportion of CDR2L-specific mAbs found in

this study may indirectly suggest that CDR2L is also more abundant in the Yo-OC sample. Alternatively, higher frequencies of CDR2L-specific follicular T helper cells in the Yo-OC might have facilitated the selection of CDR2L-reactive clones, regardless of CDR2L and CDR2 relative abundances. Assessing the phenotypic composition of T cells infiltrating the Yo-OC, and interrogating their specificities to acquire a more thorough understanding of their contribution to Yo-directed GC responses is equally important.

Both CDR2L and CDR2 have been reported to be prevalently expressed by ovarian cancers, even in neurologically normal patients [59, 67, 68, 71] – an observation supported by my data where high-binding Yo cross-reactive mAbs also showed reactivity to frozen primary ovarian carcinoma sections from a neurologically normal cancer patient. This entails that loss of immune ignorance due to the ectopic expression of Purkinje cell-restricted antigens is not sufficient to induce autoimmunity, and that loss of tolerance happens via some other mechanism. This may re-emphasize the role of autoreactive T cells, where incomplete thymic tolerance in Yo-PCD patients could be a potential contributor to tolerance breakdown.

CDR2 and CDR2L expression has also been reported in an ovarian carcinoma model cell line, OvCar3, which has been extensively used to study the reactivities of patient-derived serum and CSF to these Yo antigens [69-71, 75]. Using the same model cell line, reactivities to CDR2L and CDR2 by Yo tumor-derived mAbs was also demonstrated in this study in immunoprecipitation experiments, representing one of the first studies to investigate the reactivities of Yo-PCD antibodies derived from the tumor. Binding of Yo antigens in the context of a tumor model by Yo OC-derived mAbs, as demonstrated by my data, is consistent with the overarching concept among paraneoplastic syndromes that the associated tumor is the origin and trigger of the autoimmune response.

The immunoprecipitation assays on lysates of OvCar3 cells also facilitated the MS-based identification of the cognate antigens of Yo mAbs, and their potential interaction partners. Apart from both CDR2 and CDR2L as the top hits, TRIM21, a cytosolic ubiquitin ligase and an intracellular Fc receptor, was also identified to be co-immunoprecipitated. TRIM21 is ubiquitously expressed by many cell types, and targets internalized IgGs and their bound cognate

antigens for degradation in an Fc-dependent manner [150]. This is typically a protective mechanism against antibody-bound virus particles that have escaped elimination from the extracellular space and have managed to make their way in the cell [151, 152]. Although a functional role of TRIM21 in autoimmunity, particularly in paraneoplastic syndromes where an immune response is commonly directed to intracellular antigens, is not yet established, its potential to mediate antibody-mediated intracellular protein degradation as a consequence of autoantibody targeting will be an interesting concept to revisit if an antibody-mediated pathogenic contribution in disorders like Yo-PCD gets substantiated.

Further insights from the immunoprecipitation experiments have stemmed from the detection of CDR2 reactivity in the immunoprecipitation experiments, even among mAbs identified to be CDR2L-specific by Yo antigen ELISA, which prompted the re-examination of the specificities of CDR2L-specific and Yo non-reactive mAbs. The absence of observable reactivity from the Yo antigen ELISA screening was likely due to weak binding to CDR2, in the case of CDR2L-specific mAbs, or to both in the case of some non-reactive antibodies, that were beyond the sensitivity thresholds of conventional indirect ELISA approaches. Using a more sensitive ELISA format where pre-crosslinking of the experimental mAbs to the HRP-labelled secondary antibody increases potential avidity to coated antigens in close proximity to each other, a small fraction of mAbs classified as “non Yo-reactive” demonstrated Yo antigen cross-reactivity, and insinuate that conventional binding assays are often likely not sensitive enough to identify such weak binding interactions.

The side benefit of testing for antigen reactivity in this high-sensitivity format is that it might also reflect the physiological situation where B cells might encounter their cognate antigens in close proximity to each other, either as processed antigens on conventional dendritic cells or immune complexes on follicular dendritic cells, such that avidity effects come into play. This is a likely scenario if antigens are highly abundant in local lymph nodes or tertiary lymphoid structures. One limitation of this assay however is that it was done on single-well measurements instead of titrated mAb concentrations. The implication of this is that signals above the defined threshold only gives a binary insight about weak cross-binding, and signal intensities should not be interpreted as a reflection of actual binding affinities, as in the case of some CDR2L-specific

mAbs which appeared to have a higher proclivity to bind to CDR2 when looking at these single-well OD values only, but in parallel tests using the conventional indirect ELISA, still displayed strong binding to CDR2L.

In the context of GC responses, the ability to cross-bind both Yo antigens might substantiate that, even though the twenty-three CDR2L-specific mAbs found to be cross-reactive have presumably lower affinities to CDR2, avidity effects towards CDR2 might have endowed B cells bearing these immunoglobulin receptors with the same edge to participate in GC reactions as B cells bearing Yo cross-reactive immunoglobulin receptors. This notion is provisionally supported by my data where mean total SHM counts and degree of clonal expansion are also not significantly different between CDR2L-specific and Yo cross-reactive mAbs (Figure 10C and 10D). How the relative abundance of CDR2 and CDR2L in Yo-associated tumors affects antigen-driven GC responses is again an additional factor to be considered, and advances in spatial-omics technologies might also be an avenue to interrogate levels of antigen and their distribution in Yo-tumors in addition to detection of TLSs.

As CDR2 and CDR2L share high protein sequence homology, particularly in the first third of their sequences [1, 75], the relative effectivity of CDR2-based Yo-PCD diagnostic panels might be explained by the detection of cross-reactive antibodies to overlapping epitopes. Examination of binding modes between two Yo high-binding cross-reactive mAbs, reveal that they target overlapping linear epitopes, that is likely constrained to the regions of high homology between CDR2 and CDR2L. Affinity measurements of the two mAbs to CDR2 and CDR2L however reveal higher affinities toward CDR2L for both, implying that the fine differences in amino acid composition within the region of high homology still influences binding preference.

The evaluation of competitive binding with the other mAbs also depicts distinct modes of binding when compared to the Yo high-binding cross-reactive antibodies. Curiously, some cross-reactive mAbs in the Q1 bin, representing competitive binding to epitopes on CDR2, do not seem to interfere with CDR2L binding of the Yo high-binding cross-reactive mAb P2_1125. This may mean that they potentially target a distinct epitope on CDR2L, or it is also possible that P2_1125 simply has a higher affinity to CDR2L, and thus is still able to outcompete the other. This might

also explain the presence of CDR2L-specific and cross-reactive mAbs in non-competitive binding modes (Q2), where higher affinity of P2_1125 to the two Yo antigens may simple outcompete those mAbs for the respective epitopes. It can however be the case that some of these mAbs do target distinct epitopes on CDR2 and/or CDR2L as well. To comprehensively evaluate different modes of binding, the nature of the targeted epitope – whether linear or conformational – needs to be determined, and binding affinities of the mAbs need to be accounted for in blocking ELISAs. Fine mapping can then be carried out by testing reactivity to peptide subunits of CDR2 and CDR2L. Resolving different epitopes targeted by Yo autoantibodies will help facilitate a more refined interpretation of CDR2 or CDR2L reactivities, especially in studies that have used commercially-derived polyclonal antibodies that are raised on specific epitopes of the Yo antigens, or that have used patient-derived sera, from which results on CDR2 or CDR2L binding may be confounded by cross-binding effects or absence thereof. Inclusion of relevant target epitopes of Yo autoantibodies in Yo-PCD diagnostic panels will also likely improve the sensitivity of these tests, if in fact CDR2L is the major target, and if indeed Yo cross-reactive antibodies are also abundant in other Yo-PCD patients.

Regarding their subcellular localization, Yo antigens have been described to be located intracellularly [68, 69, 75, 90]. Early insights into their function were surmised from their reported subcellular localization, where CDR2L was confined to the cytoplasm and endoplasmic reticulum in the perinuclear space and was found to associate with ribosomal proteins suggesting a role in translation [69]. On the other hand, CDR2 has been detected in nuclear speckles [69], which are nuclear bodies that are reported to play a role in transcription [72, 73, 153, 154]. Intracellular staining of permeabilized OvCar3 cells with the high-binding Yo cross-reactive mAbs in this study show cytoplasmic staining which appreciably intensifies in the perinuclear space and is only marginally noticeable in the nucleus, consistent with studies that used the same model cell line [69, 76]). Nuclear speckles however were not as prominent using the high-binding Yo cross-reactive mAbs, likely because the commercial antibodies used in that study was polyclonally raised against only part of the CDR2 protein (amino acids 270-392), which is outside of the region of high homology with CDR2L [69]. Interestingly, one weakly cross-reactive mAb gave a distinct

staining pattern that was only localized to the nucleus, suggesting that it might be staining CDR2 more effectively in OvCar3 cells.

The expression of Yo antigens is typically restricted to cerebellar cells, and is most prominent on Purkinje cells in humans and mice, which are the primary targets of the autoimmune response in Yo-PCD [54, 67, 76]. The high homology between the CDR2 and CDR2L protein sequences across humans and rodents suggests their similar functions across species, and enables the detection of Yo antigens in rodent sections using immunolabeling techniques. The binding to Yo antigens in Purkinje cells by Yo high-binding cross-reactive mAbs indicate that these antibodies are also able to target Yo antigens in the neuronal context. The notable staining of the monolayer of Purkinje cells is accordant with staining patterns observed in other studies using patient-derived polyclonal sera or CSF [54, 155] [69, 107]. The absence of this Purkinje layer in the cerebellum is a hallmark of Yo-PCD patient brain biopsies, and is the main cause of motor dysfunction.

Unexpectedly, patterns resembling the staining of the astrocyte marker GFAP were observed for one Yo high-binding cross-reactive mAb. I observed this astrocytic staining to be most prominent in the glia limitans – a barrier structure surrounded by astrocytes – and may suggest that Yo antigens are expressed by astrocytes below detectable thresholds, and may only be perceptible when probing with a very high-affine antibody. The alternative is that the Yo high-binding cross-reactive mAb binds to another antigen expressed by astrocytes. Interestingly, GFAP autoantibodies have also been linked to autoimmune GFAP astrocytopathies, which may also present as ataxia and movement disorders [156-158]. The cross-expression of Yo antigen on neurons, or potential cross-reactivities of Yo autoantibodies to other neuronal antigens have important implications, and may provide additional insight into the pathogenesis or progression of Yo-PCD and other related disorders.

The uptake of antibodies by neurons has been reported in other disease contexts, such as Alzheimer's disease, and other subtypes of PCD, such as Hu-PCD [159, 160]. In Yo-PCD, the uptake of Yo patient-derived IgGs by Purkinje cells has been studied and reported in mice after systemic administration and blood brain barrier disruption, and in *ex vivo* cerebellar slice cultures

[161, 162]. In the *ex vivo* cerebellar slice culture models, uptake of patient-derived polyclonal IgG was found to cause Purkinje cell cytotoxicity [92]. This observation was also what prompted contentious debates and further investigations about the pathogenic contribution of antibodies in Yo-associated paraneoplastic cerebellar degeneration. In the absence of Purkinje model cell lines, primary mixed *in vitro* cerebellar cultures were established in this study to assess whether high-binding Yo cross-reactive mAbs are also taken up by Purkinje cells. The uptake of high-binding cross-reactive monoclonal antibodies by Purkinje cells in the established *in vitro* model here independently confirms previous observations of Purkinje cell Yo- antibody uptake. Interestingly, it was found that Purkinje cells can take up IgGs with other specificities, but they do not cause the same Purkinje cell cytotoxicity mediated by Yo patient-derived antibodies [93]. Adsorption of Yo patient sera with CDR2, and subsequent incubation with slice cultures abolished the cytotoxic effect on Purkinje cells [93]. Interestingly, the effectivity of CDR2 in the adsorption experiments might suggest that CDR2 is the main target of Yo autoantibodies in Purkinje cells, or alternatively, that antibodies targeting the same epitopes on CDR2 and CDR2L were conjointly sequestered, implicating Yo cross-reactivity as an important feature in driving cytotoxicity.

An open question about the uptake of IgG's by neurons is naturally through what mechanism this happens. The advantage of using primary *in vitro* cerebellar cultures is that mechanistic theories can be tested in more controlled settings. Monoclonal antibody uptake experiments co-administered with general endocytosis blockers or specific Fc-receptor blockers might lend more insight into how antibodies enter Purkinje cells. Neurons for example have been reported to express Fcγ receptors, and the uptake of Tau antibodies has been described to be a clathrin-dependent Fcγ receptor-mediated process, which is specifically mediated by FcγRII and FcγRIII [159].

One limitation of the established murine-derived *in vitro* model however is that mouse and human FcγRs have different binding affinities and expression patterns from each other [163]. Interestingly, mouse FcγRs are able to efficiently to bind human IgG subclasses, whereas human FcγRs and FcRn do not, or only very poorly bind to the mouse IgG counterparts. The observed uptake of human IgG1 mAbs by murine-derived Purkinje cells *in vitro* could thus represent an uptake process that does not depend on good IgG-Fcγ receptor interactions; or is an Fcγ-

receptor-independent process altogether. Alternatively, murine Fcγ receptors that can efficiently bind to human IgG1 may be involved. Curiously, uptake of disease-associated Ri antibodies in Ri-associated PCD fail to induce neuronal cytotoxicity using similar *ex vivo* slice culture incubation experiments, indicating that although antibody uptake may be a more general phenomenon in neurons, the functional role of the intracellular target likely determines whether uptake will have consequential effects to the cell [160].

In a top down approach, the potential pathogenic contribution of Yo high-binding cross-reactive mAbs were directly assesses *in vivo* in mice, using an antibody administration system that allows for mAbs to be directly delivered to the CNS. This system has been used to demonstrate that $GABA_A$ monoclonal antibodies causes epileptic seizures in mice after intrathecal *in vivo* delivery [50], and the direct intrathecal delivery circumvents the interfering effects that may be imposed by an intact blood brain barrier. The accumulation of Yo high-binding cross-reactive antibodies in the Purkinje cell body was observed in the cerebellar section of a mouse harvested after continuous intrathecal mAb delivery, demonstrating uptake of IgGs by Purkinje cells in a live animal (Supplementary Figure 11). How stable this uptake is remains to be established by observing the brains of more animals, after continuous intrathecal delivery.

In relation to pathological effects on the motor system, Yo-PCD patients often exhibit severe ataxia characterized by impaired balance and coordination. The rotarod assay is a motor-behavioral test that evaluates aspects related to balance and coordination, and has been a commonly-used approach to detect cerebellar dysfunction in mice [164, 165]. Results of this motor-behavioral test may however be confounded by factors extraneous to motor function, such as the reliance on claws to cling on to and rotate with the rod, differences in weight that might affect latency time independent of motor ability, or learned adaptation behaviors such as identifying that falling from the rod does not have harmful consequences [166]. Despite these potential confounders, the observable effects after intrathecal delivery of Yo high-binding cross-reactive mAbs suggest an antigen-specific impairment of motor function induced after IgG uptake, and strongly argues for a pathogenic contribution of Yo autoantibodies. One measure to further improve the assay and reduce variability between measurements within the same treatment group might be to further optimize the period of delivery and timepoint of evaluation,

where perhaps the delivery period should not be overly prolonged, as less mAbs might be delivered in later timepoints due to natural rates of decay in the system over the course of delivery; or conversely, mAbs being highly-stable molecules, might accumulate in the system over time, causing impalpable side effects that could confound the motor readout. Orthogonal motor function assays should be carried out to corroborate the observed effects of these Yo high-binding cross-reactive mAbs, and clarify which specific motor circuits are being impaired. Overall, the results presented here so far represents one of the first studies to extensively characterize Yo autoantibodies at monoclonal level, and is the first to demonstrate Yo antibody-mediated pathogenic effects on motor function *in vivo.*

7 Outlook

For my dissertation, I aimed to resolve long-standing questions about the neuropathological contributions of antibodies in Yo-associated paraneoplastic cerebellar degeneration by examining the B cells from the associated tumor. In as much as some doors are closer to being closed, a lot of windows – that is, questions about the underlying immunobiology – have been opened.

Firstly, the extensive infiltration of the Yo ovarian carcinoma by plasmablasts that secrete Yo autoantibodies begs the question of fate – are they differentiating to become short-lived plasma cells, or will they home to the bone marrow and live on as long-lived plasma cells, producing autoantibodies throughout their lifetime? This has direct implications on how these patients might be treated, and whether antibody-depleting therapies would be beneficial for them.

In terms of origin, the highly-mutated and IgG-switched nature of these Yo-specific plasmablasts suggests that they are derived from pre-existing memory B cells. Whether this observation correlates with the stage of the tumor, and if earlier tumor stages harbor B cells and antibody-secreting cells with different features, is an open question.

The logical question that follows is where the sites of maturation are – specifically, where do the GC responses occur? Do they happen in conventional secondary lymphoid organs such as the tumor-draining lymph nodes, or do they happen in tertiary lymph structures within the tumor stroma? Are there genetic alterations in the Yo antigens CDR2 and CDR2L expressed by the tumor, as other have described? These are all questions that the recently-developed single-cell transcriptomics and high-resolution spatial-omics technologies could help address.

Additionally, would these affinity-matured cells still retain their Yo autoreactivity in their germline configuration? This lends insights into whether defects in tolerance occur in the early or GC checkpoints.

The discovery in my study that most of the Yo tumor-derived antibodies target CDR2L with high-affinity, but also CDR2 with weaker affinities, supports the notion of CDR2L being the major Yo antigen. But whether sequestration of CDR2L alone by antibodies also leads to the same pathological outcome in Purkinje cells, is yet to be settled.

Interrogating Yo antigen reactivity has also revealed the limitations of different binding assays, such that the weak Yo cross-reactivities would not have been detected if orthogonal binding tests were not carried out; but in the same vein also highlights the advantage of assessing reactivities at monoclonal resolution. Observations in this study that suggest different modes of binding by Yo autoantibodies also warrants mapping the specific epitopes that Yo autoantibodies target, which has implications both in the research and diagnostic setting. Taking all these into account would be essential in understanding functional and structural aspects about the Yo antigens and Yo autoantibodies, and ultimately in answering more mechanistic questions about Yo-PCD.

Towards the question of whether Yo autoantibodies have a pathogenic contribution, determining the exact mechanism of uptake, and resolving whether they would lead to the same functional consequences in Purkinje cells in *in vitro* systems would provide a lot of insight about the contentious role of autoantibodies in Yo-PCD.

This study is the first to demonstrate antibody-mediated motor dysfunction in mice, by Yo autoantibodies that target both CDR2L and CDR2. Whether Yo cross-reactivity is a necessary feature to elicit pathological consequences, or whether CDR2L-targeting antibodies alone would also mediate the same motor outcome, remains to be answered and would help resolve which of the two is the major Yo antigen.

Finally, whether the paradigms observed here are generalizable to other Yo-PCD patients, or whether these features are tightly linked to the tumor type, tumor stage, and extent of neurological dysfunction would only be answered by using the same approaches employed here to more patients in the future.

8 References

1. Yshii, L., C. Bost, and R. Liblau, *Immunological Bases of Paraneoplastic Cerebellar Degeneration and Therapeutic Implications.* Front Immunol, 2020. **11**: p. 991.
2. Greenlee, J.E., et al., *Paraneoplastic and Other Autoimmune Encephalitides: Antineuronal Antibodies, T Lymphocytes, and Questions of Pathogenesis.* Front Neurol, 2021. **12**: p. 744653.
3. Han, F., et al., *Antigen receptor structure and signaling.* Adv Immunol, 2023. **157**: p. 1-28.
4. De Silva, N.S. and U. Klein, *Dynamics of B cells in germinal centres.* Nat Rev Immunol, 2015. **15**(3): p. 137-48.
5. Batista, F.D. and N.E. Harwood, *The who, how and where of antigen presentation to B cells.* Nat Rev Immunol, 2009. **9**(1): p. 15-27.
6. Helmink, B.A., et al., *B cells and tertiary lymphoid structures promote immunotherapy response.* Nature, 2020. **577**(7791): p. 549-555.
7. Brezski, R.J. and J.G. Monroe, *B-cell receptor.* Adv Exp Med Biol, 2008. **640**: p. 12-21.
8. Wang, Y., et al., *B Cell Development and Maturation.* Adv Exp Med Biol, 2020. **1254**: p. 1-22.
9. Hardy, R.R. and K. Hayakawa, *B cell development pathways.* Annu Rev Immunol, 2001. **19**: p. 595-621.
10. Pieper, K., B. Grimbacher, and H. Eibel, *B-cell biology and development.* J Allergy Clin Immunol, 2013. **131**(4): p. 959-71.
11. Amin, R.H. and M.S. Schlissel, *Foxo1 directly regulates the transcription of recombination-activating genes during B cell development.* Nat Immunol, 2008. **9**(6): p. 613-22.
12. LeBien, T.W. and T.F. Tedder, *B lymphocytes: how they develop and function.* Blood, 2008. **112**(5): p. 1570-80.
13. LeBien, T.W., *Fates of human B-cell precursors.* Blood, 2000. **96**(1): p. 9-23.
14. Nemazee, D., *Mechanisms of central tolerance for B cells.* Nat Rev Immunol, 2017. **17**(5): p. 281-294.
15. Saijo, K., et al., *Essential role of Src-family protein tyrosine kinases in NF-kappaB activation during B cell development.* Nat Immunol, 2003. **4**(3): p. 274-9.
16. Schlissel, M., *Allelic exclusion of immunoglobulin gene rearrangement and expression: why and how?* Semin Immunol, 2002. **14**(3): p. 207-212; discussion 225-6.
17. Thien, M., et al., *Excess BAFF rescues self-reactive B cells from peripheral deletion and allows them to enter forbidden follicular and marginal zone niches.* Immunity, 2004. **20**(6): p. 785-98.
18. Rowland, S.L., et al., *BAFF receptor signaling aids the differentiation of immature B cells into transitional B cells following tonic BCR signaling.* J Immunol, 2010. **185**(8): p. 4570-81.
19. Inoue, T. and T. Kurosaki, *Memory B cells.* Nat Rev Immunol, 2024. **24**(1): p. 5-17.
20. Roco, J.A., et al., *Class-Switch Recombination Occurs Infrequently in Germinal Centers.* Immunity, 2019. **51**(2): p. 337-350 e7.
21. Victora, G.D. and M.C. Nussenzweig, *Germinal Centers.* Annu Rev Immunol, 2022. **40**: p. 413-442.
22. Sun, B., et al., *The B cell immunobiology that underlies CNS autoantibody-mediated diseases.* Nat Rev Neurol, 2020. **16**(9): p. 481-492.
23. Casellas, R., et al., *Contribution of receptor editing to the antibody repertoire.* Science, 2001. **291**(5508): p. 1541-4.
24. Tsubata, T., *B-cell tolerance and autoimmunity.* F1000Res, 2017. **6**: p. 391.
25. Cambier, J.C., et al., *B-cell anergy: from transgenic models to naturally occurring anergic B cells?* Nat Rev Immunol, 2007. **7**(8): p. 633-43.

26. Wardemann, H. and M.C. Nussenzweig, *B-cell self-tolerance in humans.* Adv Immunol, 2007. **95**: p. 83-110.
27. Cyster, J.G., S.B. Hartley, and C.C. Goodnow, *Competition for follicular niches excludes self-reactive cells from the recirculating B-cell repertoire.* Nature, 1994. **371**(6496): p. 389-95.
28. Cambier, J.C. and A. Getahun, *B cell activation versus anergy; the antigen receptor as a molecular switch.* Immunol Lett, 2010. **128**(1): p. 6-7.
29. Burnett, D.L., et al., *Clonal redemption and clonal anergy as mechanisms to balance B cell tolerance and immunity.* Immunol Rev, 2019. **292**(1): p. 61-75.
30. Yarkoni, Y., A. Getahun, and J.C. Cambier, *Molecular underpinning of B-cell anergy.* Immunol Rev, 2010. **237**(1): p. 249-63.
31. Zikherman, J., R. Parameswaran, and A. Weiss, *Endogenous antigen tunes the responsiveness of naive B cells but not T cells.* Nature, 2012. **489**(7414): p. 160-4.
32. Shlomchik, M.J., *Sites and stages of autoreactive B cell activation and regulation.* Immunity, 2008. **28**(1): p. 18-28.
33. Platt, J.L., M. Garcia de Mattos Barbosa, and M. Cascalho, *The five dimensions of B cell tolerance.* Immunol Rev, 2019. **292**(1): p. 180-193.
34. Vinuesa, C.G., I. Sanz, and M.C. Cook, *Dysregulation of germinal centres in autoimmune disease.* Nat Rev Immunol, 2009. **9**(12): p. 845-57.
35. Rawlings, D.J., et al., *Altered B cell signalling in autoimmunity.* Nat Rev Immunol, 2017. **17**(7): p. 421-436.
36. Chan, T.D., et al., *Elimination of germinal-center-derived self-reactive B cells is governed by the location and concentration of self-antigen.* Immunity, 2012. **37**(5): p. 893-904.
37. Sng, J., et al., *AIRE expression controls the peripheral selection of autoreactive B cells.* Sci Immunol, 2019. **4**(34).
38. Young, C. and R. Brink, *Germinal centers and autoantibodies.* Immunol Cell Biol, 2020. **98**(6): p. 480-489.
39. Ma, H., et al., *Autoantibodies - enemies, and/or potential allies?* Front Immunol, 2022. **13**: p. 953726.
40. Wardemann, H., et al., *Predominant autoantibody production by early human B cell precursors.* Science, 2003. **301**(5638): p. 1374-7.
41. Pisetsky, D.S., *Pathogenesis of autoimmune disease.* Nat Rev Nephrol, 2023. **19**(8): p. 509-524.
42. Shao, W.H. and P.L. Cohen, *Disturbances of apoptotic cell clearance in systemic lupus erythematosus.* Arthritis Res Ther, 2011. **13**(1): p. 202.
43. Dalmau, J. and M.R. Rosenfeld, *Paraneoplastic syndromes of the CNS.* Lancet Neurol, 2008. **7**(4): p. 327-40.
44. Graus, F. and J. Dalmau, *Paraneoplastic neurological syndromes in the era of immune-checkpoint inhibitors.* Nat Rev Clin Oncol, 2019. **16**(9): p. 535-548.
45. Binks, S., et al., *Paraneoplastic neurological syndromes: a practical approach to diagnosis and management.* Pract Neurol, 2022. **22**(1): p. 19-31.
46. Graus, F., et al., *Updated Diagnostic Criteria for Paraneoplastic Neurologic Syndromes.* Neurol Neuroimmunol Neuroinflamm, 2021. **8**(4).
47. Darnell, R.B. and J.B. Posner, *Paraneoplastic syndromes involving the nervous system.* N Engl J Med, 2003. **349**(16): p. 1543-54.
48. Pelosof, L.C. and D.E. Gerber, *Paraneoplastic syndromes: an approach to diagnosis and treatment.* Mayo Clin Proc, 2010. **85**(9): p. 838-54.
49. Pruss, H., *Autoantibodies in neurological disease.* Nat Rev Immunol, 2021. **21**(12): p. 798-813.
50. Kreye, J., et al., *Encephalitis patient-derived monoclonal GABAA receptor antibodies cause epileptic seizures.* J Exp Med, 2021. **218**(11).

51. Kreye, J., et al., *Human cerebrospinal fluid monoclonal N-methyl-D-aspartate receptor autoantibodies are sufficient for encephalitis pathogenesis.* Brain, 2016. **139**(Pt 10): p. 2641-2652.
52. Wenke, N.K., et al., *N-methyl-D-aspartate receptor dysfunction by unmutated human antibodies against the NR1 subunit.* Ann Neurol, 2019. **85**(5): p. 771-776.
53. Shams'ili, S., et al., *An uncontrolled trial of rituximab for antibody associated paraneoplastic neurological syndromes.* J Neurol, 2006. **253**(1): p. 16-20.
54. Greenlee, J.E. and H.R. Brashear, *Antibodies to cerebellar Purkinje cells in patients with paraneoplastic cerebellar degeneration and ovarian carcinoma.* Ann Neurol, 1983. **14**(6): p. 609-13.
55. Hammack, J.E., et al., *Paraneoplastic cerebellar degeneration: a clinical comparison of patients with and without Purkinje cell cytoplasmic antibodies.* Mayo Clin Proc, 1990. **65**(11): p. 1423-31.
56. Hoftberger, R., M.R. Rosenfeld, and J. Dalmau, *Update on neurological paraneoplastic syndromes.* Curr Opin Oncol, 2015. **27**(6): p. 489-95.
57. Peterson, K., et al., *Paraneoplastic cerebellar degeneration. I. A clinical analysis of 55 anti-Yo antibody-positive patients.* Neurology, 1992. **42**(10): p. 1931-7.
58. Loehrer, P.A., L. Zieger, and O.J. Simon, *Update on Paraneoplastic Cerebellar Degeneration.* Brain Sci, 2021. **11**(11).
59. Albert, M.L., L.M. Austin, and R.B. Darnell, *Detection and treatment of activated T cells in the cerebrospinal fluid of patients with paraneoplastic cerebellar degeneration.* Ann Neurol, 2000. **47**(1): p. 9-17.
60. Herdlevaer, I., et al., *Paraneoplastic Cerebellar Degeneration: The Importance of Including CDR2L as a Diagnostic Marker.* Neurol Neuroimmunol Neuroinflamm, 2021. **8**(2).
61. Faure, F., et al., *A Pilot Study to Develop Paraneoplastic Cerebellar Degeneration Mouse Model.* Cerebellum, 2024. **23**(1): p. 181-196.
62. Tanaka, M., et al., *Trial to establish an animal model of paraneoplastic cerebellar degeneration with anti-Yo antibody. 1. Mouse strains bearing different MHC molecules produce antibodies on immunization with recombinant Yo protein, but do not cause Purkinje cell loss.* Clin Neurol Neurosurg, 1995. **97**(1): p. 95-100.
63. Candler, P.M., et al., *A follow up study of patients with paraneoplastic neurological disease in the United Kingdom.* J Neurol Neurosurg Psychiatry, 2004. **75**(10): p. 1411-5.
64. Venkatraman, A. and P. Opal, *Paraneoplastic cerebellar degeneration with anti-Yo antibodies - a review.* Ann Clin Transl Neurol, 2016. **3**(8): p. 655-63.
65. Shams'ili, S., et al., *Paraneoplastic cerebellar degeneration associated with antineuronal antibodies: analysis of 50 patients.* Brain, 2003. **126**(Pt 6): p. 1409-18.
66. Albert, M.L., et al., *Tumor-specific killer cells in paraneoplastic cerebellar degeneration.* Nat Med, 1998. **4**(11): p. 1321-4.
67. Darnell, J.C., M.L. Albert, and R.B. Darnell, *Cdr2, a target antigen of naturally occuring human tumor immunity, is widely expressed in gynecological tumors.* Cancer Res, 2000. **60**(8): p. 2136-9.
68. Totland, C., et al., *CDR2 antigen and Yo antibodies.* Cancer Immunol Immunother, 2011. **60**(2): p. 283-9.
69. Herdlevaer, I., et al., *Localization of CDR2L and CDR2 in paraneoplastic cerebellar degeneration.* Ann Clin Transl Neurol, 2020. **7**(11): p. 2231-2242.
70. Raspotnig, M., et al., *Expression of cerebellar degeneration-related proteins CDR2 and CDR2L in human and rat brain tissue.* J Neuroimmunol, 2022. **362**: p. 577766.
71. Raspotnig, M., et al., *Cerebellar degeneration-related proteins 2 and 2-like are present in ovarian cancer in patients with and without Yo antibodies.* Cancer Immunol Immunother, 2017. **66**(11): p. 1463-1471.

72. Sakai, K., et al., *Interaction of a paraneoplastic cerebellar degeneration-associated neuronal protein with the nuclear helix-loop-helix leucine zipper protein MRG X.* Mol Cell Neurosci, 2002. **19**(4): p. 477-84.
73. O'Donovan, K.J., et al., *The onconeural antigen cdr2 is a novel APC/C target that acts in mitosis to regulate c-myc target genes in mammalian tumor cells.* PLoS One, 2010. **5**(4): p. e10045.
74. Schubert, M., et al., *Paraneoplastic CDR2 and CDR2L antibodies affect Purkinje cell calcium homeostasis.* Acta Neuropathol, 2014. **128**(6): p. 835-52.
75. Eichler, T.W., et al., *CDR2L Antibodies: A New Player in Paraneoplastic Cerebellar Degeneration.* PLoS One, 2013. **8**(6): p. e66002.
76. Krakenes, T., et al., *CDR2L Is the Major Yo Antibody Target in Paraneoplastic Cerebellar Degeneration.* Ann Neurol, 2019. **86**(2): p. 316-321.
77. Furneaux, H.M., et al., *Selective expression of Purkinje-cell antigens in tumor tissue from patients with paraneoplastic cerebellar degeneration.* N Engl J Med, 1990. **322**(26): p. 1844-51.
78. Greenlee, J.E. and N.G. Carlson, *CDR2 and CDR2L Yo Antigens in Paraneoplastic Cerebellar Degeneration.* Ann Neurol, 2020. **88**(2): p. 428.
79. Zavala, F., et al., *Circumsporozoite proteins of malaria parasites contain a single immunodominant region with two or more identical epitopes.* The Journal of experimental medicine, 1983. **157**(6): p. 1947-1957.
80. Triller, G., et al., *Natural parasite exposure induces protective human anti-malarial antibodies.* Immunity, 2017. **47**(6): p. 1197-1209. e10.
81. Busse, C.E., et al., *Single-cell based high-throughput sequencing of full-length immunoglobulin heavy and light chain genes.* Eur J Immunol, 2014. **44**(2): p. 597-603.
82. Murugan, R., et al., *Direct high-throughput amplification and sequencing of immunoglobulin genes from single human B cells.* Eur J Immunol, 2015. **45**(9): p. 2698-700.
83. Masella, A.P., et al., *PANDAseq: paired-end assembler for illumina sequences.* BMC bioinformatics, 2012. **13**: p. 1-7.
84. Busse, C.E., et al., *Single-cell based high-throughput sequencing of full-length immunoglobulin heavy and light chain genes.* European journal of immunology, 2014. **44**(2): p. 597-603.
85. Imkeller, K., et al., *sciReptor: analysis of single-cell level immunoglobulin repertoires.* BMC Bioinformatics, 2016. **17**: p. 67.
86. Ye, J., et al., *IgBLAST: an immunoglobulin variable domain sequence analysis tool.* Nucleic acids research, 2013. **41**(W1): p. W34-W40.
87. Oludada, O.E., et al., *Molecular and functional properties of human Plasmodium falciparum CSP C-terminus antibodies.* EMBO Mol Med, 2023. **15**(6): p. e17454.
88. Li, L.Y., et al., *Brain blood vessel autoantibodies in patients with NMDA and GABA(A) receptor encephalitis: identification of unconventional Myosin-X as target antigen.* Front Cell Neurosci, 2023. **17**: p. 1077204.
89. Bunger, I., et al., *Synapsin autoantibodies during pregnancy are associated with fetal abnormalities.* Brain Behav Immun Health, 2023. **33**: p. 100678.
90. Corradi, J.P., et al., *A post-transcriptional regulatory mechanism restricts expression of the paraneoplastic cerebellar degeneration antigen cdr2 to immune privileged tissues.* J Neurosci, 1997. **17**(4): p. 1406-15.
91. Greenlee, J.E., et al., *Editorial: Autoimmunity and the Brain: Paraneoplastic Neurological Injury and Beyond.* Front Neurol, 2022. **13**: p. 900130.
92. Greenlee, J.E., et al., *Purkinje cell death after uptake of anti-Yo antibodies in cerebellar slice cultures.* J Neuropathol Exp Neurol, 2010. **69**(10): p. 997-1007.
93. Greenlee, J.E., et al., *Anti-Yo antibody uptake and interaction with its intracellular target antigen causes Purkinje cell death in rat cerebellar slice cultures: a possible mechanism for*

paraneoplastic cerebellar degeneration in humans with gynecological or breast cancers. PLoS One, 2015. **10**(4): p. e0123446.
94. Mosele, F., et al., *Recommendations for the use of next-generation sequencing (NGS) for patients with metastatic cancers: a report from the ESMO Precision Medicine Working Group.* Ann Oncol, 2020. **31**(11): p. 1491-1505.
95. Endrullat, C., et al., *Standardization and quality management in next-generation sequencing.* Appl Transl Genom, 2016. **10**: p. 2-9.
96. Liu, X., et al., *Clinical challenges of tissue preparation for spatial transcriptome.* Clin Transl Med, 2022. **12**(1): p. e669.
97. Kucharski, M., et al., *A comprehensive RNA handling and transcriptomics guide for high-throughput processing of Plasmodium blood-stage samples.* Malar J, 2020. **19**(1): p. 363.
98. Hudry, D., et al., *Tumor-Infiltrating Lymphocytes (TILs) in Epithelial Ovarian Cancer: Heterogeneity, Prognostic Impact, and Relationship with Immune Checkpoints.* Cancers (Basel), 2022. **14**(21).
99. Schatton, T., et al., *Tumor-infiltrating lymphocytes and their significance in melanoma prognosis.* Methods Mol Biol, 2014. **1102**: p. 287-324.
100. Maibach, F., et al., *Tumor-Infiltrating Lymphocytes and Their Prognostic Value in Cutaneous Melanoma.* Front Immunol, 2020. **11**: p. 2105.
101. Stanton, S.E. and M.L. Disis, *Clinical significance of tumor-infiltrating lymphocytes in breast cancer.* J Immunother Cancer, 2016. **4**: p. 59.
102. Farhood, B., M. Najafi, and K. Mortezaee, *CD8(+) cytotoxic T lymphocytes in cancer immunotherapy: A review.* J Cell Physiol, 2019. **234**(6): p. 8509-8521.
103. Whiteside, T.L., *Tumor-Infiltrating Lymphocytes and Their Role in Solid Tumor Progression.* Exp Suppl, 2022. **113**: p. 89-106.
104. Zhu, J. and W.E. Paul, *Peripheral CD4+ T-cell differentiation regulated by networks of cytokines and transcription factors.* Immunol Rev, 2010. **238**(1): p. 247-62.
105. Knutson, K.L. and M.L. Disis, *Tumor antigen-specific T helper cells in cancer immunity and immunotherapy.* Cancer Immunol Immunother, 2005. **54**(8): p. 721-8.
106. Kalams, S.A. and B.D. Walker, *The critical need for CD4 help in maintaining effective cytotoxic T lymphocyte responses.* J Exp Med, 1998. **188**(12): p. 2199-204.
107. Verschuuren, J., et al., *Inflammatory infiltrates and complete absence of Purkinje cells in anti-Yo-associated paraneoplastic cerebellar degeneration.* Acta Neuropathol, 1996. **91**(5): p. 519-25.
108. Paijens, S.T., et al., *Tumor-infiltrating lymphocytes in the immunotherapy era.* Cell Mol Immunol, 2021. **18**(4): p. 842-859.
109. Sato, E., et al., *Intraepithelial CD8+ tumor-infiltrating lymphocytes and a high CD8+/regulatory T cell ratio are associated with favorable prognosis in ovarian cancer.* Proc Natl Acad Sci U S A, 2005. **102**(51): p. 18538-43.
110. Kroeger, D.R., K. Milne, and B.H. Nelson, *Tumor-Infiltrating Plasma Cells Are Associated with Tertiary Lymphoid Structures, Cytolytic T-Cell Responses, and Superior Prognosis in Ovarian Cancer.* Clin Cancer Res, 2016. **22**(12): p. 3005-15.
111. Nielsen, J.S., et al., *CD20+ tumor-infiltrating lymphocytes have an atypical CD27- memory phenotype and together with CD8+ T cells promote favorable prognosis in ovarian cancer.* Clin Cancer Res, 2012. **18**(12): p. 3281-92.
112. Laumont, C.M., et al., *Tumour-infiltrating B cells: immunological mechanisms, clinical impact and therapeutic opportunities.* Nat Rev Cancer, 2022. **22**(7): p. 414-430.
113. Fridman, W.H., et al., *B cells and cancer: To B or not to B?* J Exp Med, 2021. **218**(1).
114. Small, M., et al., *Genetic alterations and tumor immune attack in Yo paraneoplastic cerebellar degeneration.* Acta Neuropathol, 2018. **135**(4): p. 569-579.

115. Sundling, C., et al., *Positive selection of IgG(+) over IgM(+) B cells in the germinal center reaction.* Immunity, 2021. **54**(5): p. 988-1001 e5.
116. Dhenni, R. and T.G. Phan, *The geography of memory B cell reactivation in vaccine-induced immunity and in autoimmune disease relapses.* Immunol Rev, 2020. **296**(1): p. 62-86.
117. Ribatti, D., *The discovery of plasma cells: An historical note.* Immunol Lett, 2017. **188**: p. 64-67.
118. Palaiologou, M., I. Delladetsima, and D. Tiniakos, *CD138 (syndecan-1) expression in health and disease.* Histol Histopathol, 2014. **29**(2): p. 177-89.
119. Nutt, S.L., et al., *The generation of antibody-secreting plasma cells.* Nat Rev Immunol, 2015. **15**(3): p. 160-71.
120. Sprumont, A., et al., *Germinal centers output clonally diverse plasma cell populations expressing high- and low-affinity antibodies.* Cell, 2023. **186**(25): p. 5486-5499 e13.
121. Thone, J., et al., *Effective immunosuppressant therapy with cyclophosphamide and corticosteroids in paraneoplastic cerebellar degeneration.* J Neurol Sci, 2008. **272**(1-2): p. 171-3.
122. Meloni, C., et al., *A case report of plasma exchange therapy in non-paraneoplastic cerebellar ataxia associated with anti-Yo antibody.* Ther Apher Dial, 2004. **8**(6): p. 500-2.
123. Vernino, S., et al., *Immunomodulatory treatment trial for paraneoplastic neurological disorders.* Neuro Oncol, 2004. **6**(1): p. 55-62.
124. Turner, J.S., et al., *Human germinal centres engage memory and naive B cells after influenza vaccination.* Nature, 2020. **586**(7827): p. 127-132.
125. Lee, J.H., et al., *Long-primed germinal centres with enduring affinity maturation and clonal migration.* Nature, 2022. **609**(7929): p. 998-1004.
126. Murugan, R., et al., *Clonal selection drives protective memory B cell responses in controlled human malaria infection.* Sci Immunol, 2018. **3**(20).
127. Vanhersecke, L., et al., *Mature tertiary lymphoid structures predict immune checkpoint inhibitor efficacy in solid tumors independently of PD-L1 expression.* Nat Cancer, 2021. **2**(8): p. 794-802.
128. Sautes-Fridman, C., et al., *Tertiary lymphoid structures in the era of cancer immunotherapy.* Nat Rev Cancer, 2019. **19**(6): p. 307-325.
129. Bressan, D., G. Battistoni, and G.J. Hannon, *The dawn of spatial omics.* Science, 2023. **381**(6657): p. eabq4964.
130. Hsieh, W.C., et al., *Spatial multi-omics analyses of the tumor immune microenvironment.* J Biomed Sci, 2022. **29**(1): p. 96.
131. Chen, T.Y., et al., *Spatial Transcriptomic Technologies.* Cells, 2023. **12**(16).
132. Moses, L. and L. Pachter, *Museum of spatial transcriptomics.* Nat Methods, 2022. **19**(5): p. 534-546.
133. Baccin, C., et al., *Combined single-cell and spatial transcriptomics reveal the molecular, cellular and spatial bone marrow niche organization.* Nat Cell Biol, 2020. **22**(1): p. 38-48.
134. Kalinke, U., et al., *The role of somatic mutation in the generation of the protective humoral immune response against vesicular stomatitis virus.* Immunity, 1996. **5**(6): p. 639-52.
135. Cappelletti, F., et al., *Virus-induced preferential antibody gene-usage and its importance in humoral autoimmunity.* Semin Immunol, 2015. **27**(2): p. 138-43.
136. Manser, T., S.Y. Huang, and M.L. Gefter, *Influence of clonal selection on the expression of immunoglobulin variable region genes.* Science, 1984. **226**(4680): p. 1283-8.
137. Lima, N.S., et al., *Primary exposure to SARS-CoV-2 variants elicits convergent epitope specificities, immunoglobulin V gene usage and public B cell clones.* Nat Commun, 2022. **13**(1): p. 7733.
138. Blazso, P., et al., *Lineage Reconstruction of In Vitro Identified Antigen-Specific Autoreactive B Cells from Adaptive Immune Receptor Repertoires.* Int J Mol Sci, 2022. **24**(1).

139. Cowan, G.J.M., et al., *In Human Autoimmunity, a Substantial Component of the B Cell Repertoire Consists of Polyclonal, Barely Mutated IgG(+ve) B Cells.* Front Immunol, 2020. **11**: p. 395.
140. Tipton, C.M., et al., *Diversity, cellular origin and autoreactivity of antibody-secreting cell population expansions in acute systemic lupus erythematosus.* Nat Immunol, 2015. **16**(7): p. 755-65.
141. Wang, Q., et al., *B-Cell Receptor Repertoire: Recent Advances in Autoimmune Diseases.* Clin Rev Allergy Immunol, 2024. **66**(1): p. 76-98.
142. Sankar, K., K.H. Hoi, and I. Hotzel, *Dynamics of heavy chain junctional length biases in antibody repertoires.* Commun Biol, 2020. **3**(1): p. 207.
143. DeKosky, B.J., et al., *In-depth determination and analysis of the human paired heavy- and light-chain antibody repertoire.* Nat Med, 2015. **21**(1): p. 86-91.
144. Irac, S.E., et al., *Single-cell immune repertoire analysis.* Nat Methods, 2024. **21**(5): p. 777-792.
145. Gerard, A., et al., *High-throughput single-cell activity-based screening and sequencing of antibodies using droplet microfluidics.* Nat Biotechnol, 2020. **38**(6): p. 715-721.
146. Wardemann, H. and C.E. Busse, *Novel Approaches to Analyze Immunoglobulin Repertoires.* Trends Immunol, 2017. **38**(7): p. 471-482.
147. Friedensohn, S., T.A. Khan, and S.T. Reddy, *Advanced Methodologies in High-Throughput Sequencing of Immune Repertoires.* Trends Biotechnol, 2017. **35**(3): p. 203-214.
148. Georgiou, G., et al., *The promise and challenge of high-throughput sequencing of the antibody repertoire.* Nat Biotechnol, 2014. **32**(2): p. 158-68.
149. Fathallah-Shaykh, H., et al., *Cloning of a leucine-zipper protein recognized by the sera of patients with antibody-associated paraneoplastic cerebellar degeneration.* Proc Natl Acad Sci U S A, 1991. **88**(8): p. 3451-4.
150. Rhodes, D.A. and D.A. Isenberg, *TRIM21 and the Function of Antibodies inside Cells.* Trends Immunol, 2017. **38**(12): p. 916-926.
151. Foss, S., et al., *TRIM21-From Intracellular Immunity to Therapy.* Front Immunol, 2019. **10**: p. 2049.
152. Bottermann, M., et al., *TRIM21 mediates antibody inhibition of adenovirus-based gene delivery and vaccination.* Proc Natl Acad Sci U S A, 2018. **115**(41): p. 10440-10445.
153. Takanaga, H., et al., *PKN interacts with a paraneoplastic cerebellar degeneration-associated antigen, which is a potential transcription factor.* Exp Cell Res, 1998. **241**(2): p. 363-72.
154. Sakai, K., et al., *Effect of a paraneoplastic cerebellar degeneration-associated neural protein on B-myb promoter activity.* Neurobiol Dis, 2004. **15**(3): p. 529-33.
155. Storstein, A., B.K. Krossnes, and C.A. Vedeler, *Morphological and immunohistochemical characterization of paraneoplastic cerebellar degeneration associated with Yo antibodies.* Acta Neurol Scand, 2009. **120**(1): p. 64-7.
156. Kunchok, A., A. Zekeridou, and A. McKeon, *Autoimmune glial fibrillary acidic protein astrocytopathy.* Curr Opin Neurol, 2019. **32**(3): p. 452-458.
157. Dubey, D., et al., *Autoimmune GFAP astrocytopathy: Prospective evaluation of 90 patients in 1 year.* J Neuroimmunol, 2018. **321**: p. 157-163.
158. Garza, M. and A.L. Piquet, *Update in Autoimmune Movement Disorders: Newly Described Antigen Targets in Autoimmune and Paraneoplastic Cerebellar Ataxia.* Front Neurol, 2021. **12**: p. 683048.
159. Congdon, E.E., et al., *Antibody uptake into neurons occurs primarily via clathrin-dependent Fcgamma receptor endocytosis and is a prerequisite for acute tau protein clearance.* J Biol Chem, 2013. **288**(49): p. 35452-65.
160. Greenlee, J.E., et al., *Neuronal uptake of anti-Hu antibody, but not anti-Ri antibody, leads to cell death in brain slice cultures.* J Neuroinflammation, 2014. **11**: p. 160.

161. Greenlee, J.E., et al., *Uptake of systemically administered human anticerebellar antibody by rat Purkinje cells following blood-brain barrier disruption.* Acta Neuropathol, 1995. **89**(4): p. 341-5.
162. Hill, K.E., et al., *Cerebellar Purkinje cells incorporate immunoglobulins and immunotoxins in vitro: implications for human neurological disease and immunotherapeutics.* J Neuroinflammation, 2009. **6**: p. 31.
163. Bruhns, P. and F. Jonsson, *Mouse and human FcR effector functions.* Immunol Rev, 2015. **268**(1): p. 25-51.
164. Shiotsuki, H., et al., *A rotarod test for evaluation of motor skill learning.* J Neurosci Methods, 2010. **189**(2): p. 180-5.
165. Carter, R.J., J. Morton, and S.B. Dunnett, *Motor coordination and balance in rodents.* Curr Protoc Neurosci, 2001. **Chapter 8**: p. Unit 8 12.
166. Brooks, S.P. and S.B. Dunnett, *Tests to assess motor phenotype in mice: a user's guide.* Nat Rev Neurosci, 2009. **10**(7): p. 519-29.

9 Supplementary Data

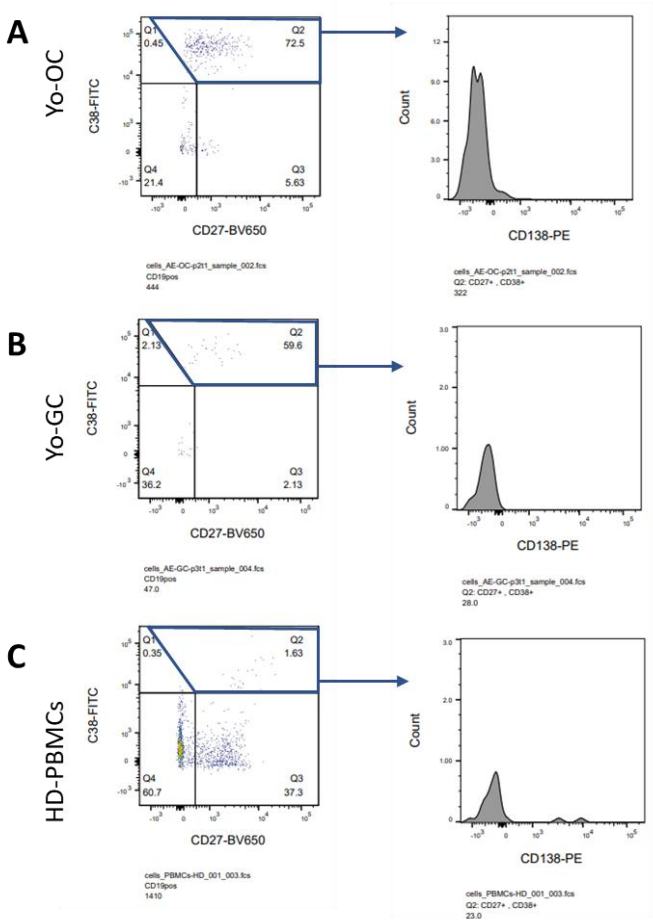

Suppl. Figure 1. CD138 expression of plasmablasts in Yo-tumors and HD-PBMCs. CD138 expression of plasmablasts in the A) Yo-OC B) Yo-GC and C) HD-PBMC samples depicted as a histogram.

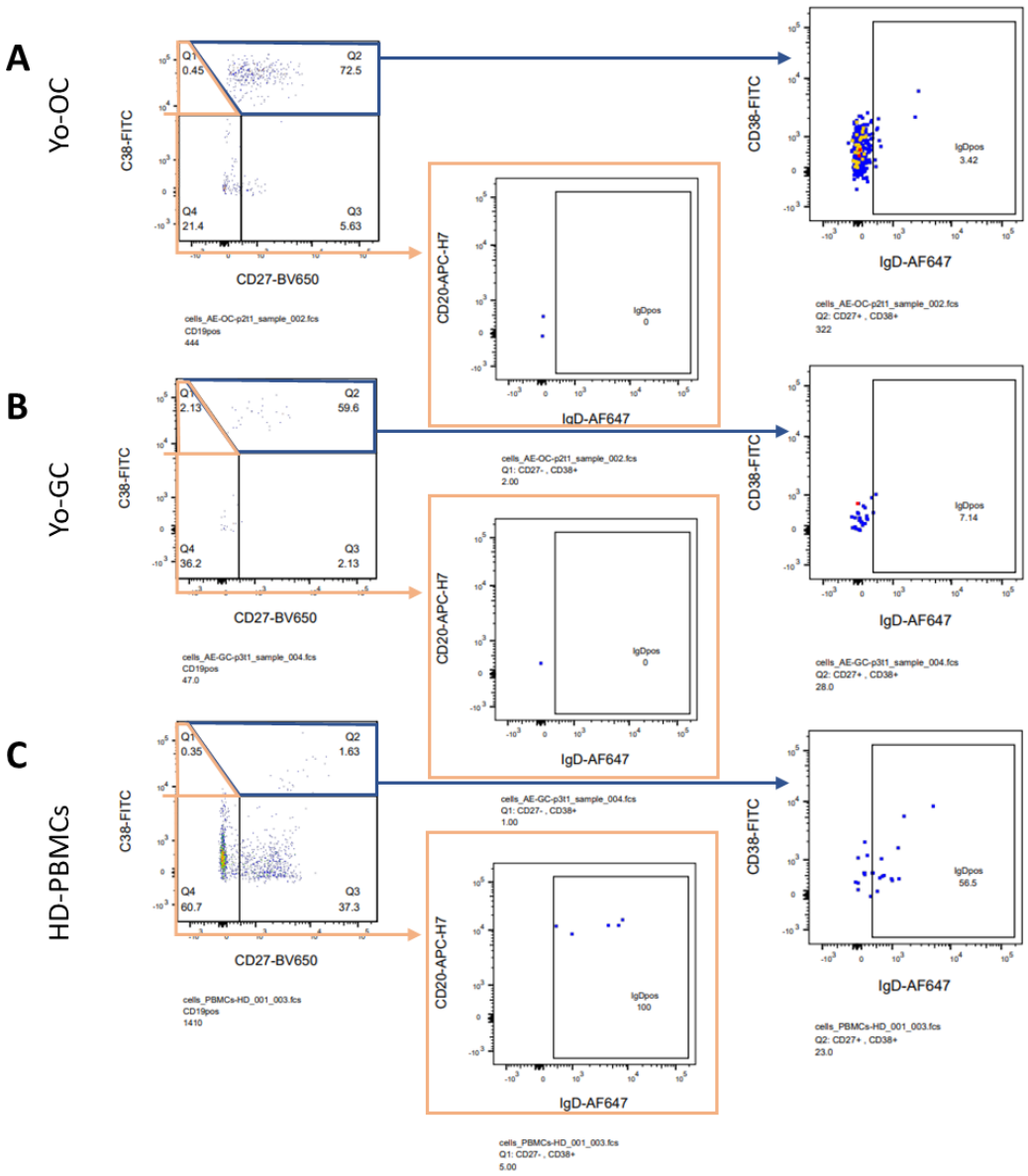

Suppl. Figure 2. IgD expression of plasmablast and PB-like subsets from Yo-tumors and HD-PBMCs. IgD vs CD38 expression of the PB-like (orange) and PB (blue) subsets for the A) Yo-OC B) Yo-GC and C) HD-PBMC samples

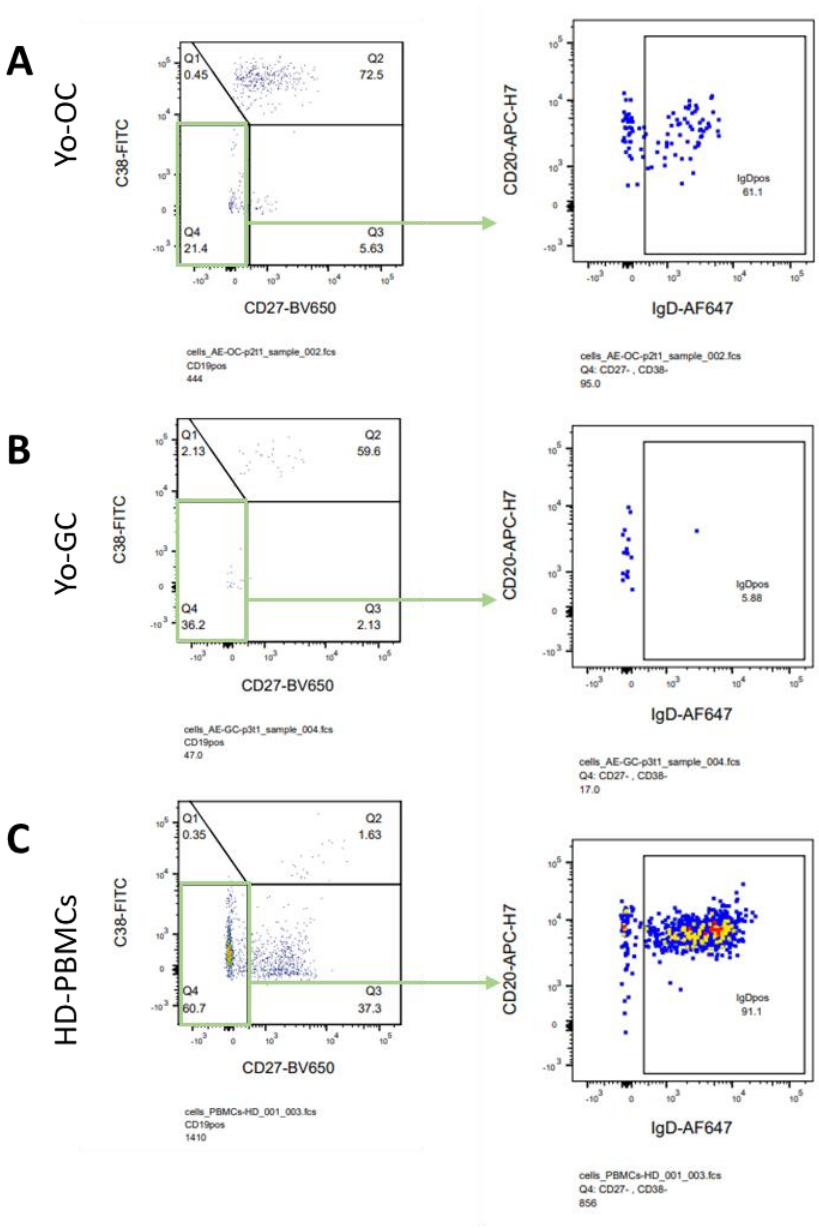

Suppl. Figure 3. IgD expression of naive B cells in Yo-tumors and HD-PBMCs. IgD vs CD20 expression of the naive B cell subset in the A) Yo-OC B) Yo-GC and C) HD-PBMC samples

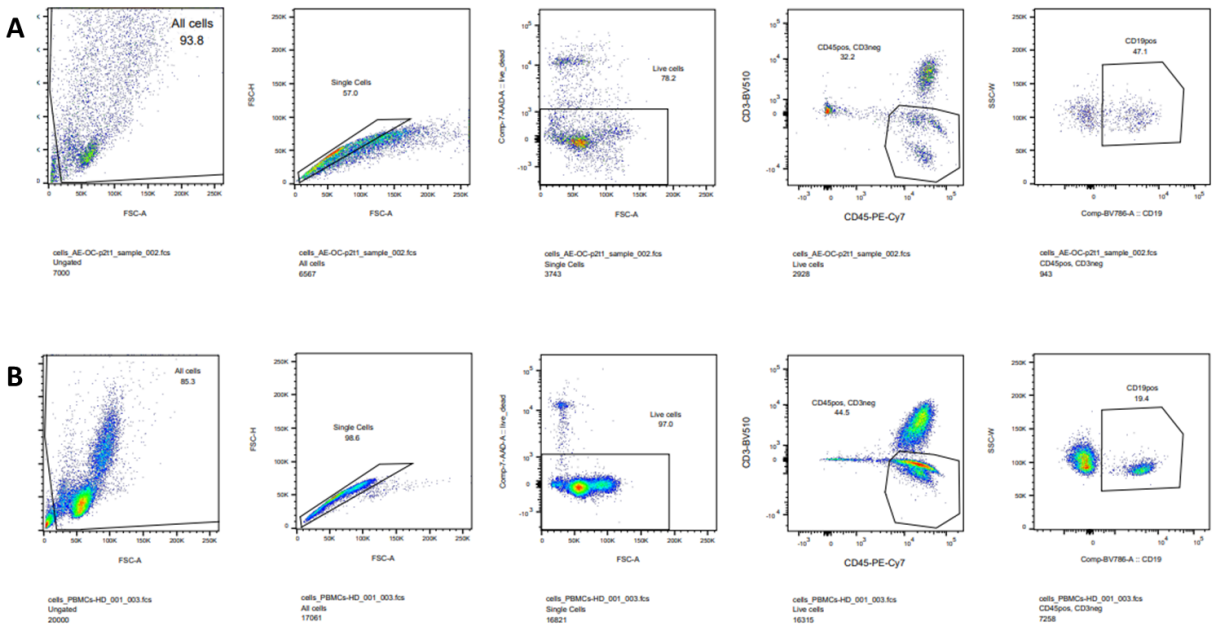

Suppl. Figure 4. Sort gate strategy for the single-cell index sortin of CD19pos B cells from Yo-tumors. A) Gating for the Yo-OC sample. B) Gating for the HD-PBMC sample stained simultaneously with Yo-OC

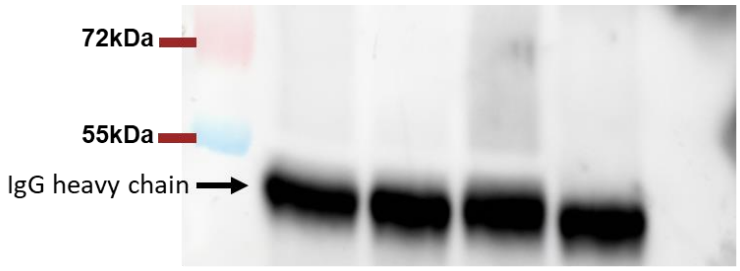

Suppl. Figure 5. Re-probing of the Western Blots of IP for anti-human IgG after mild stripping. Blots of IP products from CDR2L-specific mAbs initially probed for CDR2L (*as described in Figure 14B, left blot)* show intense staining of the IgG1 heavy chain at 50kDa.

Suppl. Table 1. List of proteins, calculated p-values and confidence call scores (Contrast Max Score) from MS results of OvCar3 lysate IP products of P2_1125

Majority.protein.IDs	Gene.names	logFC_of_imputed_values	adj.P.Val_of_imputed_values	Contrast.Max.Score
A0A087WSY6;P01624	IGKV3D-15	10.96223803	4.20E-08	0.663833333
A0A0B4J1X5;A0A0B4J1V1;P01780;P01763;P01762;A0A075B7F0;A0A0C4DH32;P01782	IGHV3-74;IGHV3-21;IGHV3OR16-10;IGHV3-20	12.77492109	1.45E-08	0.613873016
A0A286YFJ8;P01861	IGHG4	8.666705491	1.62E-07	0.573568057
A0A2R8YEM3;E7EQV9;P61313;E7EX53;A0A2R8Y738;E7ENU7	RPL15	3.276729318	9.19E-05	0.513563004
A0A4W9A917;P01860;A0A286YES1	IGHG3	6.528500567	0.000114957	0.654553377
A0A6Q8PFJ0;P02545;A0A804HL68;A0A6Q8PHQ9;A0A6Q8PF80	LMNA	3.919599916	2.28E-06	0.848135802
CON__P02533;P02533	KRT14	1.709758066	0.001303651	0.869884696
CON__P02538;P02538	KRT6A	1.991447099	0.004551755	0.812820988
CON__P02662		1.14533658	0.034001919	0.747671296
CON__P05787;P05787;F8VUG2	KRT8	1.090030368	0.008213241	0.943736111
CON__P08729		5.449109493	5.75E-06	0.629074595
CON__P08779;P08779	KRT16	2.196540048	0.042694353	0.920823755
CON__P13645;A0A1B0GVI3;P13645	KRT10	1.165730762	0.019194263	0.929122739
CON__P13647;P13647	KRT5	1.430663391	0.00453013	0.869814815
CON__P35908v2;P35908	KRT2	1.154490059	0.008334994	0.817
CON__Q04695;Q04695;F5GWP8	KRT17	2.07143421	0.003528005	0.760007732
CON__Q5D862;Q5D862	FLG2	1.621755531	0.037782331	0.737958624
CON__Q86YZ3;Q86YZ3	HRNR	1.698054314	0.035352936	0.713507354
CON__Q9C075;Q9C075;J3QR55	KRT23	3.548310475	0.000169966	0.552289741
E9PHI4;O94901;H0Y6N5;H0Y742	SUN1	2.128001103	0.000191846	0.602021047
P01040;C9J0E4	CSTA	1.535598841	0.012193495	0.684343258
P01834;A0A5H1ZRQ3	IGKC	7.087376768	0.000396942	0.922547138
P01857;A0A0A0MS08;A0A0A0MS07	IGHG1	9.81965349	1.43E-05	0.918490442
P01859;A0A286YEY4	IGHG2	9.771374352	4.20E-08	0.596608262
P04264;CON__P04264	KRT1	1.290460644	0.012335829	0.948977456
P04406;E7EUT5	GAPDH	1.126244869	0.017846549	0.898910675
P05783;F8VZY9	KRT18	1.260848303	0.003200976	0.782023525
P10599	TXN	2.45284172	0.018772128	0.591945443
P19474	TRIM21	2.212296463	0.000151737	0.687688419
P20700;E9PBF6;A0A0D9SFE5	LMNB1	1.547587946	0.000416814	0.863569391
P23490	LOR	1.631537595	0.01309493	0.617943663
P29508;H0Y5H9;P48594	SERPINB3;SERPINB4	4.908767095	7.03E-05	0.553304201
P35321	SPRR1A	2.03815004	0.000861699	0.613405436
P35527;CON__P35527;K7EQQ3	KRT9	1.234399105	0.011888511	0.934153846
P47929	LGALS7	2.710097625	8.22E-05	0.548619628
P49756;E9PQU5	RBM25	1.08632236	0.00845038	0.565722967
Q01469;I6L8B7	FABP5	1.263061774	0.01168196	0.833228687
Q01850;H3BU23	CDR2	6.235652978	2.28E-06	0.910227841
Q02878	RPL6	5.087431742	2.82E-05	0.508787997
Q03252	LMNB2	1.045216143	0.024029724	0.574835107
Q16610	ECM1	4.25660857	2.82E-05	0.558693088
Q3BDU5	LMNA	5.029608233	1.67E-06	0.646402863
Q5T749	KPRP	1.152062491	0.010298692	0.902944444
Q5T750	XP32	2.307026556	0.000350701	0.743173232
Q7Z794;CON__Q7Z794	KRT77	1.542547545	0.009764399	0.791254884
Q86X02	CDR2L	8.89014562	7.85E-06	0.934207207
Q8N1N4;CON__Q7RTT2;CON__Q8N1N4-2	KRT78	1.013705799	0.048022314	0.847938061
Q8TF05	PPP4R1	1.12589283	0.01137432	0.734778898
Q96EN8	MOCOS	3.346122181	6.46E-05	0.740700066
Q96QK1	VPS35	2.945456079	4.36E-05	0.910268116
Q9BVA1;Q13885	TUBB2B;TUBB2A	1.429296862	0.003824126	0.653285116
Q9HCY8	S100A14	1.254357048	0.005590628	0.518880624
Q9UHB6;F8VQE1;F8VRN8;F8VS07	LIMA1	1.118029002	0.017415944	0.657514655
Q9UHY1;F8W6G1	NRBP1	1.399157725	0.016861839	0.536455564
Q9Y2U8	LEMD3	2.107471511	0.000457172	0.681157038

A

Top Canonical Pathways

Name	p-value	Overlap	
Keratinization	2.06E-23	7.9 %	17/214
Glucocorticoid Receptor Signaling	4.06E-12	2.4 %	14/582
Primary Immunodeficiency Signaling	1.34E-07	8.2 %	5/61
Complement cascade	6.98E-06	3.7 %	5/135
Fcgamma receptor (FCGR) dependent phagocytosis	1.45E-05	3.2 %	5/157

B

ID	Molecules in Network	Score	Focus Molec...	Top Diseases and Functions
	AKT, CDK4/6, Cornified envelope, Cornified envelope:CDSN, ↑**CSTA**, cytokeratin, Early cornified envelope, FLG fragment:Keratin tonofila... ...all 35	49	19	Dermatological Diseases and Conditions, Organismal Injury an... ...all 3
	actin, Ap1, caspase, CD3 (complex), ↑**ECM1**, EMD/TMPO/LEMD3/LEMD2:Lamin filaments, EMD/TMPO/LEMD3/LEMD2:Lamin filaments:BAN... ...all 35	28	12	Cell Morphology, Cellular Compromise, Organismal Injury and ... ...all 3
	Antigen:IgG, Antigen:IgG:C1Q:2xActivated C1R:SERPING1:2xActivated C1S:SERPING1, Antigen:IgG:C1Q:2xC1R:2xC1S, BCR (complex), C4 ac... ...all 35	19	9	Cell Death and Survival, Cell Morphology, Cellular Assembly an... ...all 3
	26S proteasome, AIFM2, AKR1A1, ARMC10, C4orf46, CCDC153, CCDC187, ↑**CDR2**, ↑**CDR2L**, CHCHD4 ...all 35	17	8	Drug Metabolism, Nucleic Acid Metabolism, Organismal Injury a... ...all 3

Suppl. Figure 6. Qiagen IPA analysis results from the list of proteins identified from the MS-IP. A) Top canonical pathways inferred from the protein list, none of which involved CDR2 and CDR2L B) Molecular networks where CDR2 and CDR2L (bottom row, marked by red arrows) may be involved , and the inferred function of proteins within that network

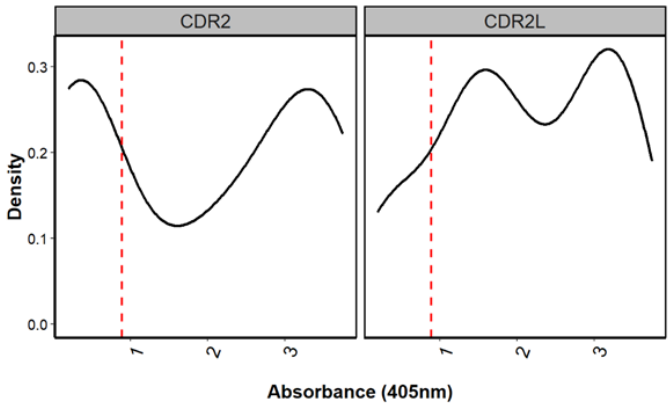

Suppl. Figure 7. Density curves and calculated points of inflection for antibodies testing in the High-sensitivty crosslinking ELISA against CDR2 and CDR2L. Red line represents the first point of inflection, that determined the threshold for binding vs non-binding and informed by the absorbance measurements of the mGO53 antibody as the negative control.

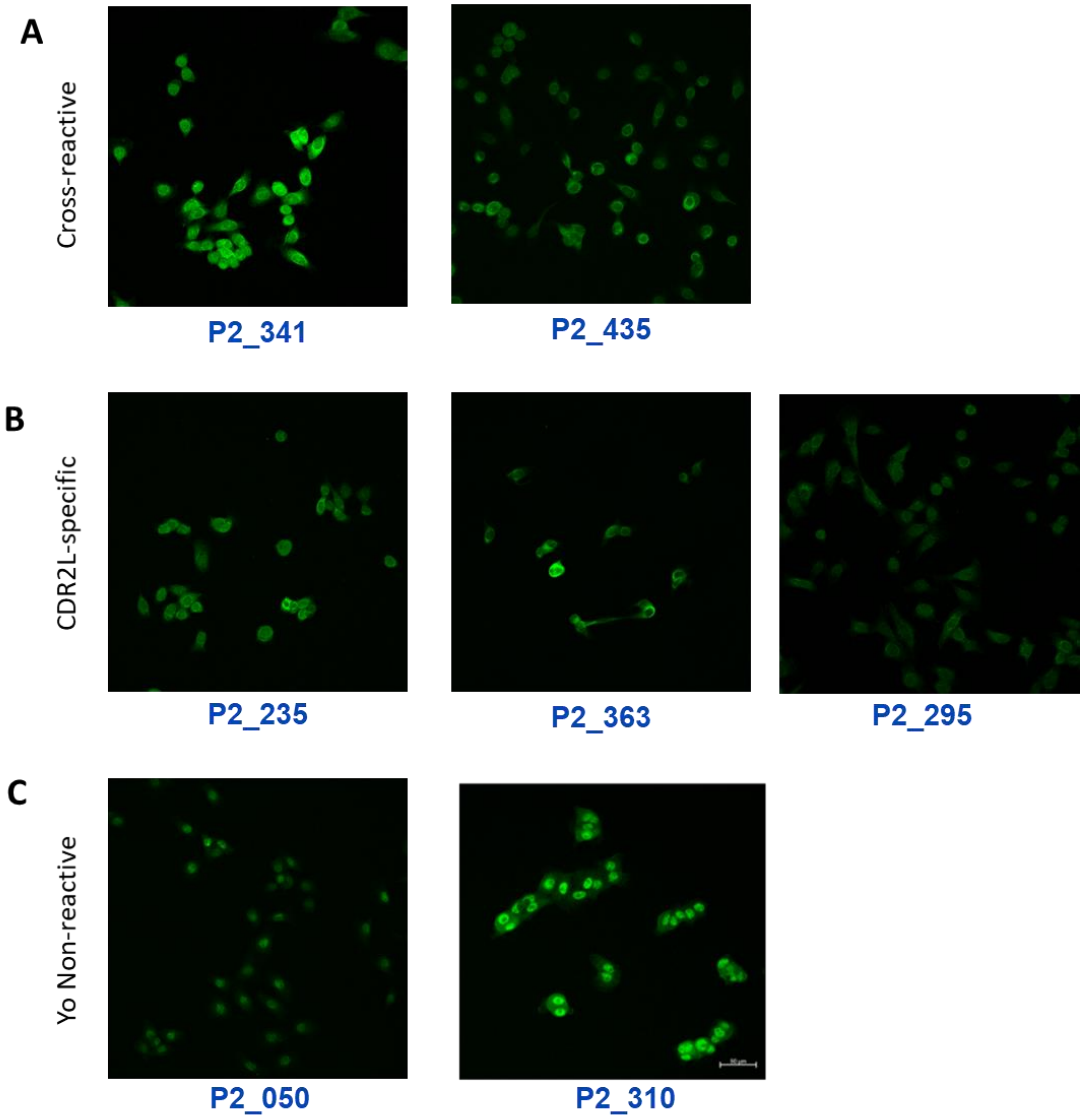

Suppl. Figure 8. IF staining and confocal images of OvCar3 with other mAbs. Staining of permeabilzed OvCar3 with A) cross-reactive mAbs, B) CDR2L-specific mAbs and C) Yo non-reactive mAbs, whose reactivities were assigned based on Yo antigen ELISA AUCs.

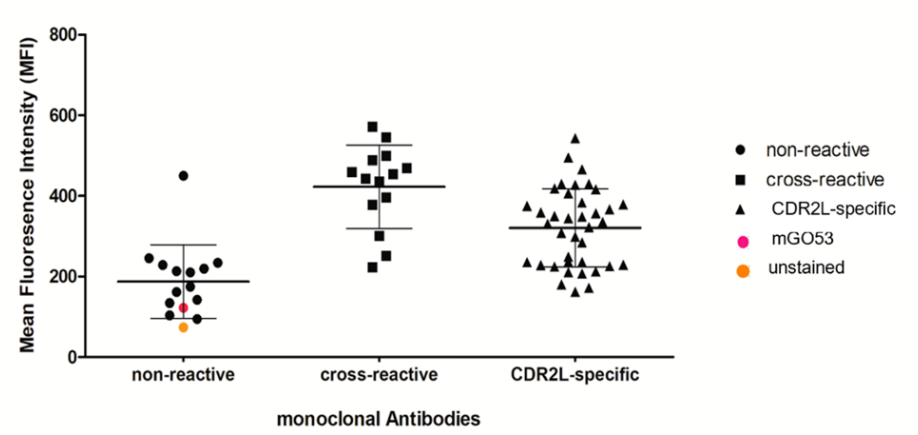

Suppl. Figure 9. Mean MFI values of permeabilized OvCar3 cells stained with the 65 mAbs and separated based on reactivity groups from Yo antigen ELISA . MFI values as a mean of two experiments, and data was generated by Shaumya Kulendran, an MSc student I directly supervised.

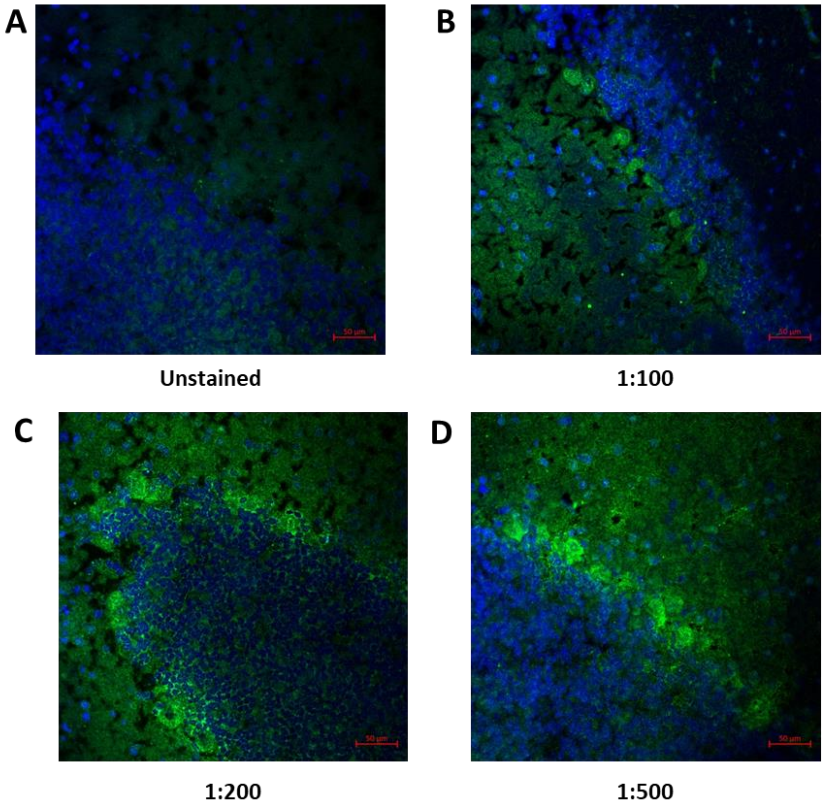

Suppl. Figure 10. Staining of Rat cerebellar sections with anti-calbindin as a positive marker for Purkinje cells. Optimization of the optimial dilution for the commercial anti-calbinding antibody was carriedout here. A) Unstained fixed permeabilized rat cerebellar sections. B) Stained with 1:100 anti-calbindin. C) Stained with 1:200 anti-calbindin. D). Stained with 1:500 anti-calbindin. The 1:100 dilution was identified to be the optimal concentration for IF staining.

Suppl. Table 2. Relevant features of 65 cloned and expressed mAbs from the Yo-OC tumor.

cloning_id	blocking_	igh_segment_v	igh_segment_d	igh_segment_j	igh_cdr3	igh_segm	igh_shm	igk_segment_v	igk_segment_j	igk_cdr3	igk_segm	igk_shm	igl_segme	igl_segmen	igl_cdr3	igl_segme	igl_shm	nodes	pairing	expansior	phenotyp	reactivity	mean_mf	polyreacti	hs_reactivity
JJOCBCP2_050	Q2	IGHV3-23*01	IGHD3-22*01	IGHJ4*02	AKIGKSAYDPGPFDY	IGHG1	17	NULL	NULL	NULL	NULL	NULL	IGLV3-21*	IGLJ2*01	QVWDSSSGHRRA	IGLC3	10	5	H-L	expanded	Plasmabla	non-reactive	142.5	no	non-reactive
JJOCBCP2_1010	Q2	IGHV4-59*01	IGHD1-1*01	IGHJ4*02	ARGVTKRDPGDN	IGHG1	13	NULL	NULL	NULL	NULL	NULL	IGLV1-51*	IGLJ2*01	GTWDSSLSAVV	IGLC7	3	3	H-L	expanded	Plasmabla	cdr2l	416.5	no	hs_cross
JJOCBCP2_1039	Q2	IGHV3-7*01	IGHD1-26*01	IGHJ4*02	ARRSGYSGTYGGFDF	IGHG1	14	NULL	NULL	NULL	NULL	NULL	IGLV2-11*	IGLJ2*01	CSYAGRYTFV	IGLC3	5	2	H-L	expanded	Plasmabla	non-reactive	161.5	no	hs_cross
JJOCBCP2_104	Q4	IGHV3-11*01	IGHD3-3*01	IGHJ6*02	ARGVVRFLRSSMDV	IGHG1	14	IGKV3-20*01	IGKJ2*01	QQYGNSPYT	IGKC	8	NULL	NULL	NULL	NULL	NULL	3	H-K	expanded	Plasmabla	cdr2l	298.5	no	cdr2l
JJOCBCP2_1047	Q2	IGHV3-23*01	IGHD3-10*01	IGHJ6*02	AKDKIRGVRGFLDV	IGHG1	17	IGKV1-39*01	IGKJ1*01	QQSYTDTWT	IGKC	14	NULL	NULL	NULL	NULL	NULL	2	H-K	expanded	Plasmabla	cdr2l	429.5	no	hs_cross
JJOCBCP2_1055	Q2	IGHV1-69*06	IGHD6-19*01	IGHJ6*02	AATSRYSIGWQHVLHNGMDV	IGHG1	17	NULL	NULL	NULL	NULL	NULL	IGLV7-43*	IGLJ2*01	LLYYGGTQGVV	IGLC3	13	3	H-L	expanded	Plasmabla	cross-reactive	436.5	no	cross-reactive
JJOCBCP2_1064	Q2	IGHV3-11*01	IGHD3-16*01	IGHJ4*02	ARRLAMRSRGSDY	IGHG1	17	IGKV3-15*01	IGKJ4*01	QQDNNWPFT	IGKC	7	NULL	NULL	NULL	NULL	NULL	2	H-K	expanded	Plasmabla	cdr2l	406.5	no	hs_cross
JJOCBCP2_1141	Q3	IGHV3-21*03	IGHD3-10*01	IGHJ4*02	VRDGNQMTTIRGVMFDY	IGHG1	17	IGKV1-39*01	IGKJ4*01	QQSYSTPLT	IGKC	13	NULL	NULL	NULL	NULL	NULL	3	H-K	expanded	Plasmabla	cross-reactive	545.5	no	cross-reactive
JJOCBCP2_115	Q2	IGHV3-23*01	IGHD3-10*01	IGHJ4*02	AKDLWTYYYGSGSH	IGHA1	9	NULL	NULL	NULL	NULL	NULL	IGLV2-14*	IGLJ3*02	SSYTTINTVVV	IGLC7	7	2	H-L	expanded	Plasmabla	cdr2l	236.5	no	cdr2l
JJOCBCP2_116	Q2	IGHV3-21*01	IGHD4-23*01	IGHJ4*02	ARVPKGCGSGNCRTQYLDY	IGHG1	21	IGKV3-11*01	IGKJ4*01	QQRRNWPLLT	IGKC	6	NULL	NULL	NULL	NULL	NULL	3	H-K	expanded	Plasmabla	cdr2l	357	no	hs_cross
JJOCBCP2_1179	Q4	IGHV3-7*01	IGHD1-20*01	IGHJ4*02	ARDNWLGAIDY	IGHG1	9	IGKV1-9*01	IGKJ4*01	QQFKSYSLT	IGKC	9	NULL	NULL	NULL	NULL	NULL	2	H-K	expanded	Plasmabla	cdr2l	495	no	hs_cross
JJOCBCP2_1182	Q2	IGHV3-23*01	NULL	IGHJ4*02	AKRDLGSRSFDY	IGHG1	19	IGKV1-39*01	IGKJ4*01	QQSYGTLALT	IGKC	14	NULL	NULL	NULL	NULL	NULL	2	H-K	expanded	Plasmabla	cdr2l	330.5	no	hs_cross
JJOCBCP2_144	Q2	IGHV1-18*04	IGHD2-2*01	IGHJ4*02	ARDYLGDIVVVPAAITLDY	IGHG1	14	IGKV1-39*01	IGKJ1*01	QQSYSTPLA	IGKC	15	IGLV3-21*	IGLJ2*01	QVWDSGSAS	IGLC7	7	2	both	expanded	Plasmabla	cdr2l	236	no	cdr2l
JJOCBCP2_151	Q2	IGHV3-11*01	IGHD3-3*01	IGHJ6*02	ARATLRFLKAGMDV	IGHG1	13	IGKV3-20*01	IGKJ1*01	QQYGGSRWT	IGKC	6	IGLV1-51*	IGLJ2*01	ATWDSSLSGVV	IGLC7	7	2	both	expanded	Plasmabla	non-reactive	103.6	no	non-reactive
JJOCBCP2_171	Q2	IGHV1-18*04	IGHD1-1*01	IGHJ4*02	AREGSPERGRGWLGY	IGHG1	26	NULL	NULL	NULL	NULL	NULL	IGLV3-21*	IGLJ3*02	QVWDSSSDHQV	IGLC7	5	5	H-L	expanded	Plasmabla	non-reactive	175	no	non-reactive
JJOCBCP2_182	Q3	IGHV3-11*01	IGHD3-3*01	IGHJ6*02	AREVKRFLRGGMDV	IGHG1	13	IGKV3-20*01	IGKJ1*01	QQYGGSPGT	IGKC	9	NULL	NULL	NULL	NULL	NULL	12	H-K	expanded	Plasmabla	cdr2l	367	no	hs_cross
JJOCBCP2_235	Q2	IGHV3-30*10	IGHD4-23*01	IGHJ5*02	ARVGSRPPVGWFDA	IGHG1	24	IGKV3-11*01	IGKJ4*01	QQRNNWPPLT	IGKC	8	NULL	NULL	NULL	NULL	NULL	2	H-K	expanded	Plasmabla	cdr2l	465.5	no	hs_cross
JJOCBCP2_272	Q2	IGHV1-2*02	IGHD1-1*01	IGHJ4*02	ALTAFTTGSSMEY	IGHG1	17	IGKV2-28*01	IGKJ4*01	MQALQSPT	IGKC	3	NULL	NULL	NULL	NULL	NULL	5	H-K	expanded	Plasmabla	cdr2l	207.5	no	cdr2l
JJOCBCP2_290	Q3	IGHV3-23*01	IGHD5-12*01	IGHJ4*02	AKAAATSGYYRMYFDN	IGHG1	12	IGKV3-15*01	IGKJ1*01	QQYSNWPPWT	IGKC	5	NULL	NULL	NULL	NULL	NULL	2	H-K	expanded	Plasmabla	cross-reactive	469.5	no	cross-reactive
JJOCBCP2_295	Q2	IGHV3-33*01	IGHD3-10*01	IGHJ6*02	ARDRFFGSGSDYVLHGMDV	IGHG1	17	IGKV3-20*01	IGKJ3*01	QQYGSSPPVFT	IGKC	4	NULL	NULL	NULL	NULL	NULL	4	H-K	expanded	Plasmabla	cdr2l	379	no	hs_cross
JJOCBCP2_310	Q2	IGHV4-61*02	IGHD3-10*01	IGHJ4*02	ARGNYGNGGLDY	IGHG1	15	NULL	NULL	NULL	NULL	NULL	IGLV1-47*	IGLJ1*01	AAWDDSLSGLV	IGLC1	5	2	H-L	expanded	Plasmabla	non-reactive	450	no	hs_cross
JJOCBCP2_320	Q2	IGHV3-23*01	IGHD6-25*01	IGHJ4*02	ATRPYSSGPD	IGHG1	20	IGKV1-9*01	IGKJ4*01	QQLNSYPLT	IGKC	9	NULL	NULL	NULL	NULL	NULL	2	H-K	expanded	Plasmabla	cdr2l	228	no	hs_cross
JJOCBCP2_325	Q3	IGHV4-4*07	IGHD4-11*01	IGHJ6*02	TRGRYSSYGYGLDV	IGHG1	12	IGKV1-39*01	IGKJ2*01	QQGYSTPHT	IGKC	13	NULL	NULL	NULL	NULL	NULL	5	H-K	expanded	Plasmabla	cross-reactive	572	no	cross-reactive
JJOCBCP2_341	Q1	IGHV1-69*06	IGHD5-12*01	IGHJ1*01	ASSKSREWLRWNLHH	IGHG1	22	NULL	NULL	NULL	NULL	NULL	IGLV2-14*	IGLJ1*01	SSYTTSSTF	IGLC1	12	8	H-L	expanded	Plasmabla	cross-reactive	443	poly	cross-reactive
JJOCBCP2_363	Q4	IGHV3-48*03	IGHD3-16*01	IGHJ4*02	ARDGETTMITRGLRLDY	IGHG1	13	IGKV1-39*01	IGKJ2*01	QQSYSTPQT	IGKC	7	NULL	NULL	NULL	NULL	NULL	11	H-K	expanded	Plasmabla	cdr2l	383.5	no	hs_cross
JJOCBCP2_371	Q2	IGHV4-39*01	IGHD3-22*01	IGHJ4*02	ASLPVYYFDGCD	IGHG1	17	IGKV3-15*01	IGKJ3*01	QQYNKWPEFT	IGKC	8	NULL	NULL	NULL	NULL	NULL	9	H-K	expanded	Plasmabla	cdr2l	335.5	no	cdr2l
JJOCBCP2_372	Q2	IGHV3-23*01	IGHD3/OR15-3a*	IGHJ4*02	AKAQGLD	IGHG1	18	IGKV4-1*01	IGKJ1*01	QQYYGSEWA	IGKC	10	NULL	NULL	NULL	NULL	NULL	2	H-K	expanded	Plasmabla	cdr2l	359	no	cdr2l
JJOCBCP2_417	Q2	IGHV1-18*01	IGHD5-18*01	IGHJ4*02	ARDPRPARGYRDYFDF	IGHG1	29	NULL	NULL	NULL	NULL	NULL	IGLV3-21*	IGLJ2*01	QVWDSVGDHPV	IGLC3	13	2	H-L	expanded	Plasmabla	non-reactive	210.5	no	non-reactive
JJOCBCP2_418	Q2	IGHV3-23*01	IGHD3-16*01	IGHJ3*02	ARRGIASLSRAFDI	IGHG1	14	IGKV1-39*01	IGKJ2*03	QQSYTTLSYS	IGKC	6	NULL	NULL	NULL	NULL	NULL	2	H-K	expanded	Plasmabla	cdr2l	344.5	no	hs_cross
JJOCBCP2_431	Q2	IGHV3-7*01	IGHD6-13*01	IGHJ4*02	ARVGPGGGDSSWFGWGYLDY	IGHG1	6	NULL	NULL	NULL	NULL	NULL	IGLV1-44*	IGLJ3*02	AAWDDSLNGCV	IGLC3	3	5	H-L	expanded	Plasmabla	non-reactive	134.5	no	non-reactive
JJOCBCP2_435	Q3	IGHV4-4*07	IGHD1-26*01	IGHJ5*02	ARITVGGTRDS	IGHG1	13	IGKV3-11*01	IGKJ5*01	QHRSNWIT	IGKC	4	NULL	NULL	NULL	NULL	NULL	6	H-K	expanded	Plasmabla	cross-reactive	459	no	cross-reactive
JJOCBCP2_469	Q2	IGHV3-21*01	IGHD1-1*01	IGHJ3*02	ARDLTTGDAFDI	IGHG1	10	IGKV3-15*01	IGKJ1*01	QQYNTWPT	IGKC	5	NULL	NULL	NULL	NULL	NULL	3	H-K	expanded	Plasmabla	cdr2l	224.5	no	cdr2l
JJOCBCP2_489	Q2	IGHV1-18*04	IGHD3-10*01	IGHJ5*02	ARGPRALVRGALNWFDT	IGHG1	20	NULL	NULL	NULL	NULL	NULL	IGLV1-44*	IGLJ2*01	TVWDDSLNGVV	IGLC3	3	4	H-L	expanded	Plasmabla	cdr2l	249	no	cdr2l
JJOCBCP2_504	Q2	IGHV1-69*06	IGHD5-24*01	IGHJ6*01	ARARSRDAYFGYAMDV	IGHG1	17	IGKV3-11*01	IGKJ4*01	QLRSNWPS	IGKC	9	NULL	NULL	NULL	NULL	NULL	3	H-K	expanded	Plasmabla	cross-reactive	302	poly	cross-reactive
JJOCBCP2_506	Q2	IGHV3-21*01	IGHD1-1*01	IGHJ4*02	TRHRAVERRKFDY	IGHG1	14	NULL	NULL	NULL	NULL	NULL	IGLV3-21*	IGLJ2*01	QVWDSSSAS	IGLC7	9	7	H-L	expanded	Plasmabla	cdr2l	418.5	no	hs_cross
JJOCBCP2_512	Q2	IGHV3-30*04	IGHD3-16*01	IGHJ4*02	ARSGRGSFLGDY	IGHG1	23	IGKV1-5*03	IGKJ1*01	QQYNTYMWT	IGKC	7	NULL	NULL	NULL	NULL	NULL	2	H-K	expanded	Plasmabla	non-reactive	245.5	no	non-reactive
JJOCBCP2_522	Q2	IGHV4-39*01	IGHD2-15*01	IGHJ5*02	ASSAVFVMGCFDP	IGHG1	14	IGKV3-11*01	IGKJ3*01	QQRSSWPRGIT	IGKC	5	NULL	NULL	NULL	NULL	NULL	2	H-K	expanded	Plasmabla	non-reactive	219.5	no	hs_cross
JJOCBCP2_530	Q4	IGHV3-23*01	IGHD2-2*01	IGHJ5*02	AKGPGGLPTFLDS	IGHG1	13	IGKV1-27*01	IGKJ3*01	QNYNSSPFT	IGKC	6	NULL	NULL	NULL	NULL	NULL	2	H-K	expanded	Plasmabla	cdr2l	375.5	no	hs_cross
JJOCBCP2_545	Q2	IGHV3-23*01	IGHD4-23*01	IGHJ3*02	AKRHDGHGAFDI	IGHG1	12	IGKV1-16*01	IGKJ5*01	QQYNSYPIT	IGKC	9	NULL	NULL	NULL	NULL	NULL	2	H-K	expanded	Plasmabla	cdr2l	237.5	no	cdr2l
JJOCBCP2_548	Q2	IGHV3-23*01	IGHD1-26*01	IGHJ4*02	AKDTTVYSGSVD	IGHG1	17	NULL	NULL	NULL	NULL	NULL	IGLV1-47*	IGLJ3*02	AAWDDSLIGRV	IGLC7	5	3	H-L	expanded	Plasmabla	non-reactive	74.1	no	non-reactive
JJOCBCP2_562	Q2	IGHV4-39*01	IGHD3-16*01	IGHJ2*01	ARLMISSRDFDL	IGHG1	16	NULL	NULL	NULL	NULL	NULL	IGLV7-43*	IGLJ1*01	LLYVGSSQLGV	IGLC1	12	19	H-L	expanded	Plasmabla	non-reactive	228.5	no	hs_cross
JJOCBCP2_592	Q2	IGHV3-33*01	IGHD2-15*01	IGHJ4*02	ARDRGSPLLNYIDH	IGHG1	13	NULL	NULL	NULL	NULL	NULL	IGLV1-40*	IGLJ1*01	QSYDSSLSALYV	IGLC1	9	4	H-L	expanded	Plasmabla	cdr2l	285	no	hs_cross
JJOCBCP2_605	Q2	IGHV1-18*01	IGHD2-8*01	IGHJ4*02	ARGSGTFDY	IGHG1	19	IGKV3-20*01	IGKJ4*01	QQFASSLT	IGKC	9	NULL	NULL	NULL	NULL	NULL	2	H-K	expanded	Plasmabla	cdr2l	429.5	no	hs_cross
JJOCBCP2_632	Q2	IGHV3-30*18	IGHD3-10*01	IGHJ4*02	AKERFSNSGDLNYFHY	IGHG1	14	IGKV2-28*01	IGKJ4*01	MQTLQTPLT	IGKC	8	NULL	NULL	NULL	NULL	NULL	2	H-K	expanded	Plasmabla	cdr2l	172	no	hs_cross
JJOCBCP2_638	Q2	IGHV3-30*18	IGHD6-19*01	IGHJ4*02	AKERGVTKIAVLDH	IGHG1	10	IGKV1-16*02	IGKJ4*01	QQYISYPLT	IGKC	5	NULL	NULL	NULL	NULL	NULL	2	H-K	expanded	Plasmabla	non-reactive	213.5	no	hs_cross
JJOCBCP2_643	Q1	IGHV3-48*03	IGHD1-7*01	IGHJ6*02	ARTRAGYYGLNV	IGHG1	15	IGKV1-5*03	IGKJ1*01	QLYSTYSRT	IGKC	8	NULL	NULL	NULL	NULL	NULL	2	H-K	expanded	Plasmabla	cross-reactive	454	no	cross-reactive
JJOCBCP2_658	Q1	IGHV4-38-2*01	IGHD2-21*02	IGHJ4*02	ASTRAVTATDY	IGHG1	14	IGKV3-20*01	IGKJ5*01	QQYGTSPPVT	IGKC	4	NULL	NULL	NULL	NULL	NULL	3	H-K	expanded	Plasmabla	cross-reactive	378	no	cross-reactive
JJOCBCP2_677	Q3	IGHV4-61*02	IGHD4-23*01	IGHJ5*02	ARARFGGNILDP	IGHG1	11	IGKV3-20*01	IGKJ5*01	QHYDNSPIT	IGKC	5	NULL	NULL	NULL	NULL	NULL	2	H-K	expanded	Plasmabla	cross-reactive	223	no	cross-reactive
JJOCBCP2_687	Q4	IGHV4-31*03	IGHD1-1*01	IGHJ1*01	ACGRGTPAYFKH	IGHG1	9	NULL	NULL	NULL	NULL	NULL	IGLV1-40*	IGLJ3*02	QSYDSSLSGSV	IGLC3	3	2	H-L	expanded	Plasmabla	cdr2l	225.5	no	hs_cross
JJOCBCP2_691	Q2	IGHV4-4*07	IGHD3-10*01	IGHJ3*02	ARGPGPFDI	IGHG1	19	IGKV3-11*01	IGKJ4*01	QQRFNWPPEVT	IGKC	6	NULL	NULL	NULL	NULL	NULL	8	H-K	expanded	Plasmabla	non-reactive	234.5	no	non-reactive
JJOCBCP2_738	Q2	IGHV3-11*01	IGHD2-15*01	IGHJ3*02	ARRIPQIVMGGGYAFDI	IGHG1	16	IGKV1-39*01	IGKJ4*01	QQSYITPLT	IGKC	7	NULL	NULL	NULL	NULL	NULL	3	H-K	expanded	Plasmabla	cdr2l	308.5	no	cdr2l
JJOCBCP2_742	Q2	IGHV5-51*01	IGHD3-10*01	IGHJ4*02	TIPPGGSGSEHFDF	IGHG1	9	NULL	NULL	NULL	NULL	NULL	IGLV3-25*	IGLJ2*01	QSADISSSYRV	IGLC7	6	3	H-L	expanded	Plasmabla	cdr2l	349	no	cdr2l
JJOCBCP2_745	Q3	IGHV3-48*01	IGHD5-24*01	IGHJ4*02	ARDGTWHYAFDF	IGHG1	10	IGKV1-27*01	IGKJ3*01	QGYKSALGIT	IGKC	5	NULL	NULL	NULL	NULL	NULL	6	H-K	expanded	Plasmabla	cross-reactive	396	no	cross-reactive
JJOCBCP2_765	Q3	IGHV1-18*04	IGHD5-18*01	IGHJ6*02	ARSRDTSSYAMDV	IGHG1	14	IGKV3-11*01	IGKJ5*01	QQRSRWPPSIT	IGKC	7	NULL	NULL	NULL	NULL	NULL	2	H-K	expanded	Plasmabla	cross-reactive	500	no	cross-reactive
JJOCBCP2_772	Q1	IGHV3-23*01	IGHD6-19*01	IGHJ4*02	AKAAVAGVVRMGFDS	IGHG1	13	IGKV1-27*01	IGKJ1*01	QKYDTDPWT	IGKC	8	NULL	NULL	NULL	NULL	NULL	7	H-K	expanded	Plasmabla	cdr2l	229	no	hs_cross
JJOCBCP2_834	Q2	IGHV3-23*01	IGHD3-3*01	IGHJ4*02	AKDSWSTLYSAGDY	IGHG1	17	NULL	NULL	NULL	NULL	NULL	IGLV2-14*	IGLJ2*01	SSYTTYDTLVV	IGLC3	6	3	H-L	expanded	Plasmabla	cdr2l	350	no	cdr2l
JJOCBCP2_858	Q2	IGHV3-48*01	IGHD3-10*01	IGHJ4*02	ARDLRRRVPFDY	IGHG1	11	IGKV1-39*01	IGKJ5*01	QQSYTTLSVT	IGKC	8	NULL	NULL	NULL	NULL	NULL	3	H-K	expanded	Plasmabla	cdr2l	543.5	no	hs_cross
JJOCBCP2_870	Q2	IGHV3-23*01	IGHD1-14*01	IGHJ4*02	ARKNPFDY	IGHG1	19	IGKV4-1*01	IGKJ2*01	QQYYSAPYT	IGKC	10	NULL	NULL	NULL	NULL	NULL	4	H-K	expanded	Plasmabla	cdr2l	210.5	no	cdr2l
JJOCBCP2_893	Q2	IGHV1-18*04	IGHD2-2*01	IGHJ4*02	ARDLLGDIIVHPVAITLDY	IGHG1	8	IGKV1-39*01	IGKJ1*01	QQSYSTPLA	IGKC	10	NULL	NULL	NULL	NULL	NULL	2	H-K	expanded	Plasmabla	cdr2l	213	no	cdr2l
JJOCBCP2_907	Q4	IGHV3-48*03	IGHD2-8*01	IGHJ4*02	ARDGEGLMASSGAYFDY	IGHG1	16	IGKV1-39*01	IGKJ4*01	QHTYSTPLT	IGKC	2	NULL	NULL	NULL	NULL	NULL	6	H-K	expanded	Plasmabla	cdr2l	427	no	hs_cross
JJOCBCP2_921	Q1	IGHV3-23*01	IGHD6-6*01	IGHJ4*02	AKGHIAARPYYFDS	IGHG1	8	IGKV1-5*03	IGKJ1*01	QQYSSYSLWT	IGKC	5	NULL	NULL	NULL	NULL	NULL	2	H-K	expanded	Plasmabla	cross-reactive	252	no	cross-reactive
JJOCBCP2_927	Q2	IGHV3-30*18	IGHD2-2*01	IGHJ4*02	AKTKFKKVVAPLDY	IGHG1	20	IGKV1-39*01	IGKJ5*01	QQSYSLRAIT	IGKC	12	NULL	NULL	NULL	NULL	NULL	11	H-K	expanded	Plasmabla	cdr2l	322.5	no	hs_cross
JJOCBCP2_936	Q2	IGHV4-59*01	IGHD2-8*01	IGHJ6*02	ARERRYLFGMVSNFDYGMGV	IGHG1	17	IGKV2-28*01	IGKJ2*01	MQALQTPPYT	IGKC	5	NULL	NULL	NULL	NULL	NULL	8	H-K	expanded	Plasmabla	cdr2l	162	no	hs_cross
JJOCBCP2_994	Q4	IGHV4-38-2*01	IGHD2-15*01	IGHJ6*02	VRDSIVVVVAAEGYYGMDV	IGHG1	4	IGKV1-39*01	IGKJ1*01	QQSYSIRLRT	IGKC	7	NULL	NULL	NULL	NULL	NULL	2	H-K	expanded	Plasmabla	cdr2l	180.5	no	cdr2l
JJOCBCP2_1125	Q3	IGHV3-21*01	IGHD3-10*01	IGHJ4*02	ARVGLDSGMNRGSTDY	IGHG1	8	IGKV3-15*01	IGKJ2*01	QQYNNWPQT	IGKC	7	NULL	NULL	NULL	NULL	NULL	4	H-K	expanded	Plasmabla	cross-reactive	489	no	cross-reactive

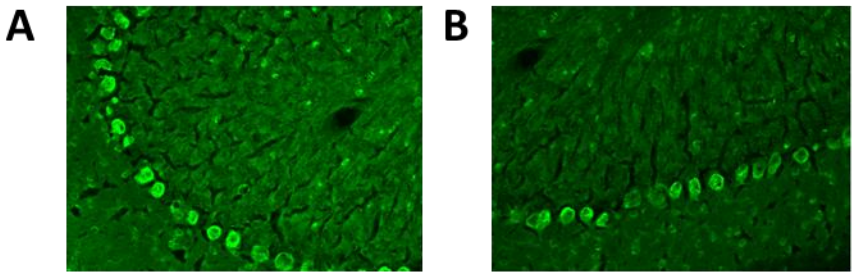

Suppl. Figure 11. Intrathecal delivery of Yo-mAbs. A & B) Cerebellar sections harvested from mice 10 days after continuous intrathecal delivery of P2_290 mAb. *Data from generated by César Cordero-Gomez.*

10 Acknowledgments

The completion of this dissertation would not be possible without so many people to be thankful for. To my family first and foremost— Mom, Dad, Deb and Frey – endless thanks. Thank you for your unwavering support throughout the years, and for all the love. I love you all a thousand times back, and I dedicate this thesis to you.

To my extended family here in Germany, the HD Pinoy fam, thanks! You brought the tropical warmth of home that has got me through the “harsh” winters. Thanks for being my constants.

To D130, both past and present members, it has been an enjoyable ride, and this whole experience would not be the same nor possible without you. There are not enough words (and sadly not enough time for now), to thank each of you properly here. Irene, Hannah, Sandro, Anna, Ernest, Julia G, Fridi, Tini, Yasmin, Zhe, Leo, Kassandra, Hendrik, Theresa, Gemma, Ilka, Christine, Claudia, Julia L, Maddie, Shaumya, Gopa, Musty, Catherine, Nyssa – too many people to mention, and so many ways I want to show my appreciation, but know that you guys are something else. You have impacted my life beyond the work and science, and made the ride so enjoyable, it’s probably why it took me a while :P

To Hedda, thank you for taking me under your wing, especially at the start when I was looking for a new “scientific” home. It took some time, but I made it. More importantly I learned a lot from you both scientifically and otherwise. Thanks for allowing me to grow as a scientist and as an individual under your mentorship.

To my friends outside work, who have kept me balanced, thanks! Michi, Berni, Patrick, Hyobin, Marvin, my Studio 54 fam Daan, Hannah and Marie, Karin, Eric, Jessi, Tilo, Johannes, Vivi and many more. How I made so many enjoyable memories with you all, despite me spending a lot of time at work, was a welcome surprise. Thanks for enriching this whole experience.

To my collaborators and SYNABS consortium friends, thanks for the trust and fun science! Been great studying these fascinating disorders with you all.

I am sure there are many more people to thank, and endless ways to thank you all, but sadly not enough time to do it here (as I have to print this now), but will make sure to let you all know how grateful I am that you were part of this experience. Ich danke Ihnen allen von ganzem Herzen!